Modeling and Numerical Analysis of Heat and Mass Transfer Phenomenon in Fluid Flow

A Thesis

submitted in partial fulfillment of the requirements for the award of the degree of

Doctor of Philosophy

in

School of Mathematics

by

Madhu Aneja
Reg no: 901511008

under the supervison of

Dr. Sapna Sharma
Associate Professor
School of Mathematics

THAPAR INSTITUTE
OF ENGINEERING & TECHNOLOGY
(Deemed to be University)

THAPAR INSTITUTE OF ENGINEERING AND TECHNOLOGY
PATIALA-147004, Punjab, India
December 16, 2021

Certificate

I hereby certify that the work, which is being presented in the thesis, entitled **Modeling and Numerical Analysis of Heat and Mass Transfer Phenomenon in Fluid Flow**, in partial fulfillment of the requirements for the award of the degree of **Doctor of Philosophy** and submitted to the institution is an authentic record of my own work carried out during the period **25 January, 2016** to **December 16, 2021** under the supervision of **Dr. Sapna Sharma**, Associate Professor, School of Mathematics School of Mathematics,Thapar Institute of Engineering and Technology, Patiala.

Date: 16/12/2021

Madhu Aneja

(Madhu Aneja)
Candidate

It is certified that the above statement made by the candidate is correct to the best of my knowledge.

Date: 16/12/2021

Dr. Sapna Sharma
Supervisor

Scanned by Scanner Go

.....dedicated to my daughter & parents

Acknowledgements

Completion of this doctoral dissertation was possible with the support of several people. I want to express my sincere gratitude to all of them.

First of all, I would like to thank the almighty for granting perseverance. After that, I would like to express my sincere gratitude to my supervisor Dr. Sapna Sharma, Associate Professor, School of Mathematics, TIET Patiala, for the continuous support of my Ph.D. study and related research, for her patience, motivation, and immense knowledge. Her guidance helped me in all the time of research and writing of this thesis. I could not have imagined having a better advisor and mentor for my Ph.D. study.

Besides my advisor, I would like to thank the rest of my doctoral committee: Dr. A.K. Lal, Dr. Kavita and Dr. Soumendu Jana, for carefully scrutinizing my progress and providing me necessary suggestions for my research work. I am also grateful to Dr. A.K. Lal, Professor & former Head, and Dr. Satish Sharma, Head, School of Mathematics, TIET Patiala for their constant support and infrastructural facilities provided for my research work. It gives me great pleasure in acknowledging the help from Dr. Avinash Chandra, Associate Professor, TIET, Patiala, Dr. Osman Anwar Beg, Professor, University of Salford, UK, Dr. M. Bilal Ashraf, Assistant Professor, Cosmat University Islamabad, Pakistan. They have been a great source of knowledge and inspiration.

I wish to express my most sincere thanks to the faculty and non-teaching staff members of the School of Mathematics, TIET, Patiala for their continuous encouragement during this work.

I am thankful to Department of Science & Technology, India, and Thapar Institute of Engineering & Technology, Patiala for providing me financial support during my research work.

I am heartfelt to my closest friends Jagbeer Kaur, Sukhveer Singh, Ashish Goyal, Arshpreet Kaur, and Richa Goyal for the stimulating discussions, for the times we work together before deadlines, and for all the moments we have fun together. I share the credit of my work with my friends Daljeet Kaur, Rajwinder kaur, Nikita Madaan. I cannot write the name of each of my friends but I would like to thank all my friends, I feel blessed to have all of you in my life.

This thesis would not have been possible without the eternal love and generous support of both my families. It is like a drop in the ocean of words that can never reach its mark to

acknowledge the tremendous sacrifice that my parents made to ensure that I had an excellent education. I can't forget to thanks my husband, Nitin Chhabra, for his continuous motivation and support. My special thanks go to my daughter, Ravya, my sister, Shallu Aneja, and my brother Anil Aneja for their unconditional love and support.

Madhu Aneja
Madhu Aneja

Scanned by Scanner Go

Abstract

The phenomenon of heat and mass transfer occurs in almost every field of science and engineering as well as in nature. In the methods of power production, fluid flow and heat transfer processes are involved. Components used in the chemical and metallurgical industries include furnaces, heat exchangers, condensers, and reactors, all of which employ thermo fluid processes. Heat transfer is frequently a limiting factor in the design of electrical machinery and electric circuits. Heat and mass transfer are significant causes of pollution in the natural environment, as are storms, floods, and fires. When the weather changes, the human body uses heat and mass transfer to maintain its temperature. Owing to these applications, investigation of heat and mass transfer in the steady-state flow of different industrial fluids through one/two-dimensional geometries has been carried out in the present research work. The current research work aims to analyze the physical problem and then develop a mathematical model that governs the fluid flow under different conditions using conservation laws for mass, momentum, energy, and concentration. For solving the modeled PDE's, a higher-order numerical technique i.e., the finite element method is applied. Further, the effect of the various embedded parameters on the flow, heat, and mass transfer traits are analyzed graphically. This thesis is comprised of seven chapters.

Chapter 1 is introductory. This chapter provides the background of the proposed study, its development, applications, and other physical aspects involved in studying heat and mass transfer problems. In addition, some basic definitions along with the motivation behind the work are discussed briefly. The work done by the various researchers in the field of heat and mass transfer by considering different geometries is also given in this chapter.

Chapter 2 is devoted to analyze the water-based bioconvection of a nanofluid containing motile gyrotactic micro-organisms (moves under the effects of gravity) over a non-linear inclined stretching sheet in the presence of a non-uniform magnetic field. This regime is encountered in the bio-nano-material electroconductive polymeric processing systems currently being considered for third-generation organic solar coatings, anti-fouling marine coatings, etc. Oberbeck-Boussinesq approximation along with ohmic dissipation (Joule heating) is considered in the problem. The governing equations of the flow are non-linear partial differential equations that are converted into ordinary differential equations via similarity transformations. These equations are then solved by the finite element method. The effect of various important parameters on non-dimensional velocity, temperature dis-

tribution, nanoparticle concentration, the density of motile micro-organisms is analyzed graphically in detail. It is observed from the obtained results that the flow velocity decreases with rising in the angle of inclination δ while temperature, nanoparticle concentration, and density of motile micro-organisms increase. The local skin friction coefficient, Nusselt number, Sherwood number, motile micro-organism's density number are calculated. It is noticed that increasing the Brownian motion and thermophoresis parameter leads to an increase in fluid temperature, which results in a reduction in Nusselt number. On the contrary, the Sherwood number rises with an increase in Brownian motion and thermophoresis parameter.

Chapter 3 deals with the bioconvective flow of nanofluids using non-Fourier's heat flux theory for heat transfer and non-Fick's mass flux theory for mass transfer. The benefits of including micro-organisms in the suspension incorporate micro-scale mixing and foreseen enhanced stability of nanofluid. For heat transfer and mass transfer processes, non-Fourier's heat flux and non-Fick's mass flux theories are employed. These theories are actively under investigation to resolve some drawbacks of the famous Fourier's Law and Fick's Law. The modified parameters in conventional laws are thermal and solutal relaxation times, respectively. The governing equations are remodeled using appropriate similarity transformations into a system of coupled ordinary differential equations. Finite Element Methodology is used to obtain the solution of non-linear coupled differential equations. The results of sundry factors are analyzed graphically on velocity, heat transfer, mass transfer, and density of micro-organisms. The computational results obtained in this letter reveal that fluid temperature and concentration of nanoparticles have an inverse relationship with thermal relaxation and solutal relaxation time.

In ***Chapter 4*** we have studied the heat and mass transfer effects in three-dimensional mixed convection flow of Eyring Powell fluid over an exponentially stretching surface with convective boundary conditions. We have employed the Cattaneo-Christov heat flux model for heat transfer that considers the interesting aspect of thermal relaxation time. First-order chemical reaction effects are also taken into account. Similarity transformations are invoked to reduce the leading boundary layer partial differential equations into the ordinary differential equations. The nonlinear, coupled ordinary differential with boundary conditions has been analyzed numerically by using the finite element method.

In chapter 5 and 6, we investigate the flow through porous cavities. The flow through cavities has its own importance because in cavities, no external source such as electric power is required for induction of convectional heat transfer. Due to the absence of power sources, convectional heat transfer in cavities is free from magnetic noise, fee, and sound. In most of the industrial and engineering applications such as air conditioning devices, food processing

industries, float glass production, disposal of nuclear waste, ceramic processing, geothermal systems cavities filled with porous media are used because dissipation area of porous is greater than conventional fins thereby enhancing heat convection. Also, The irregular motion of the fluid flow around the individual pores mixes the fluid more effectively. In ***Chapter 5***, we have examined the phenomenon of natural convection in a square porous cavity containing Casson fluid. The non-Newtonian model of Casson fluid is utilized to obtain the governing equations of a flow problem. The thermal control inside the cavity is managed by partially heating the bottom wall and symmetric cooling of the side walls while the top wall is adiabatic. The penalty finite element method is used to solve the non-linear coupled equations of the flow problem. The effect of different lengths of heated zone ε, Rayleigh number Ra and Darcy number Da has been examined on flow velocity and temperature distribution inside the cavity. The impact of effective viscosity of the fluid by varying Casson fluid parameter γ on the flow of fluid and heat transport has also been investigated. The results are demonstrated by plotting streamlines, isotherms, and average Nusselt number over wide ranges of governing parameters. The obtained results show that with an increase in Casson fluid parameter γ and Darcy number Da, heat transfer and flow circulation increase. It is also observed that the conduction dominant heat transfer takes place for low Darcy number over a wide range of the Rayleigh number ($10^2 \leq Ra \leq 10^6$).

In recent years, due to development of technology scientists are able to combine the nanofluids of different characteristic in a single host fluid which have further improved thermophysical properties. These fluids are named as hybrid nanofluid. ***Chapter 6*** is devoted to studying the heat transfer characteristics of hybrid nanofluid in a partially heated porous cavity. A partial section of the bottom wall of the cavity is being heated while the rest portion of the bottom wall and top wall are considered are adiabatic. Further, the side walls are kept at a lower temperature than the heated portion. The Penalty Finite element method is used to solve the dimensionless non-linear coupled partial differential equations of the flow problem. A comparison of results with the previous study has been made under particular cases, which shows good consistency. The results are demonstrated in terms of streamlines, isotherms, and average Nusselt number over wide ranges of governing parameters, namely Darcy number (Da), Rayleigh number (Ra), different lengths of the heated zone (ε), and volume fraction of nanoparticles (φ). The obtained results show that with an increase in the percentage of hybrid nanofluid φ and Darcy number Da, heat transfer and flow circulation increase. It is also observed that the rate of heat transfer in the porous medium increases with an increase in the volume fraction of nanoparticles.

In ***Chapter 7*** we have discussed the conclusions of all the chapters. Also, the work pre-

sented in this thesis provides the theoretical and numerical framework for investigating the steady incompressible flow of fluids through one and two-dimensional systems. Therefore, the possible future work is also described in the last chapter.

List of Publications

Published Papers

1. **M. Aneja** and S. Sharma, *Numerical study of bioconvection flow of nanofluids using non-Fouriers heat flux and non-Ficks mass flux theory*, International Journal of Modern Physics B, Vol. 33 (31), 2019, pp. 1950376, doi.org/10.1142/S0217979219503764 (**Impact Factor : 1.219**).

2. **M. Aneja**, S. Sharma, S. Kuharat and O. Anwar Beg, *Computation of electroconductive gyrotactic bioconvection under nonuniform magnetic field: Simulation of smart bio-nanopolymer coatings for solar energy*, International Journal of Modern Physics B, Vol. 34(5) pp. 2050028, 2020 , doi.org/10.1142/S0217979220500289 (**Impact Factor : 1.219**)

3. **M. Aneja**, A. Chandra and S. Sharma, *Natural convection in a partially heated porous cavity to Casson fluid*, International Communications in Heat and Mass Transfer, 114, pp. 104555, 2020, doi.org/10.1016/j.icheatmasstransfer.2020.104555 (**Impact Factor : 5.683.**)

4. M. Bilal, S. Sharma and **M. Aneja**, *Cattaneo-Christov Heat Flux Model of Eyring Powell fluid along with Convective Boundary Conditions.* Iranian Journal of Chemistry and Chemical Engineering, 40(3), pp. 971–979, 2021, doi.org/10.30492/IJCCE.2020.38021 (**Impact Factor : 0.759**)

Communicated Paper

1. **M. Aneja** and S. Sharma, *Investigation of natural convective flow of $Al_2O_3 - SiO_2$ / water hybrid nanofluid in a localized heated porous cavity* (Communicated)

Conference Papers

1. **M. Aneja** and S. Sharma, *Numerical Approach to a Mathematical Modeling of Bioconvection Due to Gyrotactic Micro-Organisms over a Nonlinear Inclined Stretching Sheet*, International Journal of Mathematical and Computational Sciences, Vol. 12(9) pp. 170-178, 2018, waset.org/Publication/10009476. (**Impact Factor : 0.456**)

2. **M. Aneja** and S. Sharma, *Heat and Mass Transfer Due to Double-Diffusion Convection in a Square Porous Enclosure Occupied by Casson Fluid*, In Advances in Fluid Mechanics and Solid Mechanics, pp. 91-99, 2020, Springer, Singapore.

International Conferences

1. **M. Aneja** and S. Sharma, *Numerical Approach to a Mathematical Modeling of Bio-convection Due to Gyrotactic Micro-Organisms over a Nonlinear Inclined Stretching Sheet* presented in 19th International Conference in Computing Science & Mathematics , November 27-29, 2017, Melbourne, Australia.

2. **M. Aneja** and S. Sharma *Free Convection in Porous Cavity with Non-newtonian (Casson) Fluid* presented in 7th International and 45th National Conference on Fluid Mechanics and Fluid Power (FMFP) December 10-12, 2018, IIT Bombay, Mumbai, India.

3. **M. Aneja** and S. Sharma, *Heat and Mass Transfer due to Double-Diffusion Convection in a Square Porous Enclosure Occupied by Casson Fluid* presented in 63rd Congress of Indian Society of Theoretical and Applied Mechanics (ISTAM) December 20-23, 2018, Dayananda Sagar University, Bengaluru.

4. **M. Aneja**, S. Sharma and A. Chandra, *Two Phase Flow analysis of Williamson fluid containing Dust particles with Marangoni convection* presented in 25th National and 3rd International ISHMT-ASTFE Heat and Mass Transfer Conference (IHMTC-2019), December 28-31, 2019, IIT Roorkee, Roorkee, India

Table of Contents

Page No.

Acknowledgements . . . . . **v**

Abstract . . . . . **vii**

List of Publications . . . . . **xi**

Table of Contents . . . . . **xiii**

List of Figures . . . . . **xvi**

List of Tables . . . . . **xviii**

List of Notations . . . . . **xix**

Chapter 1 Introduction **1**

1.1 Preface 1

1.2 Fluids 3

1.3 Brief classification of fluids 3

1.3.1 Ideal fluids 4

1.3.2 Real fluids 4

1.3.3 Newtonian fluids 4

1.3.4 non-Newtonian fluids 4

1.3.5 Nanofluids 8

1.4 Heat Transfer 10

1.4.1 Modes of Heat Transfer 10

1.5 Mass Transfer 14

1.5.1 Modes of mass transfer 14

1.6 Porous Medium 16

Chapter 2 Mathematical Analysis of Bioconvective flow of nanofluids over a non-linear stretching sheet **19**

2.1 Mathematical Model 21

2.2 Methodology 24

2.3 Validation With Published Studies 25

2.4 Results & Discussion 26
2.5 Conclusions 34

Chapter 3 Mathematical Analysis of Bioconvective flow of nanofluids using non-Fourier's heat flux and non-Fick's mass flux theory . 37
3.1 Mathematical Model 38
3.2 Methodology 41
3.3 Results & Discussion 42
3.4 Conclusions 49

Chapter 4 Theoretical Analysis of flow of Eyring-Powell fluid over a Exponential Stretching Sheet by utilizing non-Fourier Heat Flux Model 51
4.1 Introduction 51
4.2 Mathematical Model 52
4.3 Methodology 55
4.4 Validation of Results 56
4.5 Results & Discussion 56
4.6 Conclusions 62

Chapter 5 Mathematical Analysis of flow of Casson fluid in a Partially Heated Porous Cavity 63
5.1 Introduction 63
5.2 Mathematical Model 64
5.3 Methodology 67
5.3.1 Validation of the Results 67
5.4 Results & Discussion 68
5.4.1 Streamlines & Isotherms Profile 68
5.4.2 Average Nusselt number 75

Chapter 6 Numerical Analysis of flow of $Al_2O_3 - SiO_2$/water Hybrid in a Porous Cavity 83
6.1 Mathematical Model 84
6.2 Methodology & Validation of Results 87
6.3 Results & Discussion 88
6.3.1 Streamlines & Isotherms Profile 88
6.3.2 Average Nusselt number (Avg Nu) 100

Chapter 7 Summary and Future Scope 103

7.1 Summary 103
7.2 Future Scope 105

Bibliography **107**

Appendix **129**

List of Figures

Figure No.	Title	Page No.
1.1	Schematic representation of linear relationship between shear stress and shear rate	4
1.2	Curves showing different kinds of fluids	5
1.3	Modes of heat transfer (Ref: www.google/images.com)	14
2.1	Schematic model and coordinates system	22
2.2	Effect of varied thermophysical parameters on on velocity profiles	27
2.3	Effect of varied thermophysical parameters on temperature profiles	30
2.4	Effect of varied thermophysical parameters on nanoparticle concentration	31
2.5	Effect of varied thermophysical parameters on density of motile micro-organisms	32
3.1	Schematic model and coordinates system	38
3.2	Effect of varied thermophysical parameters on velocity profiles	43
3.3	Effect of varied thermophysical parameters on temperature profiles	44
3.4	Effect of varied thermophysical parameters on concentration profiles	46
3.5	Effect of varied thermophysical parameters on density profiles	47
3.6	Effect of varied thermophysical parameters on Skin Friction, Nusselt number, Sherwood number and Density number	48
4.1	Schematic model and coordinates system	53
4.2	Validation of Results with previous work	57
4.3	Effect of varied thermophysical parameters on on velocity profiles	58
4.4	Effect of varied thermophysical parameters on temperature profiles	59
4.5	Effect of varied thermophysical parameters on concentration profiles	60
4.6	Effect of varied thermophysical parameters on Nusselt number and Sherwood number	61
5.1	Physical Description and Cartesian Co-ordinates	65
5.2	Comparison of average Nusselt number with literature value for $Pr = 0.71$	68
5.3	Streamlines plots for varying Ra, Da at fixed value of $\gamma = 0.1, \varepsilon = 0.2, Pr = 7$	69
5.4	Streamlines plots for varying Ra, Da at fixed value of $\gamma = 1, \varepsilon = 0.2, Pr = 7$	71
5.5	Streamlines plots for varying Ra, Da at fixed value of $\gamma = 5, \varepsilon = 0.2, Pr = 7$	72
5.6	Streamline plots for varying ε at fixed value of $Pr = 7$	73

5.7 Isotherms plots for varying Ra, Da at fixed value of $\gamma = 0.1, \varepsilon = 0.2, Pr = 7$ 74
5.8 Isotherms plots for varying Ra, Da at fixed value of $\gamma = 1, \varepsilon = 0.2, Pr = 7$. 76
5.9 Isotherms plots for varying Ra, Da at fixed value of $\gamma = 5, \varepsilon = 0.2, Pr = 7$. 77
5.10 Isotherms plots for varying ε at fixed value of $Pr = 7$ 78
5.11 center co-ordinates plots for varying values of $Da, Ra, \gamma, \varepsilon$ 79
5.12 Average Nusselt number at hot and cold wall for varying Darcy number with Ra, γ, Pr (a) $\varepsilon = 0.5, Ra = 10^6, Pr = 7$ (b) $\varepsilon = 0.5, \gamma = 0.5, Pr = 7$ (c) $\varepsilon = 0.5, Ra = 10^6, \gamma = 0.5$ 81
5.13 Average Nusselt number at hot and cold wall for varying ε with Ra, γ, Pr (a) $Ra = 10^6, Da = 10^{-4}, Pr = 7$ (b) $Da = 10^{-4}, \gamma = 5, Pr = 7$ (c) $Da = 10^{-4}, Ra = 10^6, \gamma = 0.5$ (d) $Da = 100, Ra = 10^5, Pr = 7$ 82

6.1 Physical Description and Cartesian Co-ordinates 85
6.2 Validation of results via isotherm lines obtained in the present investigation (right side) and those in Basak et al.'s [15] work (left side) for $Pr = 0.71, Ra = 10^6, \varepsilon = 1$ in case of newtonian fluids 89
6.3 Streamlines plots for varying Ra, Da at fixed value of $\varphi = 1\%, \varepsilon = 0.8, Pr = 6.2$ 91
6.4 Streamlines plots for varying Ra, Da at fixed value of $\varphi = 2\%, \varepsilon = 0.8, Pr = 6.2$ 92
6.5 Streamlines plots for varying Ra, Da at fixed value of $\varphi = 3\%, \varepsilon = 0.8, Pr = 6.2$ 93
6.6 Streamline plots for varying ε, Ra, Da at fixed value of $Pr = 6.2$ 94
6.7 Isotherm plots for varying Ra, Da at fixed value of $\varphi = 1\%, \varepsilon = 0.8, Pr = 6.2$ 95
6.8 Isotherm plots for varying Ra, Da at fixed value of $\varphi = 2\%, \varepsilon = 0.8, Pr = 6.2$ 96
6.9 Isotherm plots for varying Ra, Da at fixed value of $\varphi = 3\%, \varepsilon = 0.8, Pr = 6.2$ 97
6.10 Isotherm plots for varying ε, Ra, Da at fixed value of $Pr = 6.2$ 98
6.11 vertical velocity component profile along horizontal midplane 98
6.12 Average Nusselt number (Avg Nu) at hot and cold wall by varying Ra with Da, φ, ε (a) $\varepsilon = 0.5, \varphi = 1\%, Pr = 6.2$ (b) $Da = 10^{-3}, \varphi = 3\%, Pr = 6.2$ (c) $\varepsilon = 0.5, Da = 10^{-3}, Pr = 6.2$ 99

List of Tables

Table No.	Title	Page No.
2.1	Comparison of results for reduced Nusselt number $-\sqrt{((n+1)/2)}\theta'(0)$, for $Le = 10, n = 1, M = Ec = Nr = Rb = Pe = Lb = \Omega = 0, \delta = 0^o$ and different values for Nt and Nb	25
2.2	Comparison of results for the density of motile micro-organisms $-\sqrt{((n+1)/2)}\chi'(0)$ for $n = 1, M = Nb = 1, Ec = 0, Nr = Nt = Gr = 0.5, Lb = Le = 2, Rb = 0.3, \delta = 0^o$, $b = 1$, and different values for Ω and Pe	26
2.3	Results for skin friction coefficient for $Gr = n = Pe = M = Lb = 1, Ec = Rb = \Omega = Nb = 0.1, Pr = 10, \delta = 0^o$ and different values for Nt and Nr	26
2.4	Results for Sherwood number for $Le = Pe = 10$, $n = 1$, $\delta = 0^o, M = Ec = Nr = Rb = Pe = Lb = \Omega = 0$ and different values for Nt and Nb	26
6.1	Thermophysical properties of fluid and nanoparticles at room temperature [7, 140]	86

List of Notations

A	temperature exponent [−]
a_f	thermal diffusivity of fluid [$a_f = \frac{k_f}{\rho C_{pf}}$]
b	chemotaxis constant [−]
B	concentration exponent [−]
c	Eyring Powell fluid characterstics [−]
C	Concentration of nanoparticles [kgm^{-3}]
$C_{f'}$	ambient fluid concentration [kgm^{-3}]
Cf_x	skin friction coefficient [−]
c_p	specific heat of fluid [$m^2K^{-1}s^{-2}$]
g	gravitational acceleration constant [ms^{-2}]
Da	Darcy number [−]
D_B	Brownian diffusion coefficient [m^2s^{-1}]
D_m	motile micro-organisms diffusivity [m^2s^{-1}]
D_T	thermophoresis diffusion coefficient [m^2s^{-1}]
Ec	Eckert number [−]
$f^{'}(\eta)$	non-dimensional velocity function [−]
$\frac{Gr}{Re^2}$	Richardson number (in terms of Grashof and Reynolds numbers) [−]
h	heat transfer coefficient $Wm^{-2}K^{-1}$
h^*	concentration transfer coefficient [ms^{-1}]
Ha	Hartmann number [−]
k	chemical reaction parameter [−]
K	thermal conductivity of fluid [$Wm^{-1}K^{-1}$]
L	reference length (m)
Lb	bioconvection Lewis number [−]
Le	Lewis number [−]
N	density of motile micro-organisms [kgm^{-3}]
n	non-linear sheet stretching parameter [-]
Nb	Brownian motion parameter [−]
Nn_x	local density number of the motile micro-organisms [−]
Nu_x	local Nusselt number [−]
$\overline{Nu}$	average Nusselt number [−]
Nr	Buoyancy ratio parameter [−]
Nt	thermophoresis parameter [−]
P	Pressure [Pa]

Pe	bioconvection Peclet number [−]
Pr	Prandtl number [−]
p_y	yield stress [−]
q_m	wall mass flux $[kgs^{-1}m^{-2}]$
q_n	wall motile micro-organisms flux $[kgs^{-1}m^{-2}]$
q_w	wall heat flux $[Wm^{-2}]$
Ra	Rayleigh number [−]
Rb	bioconvection Rayleigh number [−]
Re_x	local Reynolds number [−]
Sc	Schmidt number [−]
Sh_x	local Sherwood number [−]
T	temperature $[K]$
$T_{f'}$	ambient fluid temperature $[K]$
u, v, w	velocity components in x, y and z direction $[ms^{-1}]$
U_0, V_0, W_0	constants [−]
W_c	maximum cell swimming speed $[ms^{-1}]$

Greek Symbols

α	Thermal diffusivity $\alpha = \frac{k}{\rho C_p}$ $[m^2s^{-1}]$
$\alpha^{'}$	ratio of stretching velocities
β	Thermal expansion coefficient
β_b	Concentration expansion coefficient
β_c	non-dimensional Concentration relaxation time [−]
β_e	non-dimensional Thermal relaxation time [−]
β_v	volume expansion coefficient (K^{-1})
γ	Casson fluid parameter [−]
γ_e	micro-organism's average volume $[m^3]$
γ_1	heat transfer biot number [−]
γ_2	mass transfer biot number [−]
Γ	Penalty parameter [−]
δ	angle of inclination $[^o]$
ϵ	Erying Powell fluid parameter [−]
ε	length of heated zone [−]
$\theta(\eta)$	dimensionless temperature [−]
κ	permeability of the porous medium $[m^2]$
λ_e	Thermal buoyancy parameter [−]
λ_c	Solutal buoyancy parameter [−]

μ_B	dynamic viscosity of viscoplastic fluid
ξ	Erying Powell fluid parameter [−]
π	product of the component of the deformation rate
ρ	fluid's density $[kgm^{-3}]$
ρ_m	micro-organism's density $[kgm^{-3}]$
ρ_p	nanoparticle's density $[kgm^{-3}]$
σ	Electrical conductivity $[\Omega^{-1}m^{-1}]$
ς	Eyring Powell fluid characterstic
τ	Ratio of effective heat capacitance [-]
τ_w	wall shear stress [-]
$\phi(\eta)$	dimensionless concentration of nanoparticles [−]
φ	volume fraction of nanoparticles [−]
$\chi(\eta)$	dimensionless density of micro-organisms [−]
ψ	stream function [−]
ω	Ratio of stretching velocities [−]

subscripts

h	hot wall
c	cold wall
w	wall condition
∞	free stream condition

Chapter 1

Introduction

1.1 Preface

The main branch of applied physics is fluid mechanics, and the foundation for the understanding of many other aspects of applied sciences and engineering concerns itself with the investigation of the motion and equilibrium of fluids. This branch of science studies the static, dynamic, and kinematic characteristics of fluids. Fluid static refers to the study of fluid at rest, while fluid kinematics is studying the fluids in motion without considering pressure forces. On the other hand, fluid dynamics is the branch of science that evaluates the effect of pressure forces on fluid motion. Almost all the activities on this earth are governed by the principles of fluid dynamics as most part of the planet is water or air. The problems based on fluid dynamics are solved by using laws of conservation which say that the total amount of mass, energy, and momentum remains constant within a closed system and follows the continuum hypothesis principle. According to the continuum hypothesis principle, the properties of fluid such as density, viscosity, temperature, and velocity are assumed to be a continuous function of position and time. Mathematicians such as Bernoulli, Euler, D'Alembert, Joseph-Louis Lagrange, and Laplace were inspired to work on the part of fluids in to find solutions to many frictionless flow problems. Daniel Bernoulli (1700-1782) was the first to conduct a mathematical investigation into a fluid flow. However, the breakthrough made by Swiss mathematician Euler (1707-1783) in the "Ideal fluid theory or Non-viscous theory" was remarkable resulting in the development of non-linear field theory. During the first half of the nineteenth century, around 1822, Jean Augustin Louis Cauchy (1789-1857) introduced the concept of stress because there was a high demand for the viscous effects in the flow in the industrial and engineering sectors. After a year, a French engineer and physicist, Navier (1785-1836) presented, an equation of motion of a real (viscous) fluid contributed by Poisson, Saint-Venant, and Stokes. However, due to Stokes's outstanding contribution, the equation was eventually named the famous Navier-Stokes equations of motion.

Before 1900, the theories of ideal fluids and viscous flow were considered, separately. The ideal fluid theory was linked to some excellent papers by Euler (1707-1783) on fundamen-

tal equations, Helmholtz (1821-1894) on vortex motion, and Kelvin (1824-1907) on the circulation theorem. Many researchers also looked into some important aspects of water and sound waves. Thus, viscid flow theory was undeniably valuable. Along with the ideal fluid approach, G.G. Stokes (1819-1903) proposed viscid flow theory, which added a new dimension to flow theories. Stokes not only made our lives easier by formulating equations relating to motion, but he also discovered elementary solutions relating to viscous flow. Osborne Reynolds (1842-1912) invented the Reynolds number, which is a dimensionless number. In an influential paper published in 1851, Stokes discussed the low Reynolds number flow. H.S. Hele-Shaw (1854-1941) explored irrational streamline patterns. Despite these efforts, a significant issue of accounting for the motion of a fluid with a low viscosity past a solid body went unnoticed. Ludwing Prandtl (1875-1953) presented a paper on fluid movement with very low viscosity at the 3rd International Congress of Mathematicians in Heidelberg in 1904, which was a seminal contribution to fluid dynamics. He also recommended the theory of boundary layer, which helped the fludicist in simplifying the Navier-Stokes equations and finding its solutions.

In his classic, 'Theory of Heat', Scottish physicist James Clerk Maxwell stated a modern definition of heat. Following his theory, physicists identified heat as a type of thermal energy that flows spontaneously from higher temperature systems to lower temperature systems until thermal equilibrium is reached. When two systems of different temperatures come into thermal contact, they exchange thermal energy, i.e., thermal energy is transferred from the hotter body to the colder body until thermal equilibrium is reached. Heat transfer motion plays a vital role in industrial and environmental problems. Industrial problems include the production and conversion of energy and the generation of electrical power, the maximization of heat transfer rates for maintaining the integrity of materials in high temperature environments, the operation and design of population systems, and cryogenics. Heat transfer principles can be used to investigate the thermal effects of buildings and other structures. Many researchers like Rohsenow et al. [197], kreith et al. [121] recognized heat transfer motion as an important topic for their research work.

A system containing two or more components varies in concentration from point to point in a variety of situations, particularly in industries and chemical engineering processes. There is a natural tendency for mass transfer in this system, which reduces concentration differences within the system. The transportation of one constituent from a higher concentration region to a lower concentration region is referred to as mass transfer. Heat and mass transfer are both kinetic processes that can be studied independently or in tandem. In the case of diffusion and convection, similar mathematical equations shape both processes. As a result, considering them together is more effective. After Bird et al. [31] book's 'Trans-

port Phenomena', the concepts of heat transfer, mass transfer, and momentum transfer are regarded as a new discipline. Fick, a German physiologist, proposed the fundamental kinetic law for mass diffusion. Fick's law [71] for mass distribution was derived on a similar basis as Fourier's law [74] for heat conduction. Mass transfer, like heat transfer, has a wide range of applications, such as transpiration cooling of jet engines, rocket motors, and in ablative of space vehicles during re-entry to the atmosphere, as well as in many everyday areas such as the working system.

Fluid mechanics has many applications in the real world such as irrigation engineering, civil engineering, oceanography, mechanical engineering, chemical engineering, aeronautics, etc. The design of various types of machines such as fans, pumps, compressors and turbines are few examples in which basic principles of fluid mechanics are required. Further, heating and cooling systems for homes and industries and pipeline systems design are technical examples where fluid mechanics play a vital role. Due to its lot many applications, it becomes necessary to combine knowledge of thermodynamic, mass transfer, heat transfer, electromagnetic theory and fluid mechanics to fully understand the physical phenomena involved in the flow of fluids.

Hence, the primary goal of this research is to create a mathematical model for predicting heat and mass transfer, fluid flow, and related processes. In short, the mathematical solution outperforms all other methods of prediction.

1.2 Fluids

The materials deform when forces are applied to them, and if it deforms continually without limit, even under the action of small shearing forces, that material is known as fluid. Fluids are categorized as liquid and gases. A liquid is a type of fluid that has fixed volume but no fixed shape. It takes the shape of the vessel in which it is poured. On the other hand, gas is a type of fluid that has neither fixed shape nor volume.

1.3 Brief classification of fluids

On the basis of properties of fluids such as pressure, density, viscosity, and temperature, fluids are categorized as:

1.3.1 Ideal fluids

Ideal fluid is a fluid that is incompressible and has no viscosity. When a fluid is in motion, the shear force is zero, implying no resistance to the movement of fluid particles. This fluid is also referred to as perfect fluid. This type of fluid does not exist, but it is sometimes used to compare to existing fluids.

1.3.2 Real fluids

The fluid that is compressible and viscous is referred to as real fluid. Shear stress is always present in real fluids, which means that the fluid always provides some resistance when it is in motion. Water, oil, gases, and air are the most basic types of real fluids.

1.3.3 Newtonian fluids

Newtonian fluids are those fluids that have a linear relationship between shear stress and shearing rate. These fluids obey Newton's law of viscosity, which states that shear stress between fluid layers passing through each other is proportional to the gradient of velocity. This linear stress-strain relationship is not a hypothetical constitutive equation because it describes the flow properties of a vast class of real fluids, such as water, air, and mercury.

$$\tau = \mu \frac{\partial u}{\partial y} \tag{1.3.1}$$

Here μ is the coefficient of viscosity and it measures the resistance of fluids in motion.

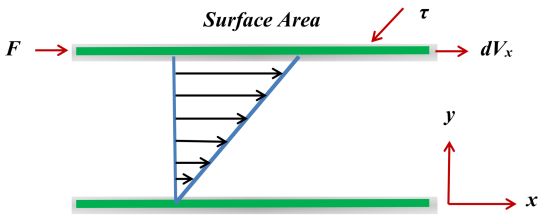

Figure 1.1: Schematic representation of linear relationship between shear stress and shear rate

1.3.4 non-Newtonian fluids

The fluids which do not obey Newton's law of viscosity, i.e., shear stress is not directly proportional to the velocity gradient are known as non-Newtonian fluids. These fluids have

a non-linear relationship between shear stress and shearing rate.

$$\tau = k^* \left(\frac{\partial u}{\partial y} \right)^n \tag{1.3.2}$$

where n, k^* denotes the flow behavior index and coefficient of consistency, respectively. Also, equation 1.3.2 can be written in the form:

$$\tau = k^* \left(\frac{\partial u}{\partial y} \right)^{n-1} \frac{\partial u}{\partial y} = \mu^{'} \frac{\partial u}{\partial y} \tag{1.3.3}$$

where $\mu^{'} = \left(\frac{\partial u}{\partial y} \right)^{n-1}$ is called apparent viscosity.

Fluids for which the value of n is less than 1, i.e., their apparent viscosity decreases with an increase in shear stress are designated as shear- thinning fluids or pseudoplastic fluids. Examples of shear-thinning fluids are polymers, colloidal suspensions. In contrast, fluids for which the value of n is greater than 1, i.e., their apparent viscosity increases with an increase in shear stress are designated as shear thickening fluids or dilatant fluids - for example, corn starch suspension, sand, etc.

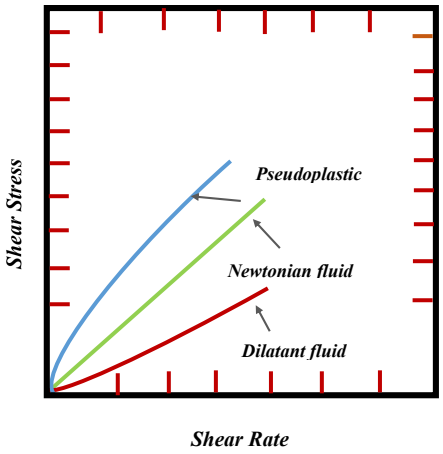

Figure 1.2: Curves showing different kinds of fluids

1.3.4.1 non-Newtonian fluid Models

Nowadays, non-Newtonian fluids have more industrial and engineering applications than Newtonian fluids. These fluids found applications in the food processing industries, metallurgical processes, extraction of petroleum products from crude oil, drilling operations, and bio-engineering processes [77]. The fluids such as clay, sand, ketchup, blood, honey, paints, slurries, melted chocolates, egg whites, mayonnaise, etc., exhibit traits of non-Newtonian

fluids. To understand the flow of these fluids, various rheological models are developed such as power-law model [41, 42], Jeffrey fluid model [203], Maxwell fluid model [8], micropolar fluid [133], and Eyring-Powell model [108, 180] and Casson fluid model [36]. Out of these models, Casson fluid model and Eyring-Powell fluid model are widely used for industrial and non-industrial problems.

Casson Fluid Model

Casson fluid model was firstly given by Casson [36] in 1959 to describe the flow behavior of pigments of printing ink. It is a kind of shear-thinning fluid i.e., the viscosity of these fluids decreases with an increase in shear stress. Casson fluid is a particular type of non-Newtonian fluid that flows only when the applied stress is more than the critical value known as yield stress and behaves as solid below the critical value of yield stress. The properties of Casson fluid are similar to the Bingham model, which is used to characterize the flow behavior of slurries, suspensions, and other complex rheological fluids. The foodstuffs such as honey, fruit juices, ketchup, soup, yogurt, and chocolate exhibit the characteristics of Casson fluid. Due to the unique properties of Casson fluid, it has various applications in industries such as food industries, biomechanics, polymer processing industries, and others. Moreover, these days the Casson model is also used for developing the rheological model for human blood [32, 39, 202, 234].

The rheological condition of state for the stress tensor [159] of Casson fluid is given by

$$\tau_{ij} = \begin{cases} 2(\mu_B + p_y/\sqrt{2\pi})e_{ij}, & \pi > \pi_c \\ 2(\mu_B + p_y/\sqrt{2\pi_c})e_{ij}, & \pi < \pi_c \end{cases} \tag{1.3.4}$$

Here $\pi = e_{ij}e_{ij}$ and e_{ij} are the (i, j)th component of the deformation rate, π denotes the product of the component of deformation rate itself, π_c designates the critical value based on the type of non-Newtonian model, μ_B represents the dynamic viscosity of viscoplastic fluids, and p_y is the yield stress.

In 1969, this model was used by Reher et al. [194] to describe the flow characteristics of cylindrical particles in viscous suspension. Casson fluid model describes the flow behavior of fluids which has a non-linear stress-strain relationship and possesses traits of pseudoplastic fluids. For example, Casson model was used to develop the rheological model for human blood [54, 238], chocolate [48] and other complex fluids [53, 75]. Dash et al. investigated the flow of Casson fluid in a pipe filled with porous medium. This model is useful to analyze the pathological condition where blood flow in arteries when fatty plaques of cholesterol and blood clots are formed. The investigation of peristaltic conveyance of non-Newtonian Casson fluid was done by Mernone et al. [145] while Misra et al. [146] presented

the mathematical model of blood as a two-layer fluid in which the core region was demonstrated by Casson fluid and the peripheral region was taken as a Newtonian viscous fluid. Boyd et al. [32] examined the Casson fluid flow as a non-Newtonian blood viscosity model in different flow geometries in the case of steady and oscillatory blood flows. Hayat et al. [91] explored the stagnation point flow of Casson fluid through a non-linear stretching surface using convective boundary conditions. Abolbashari et al. [1], Mukhopadhyay et al. [151], Bhattacharyya et al. [28] considered different models for Casson fluid flow, such as, the flow of Casson nano-fluid flow over a stretching surface, diffusion of chemically reactive species over an unsteady permeable stretching surface, Casson fluid over stretching/shrinking sheet, etc. The mixed convection over a stretching surface by considering the oblique flow of Casson fluid was explored by Rana et al. [185]. Kataria and Patel [115] examined the hydrodynamic boundary layer flow of Casson fluid over an oscillating vertical plate saturated with porous medium and obtained an analytic solution of unsteady natural convection using Laplace transformations. Further, Rahman and Pop [183] analyzed the influence of second-order slip and viscous dissipation on the steady hydrodynamic boundary layer flow of a Casson fluid past a porous shrinking sheet. Recently, Pop et al. [177] studied the buoyancy-driven convection in a square enclosure filled with Casson fluid by taking into account the effect of thermal radiation and viscous dissipation. Hamid et al. [87] investigated the free convective heat transfer characteristics of Casson fluid in a trapezoidal porous cavity.

Eyring-Powell fluid Model

The Eyring-Powell model is another fluid model used to describe the flow behavior of non-Newtonian fluids. This model is a complex rheological model in the sense that it was derived from the kinetic theory of gases instead of empirical correlations [180]. Moreover, this model mathematically describes the flow behavior of Newtonian fluids at low and high shear rates but deviates at intermediate shear stresses.

The Cauchy stress tensor T for an Eyring Powell fluid can be written as [9]:

$$T = -pI + \tau_{ij} \tag{1.3.5}$$

$$\rho a_i = -\nabla p + \nabla.\tau_{ij} \tag{1.3.6}$$

where extra stress tensor τ_{ij} is

$$\tau_{ij} = \mu \frac{\partial u_i}{\partial x_j} + \frac{1}{\xi} sinh^{-1}\left(\frac{1}{c}\frac{\partial u_i}{\partial x_j}\right) \tag{1.3.7}$$

in which ξ and c are the Eyring Powell fluid characterstics, p is the pressure and I is the identity tensor. Taking

$$sinh^{-1}\left(\frac{1}{c}\frac{\partial u_i}{\partial x_j}\right) \approx \frac{1}{c}\frac{\partial u_i}{\partial x_j} - \frac{1}{6}\left(\frac{1}{c}\frac{\partial u_i}{\partial x_j}\right)^3, \qquad \left|\frac{1}{c}\frac{\partial u_i}{\partial x_j}\right| < 1. \tag{1.3.8}$$

The Erying-Powell fluid flow through a wedge was investigated by Sirohi et al. [220]. Also, Sirohi et al. [221] studied the flow of Eyring-Powell fluid near a flat plate, which had some acceleration. Eldabe et al. [67] investigated the impact of couple stresses on the flow of Eyring-Powell fluid through porous parallel plates in the presence of the external magnetic field. The results obtained in their study may be helpful in the discussion of diseases related to blood. Patel and Timoli [171] numerically investigated the three-dimensional flow of Powell-Eyring fluid using a technique, namely, MSABC (Method of Satisfaction of Asymptotic Boundary Condition). Hayat et al. [90] examined the steady-state flow and heat transfer characteristics of Eyring -Powell fluid over a continuous moving surface. They had taken the convective boundary conditions and obtained the solution via the homotopy analysis method. Hayat et al. [92] also investigated the three-dimensional magnetohydrodynamic flow of the same fluid under the effects of thermal radiation. Many other researchers examined the flow traits of Eyring-Powell fluid by considering a different type of geometries and boundary conditions [2, 78, 94, 95, 161, 176].

1.3.5 Nanofluids

Pure fluid, oil, ethylene glycol are used as conventionally heat transfer fluid. These fluids have a low thermal conductivity which affects the heat transfer rate. To improve the thermal characteristics of these fluids, the researchers introduced the idea of adding tiny particles of size microns or millimeters in the past few decades [143]. In practical applications, these large-sized particles cause problems such as abrasion and obstruction in the flow of fluid. After that, in the late twentieth century, Choi and Eastman [51] gave us the idea of using nanosized particles instead of large-sized particles in the host fluid to enhance the heat transfer rate. The base fluids which contain nanosized particles of high thermal conductivity are named nanofluids. Mostly, the nanoparticles considered with the base fluids are metals (Cu, Ag, Au), metals in their oxide form (Al_2O_3, CuO), semiconductors (TiO_2, SiO_2), non-metals (graphite, carbon nanotubes), carbides (SiC) and nitrides (SiN). It is found that the addition of even a small amount of nanoparticles in the base fluid can enhance its thermophysical properties (viscosity, thermal conductivity, heat transfer rate). Firstly, Xuan and Li [242] gave us the procedure for the preparation of nanofluids. They prepared the nanofluid by suspending powdered nanoparticles in the

base fluid. Das et al. [60] experimentally analyzed the impact of temperature on the enhancement of thermal conductivity of nanofluids. After that, Buongiorno [33] lists out all the convective properties in the comprehensive survey for nanofluids and examined seven slip mechanisms to model the relative velocity between the nanoparticles and base fluid. In conclusion, two of these mechanisms, namely, Brownian diffusion and thermophoresis were found to be relevant for convective heat transfer. Kuznetsov and Nield [126] used both of these mechanisms to investigate the effect of nanoparticles on natural convection boundary layer flow past a vertical plate. The specific boundary conditions were incorporated in which constant temperature along with constant nanoparticle fraction were considered along the wall. The problem of natural convection past a vertical flat plate firstly proposed by Cheng and Minkowycz [46] was revisited by Nield and Kuznetsov [163] embedded in a porous medium utilizing nanofluid. It is noteworthy to mention here that the nanofluid considered in this study incorporates the effects of Brownian motion and thermophoresis for the porous medium. Sheikholeslami et al. [209] studied the problem of MHD free convection in an eccentric semi-annulus filled with nanofluid. The influence of the uniform magnetic field, radiative flux, and slip boundary conditions on the characteristics of heat transfer and flow of a nanofluid was investigated by Ibrahim and Shankar [105]. While Ferdows et al. [69] studied the boundary layer flow of a nanofluid flow over a non-linear stretching flat plate in the presence of radiative heat flux and non-uniform magnetic field. Khan et al. [117] conducted the study of the unsteady hydrodynamic flow of a nanofluid past a horizontal stretching sheet and interpreted the behavior of thermal radiation and magnetic field on the rate of heat and mass transfer. Many other scientists researched hydrodynamic flow and heat transfer attributes of nanofluids under different situations [13, 169, 170, 196, 210].

Nowadays, researchers are continuously working on improving the thermophysical properties of nanofluids. They introduced a new class of nanofluids known as hybrid nanofluids which are a combination of two different types of nanoparticles with varied thermophysical properties dispersed in a host fluid either in mixture or composite form. Hybrid nanofluids have advantages over nanofluids in terms of high thermal conductivity, high heat transfer rate, less concentration, low cost, high stability, and flexibility. Due to synergistic effects, hybrid nanofluids have more heat transfer rate compared to regular nanofluids. This innovative class of nanofluids has applications in almost every field, such as bio-nanofluids for the treatment of cancer, power generation, coolant for various machinery (computers or CPUs, microelectronics), aeronautics, refrigeration, cooling of nuclear reactors, chemical processes, and many more. Thus, in the last few decades, scientist have shown keen interest to work on hybrid nanofluids which include modeling, composition, experimental verification, and applications [112, 168, 219, 225, 231] In the context of heat transfer enhancement,

Hayat and Nadeem [96] investigated the three-dimensional rotating hybrid nanofluid flow over a stretching sheet under the effects of thermal radiation, chemical reaction, and heat generation effects. Mansour et al. [142] scrutinized the impact of heat source and sink on entropy generation and MHD flow of a hybrid nanofluid in a partially heated square porous cavity. The effect of variable magnetic field on a hybrid nanofluid flow in a circular cavity was studied by Sheikholeslami [216].

1.4 Heat Transfer

The heat transport phenomenon is an essential research topic due to its wide variety of applications in science, engineering, and industries. As illustrations, electronic devices dissipate heat that aspires to cool, textile industries, cooling and heating systems in the buildings, vehicles, phase change materials, etc. Heat transfer is a branch of science which deals with the distribution of temperature inside the body as a function of space or time. It also predicts thermal energy transfer rate due to temperature gradients at the surface or temperature difference between the bodies. Hence, heat transfer occurs whenever there is a temperature difference between two different mediums (solid, liquid, or gas) or in the same medium. Heat is always transferred from the hotter body to the colder body until thermal equilibrium is reached.

1.4.1 Modes of Heat Transfer

There are three different modes of heat transfer, namely:

1. Conduction
2. Convection
3. Radiation

1.4.1.1 Conduction

Conduction is the mode of heat transfer when there is a temperature difference within a material. For illustration, a copper rod is taken whose one end is at a higher temperature (T_1) and the other end is at low temperature (T_2). If the condition of the rod does not change with time and there is no other source of energy within the rod. Then the energy is transferred from one end to another and is known as heat transfer by conduction. The

mechanism behind the conductive heat transfer is that if one end of the rod is heated, energy is transferred from atom to atom due to collisions and movement of free electrons. Similarly, conduction in gas takes place due to collisions between the molecules which are in random motion. Fourier gave us the mathematical expression for experimentally calculating the heat transfer by conduction,

$$q = KA\frac{(T_1 - T_2)}{L} \tag{1.4.1}$$

Where K, A, L denotes the thermal conductivity, area of cross-section, characteristic length of the material, respectively. The mathematical expression for heat flux $q^{'}$, i.e., heat transfer rate per unit cross-sectional area is given by

$$\frac{q}{A} = q^{'} = K\frac{(T_1 - T_2)}{L} \tag{1.4.2}$$

The more general form of Fourier's law of heat conduction (equation 1.4.2) was given by Baron Jean Baptise Joseph Fourier [74] in 1822. The generalized mathematical expression calculates the heat transfer in more than one direction or temperature changes with time, or if the thermal conductivity of the material is variable and is written in the form:

$$q^{'} = K\frac{\partial T^{'}}{\partial n^{'}} \tag{1.4.3}$$

1.4.1.2 Convection

The mode of heat transfer is convection when energy is transferred from a solid material to an adjacent fluid (liquid or gas) that is in motion. Convective heat transfer involves the combined effect of diffusion (molecules random motion) and energy transferred due to bulk motion of the fluid. The word convection is derived from the Latin word "taking with" and occurs due to the difference in density arises from different temperature regions. This results in the mixing of hotter and colder liquid masses with each other. Hence, thermal energy is transferred with the macroscopic motion of fluid particles from one place to another within the system. Further, the rate of heat transfer by convection is determined by Newton's law of cooling and is given by

$$q^{'} = h(T_w - T_\infty) \tag{1.4.4}$$

Where $q^{'}$ is the rate of heat transfer per unit cross-sectional area, h is the coefficient of heat

transfer which is a function of surface geometry, fluid properties and velocity of fluid.

Convective heat transfer is of following types:

- Natural Convection: Natural convection is a type of heat transport in which fluid moves only due to density differences created by temperature gradients and the relative density of the fluid particles. In the presence of gravity, less dense particles of fluid move upwards while the particles of higher density take their position leading to the motion of fluid which creates natural convection. Melting of ice, the process of evaporation from water bodies are typical examples of natural convection.

- Forced Convection: Forced convection is a type of heat transport in which fluid motion is derived by some external agents such as blower, pump, fan, etc. Heat exchangers such as nuclear reactors, air conditioners are the devices where forced convection is the mechanism for the transfer of heat.

- Mixed Convection: Mixed convective heat transfer takes place when the mechanism of natural convection and forced convection both occur simultaneously. This type of heat transfer occurs in a situation when pressure forces and buoyancy forces interact with each other. Contribution from each form of heat transfer is determined by the flow, geometry, temperature, and orientation. Mixed convective heat transfer flow is observed in channel flows.

- Bioconvection: During the last few decades, a new type of convective motion has been developed termed as bioconvection. It refers to the phenomenon of macroscopic convective motion of fluid caused by a density gradient and is created by collective swimming of bottom-heavy motile micro-organisms, e.g., bacteria, single-celled algae. This happens because the density of the micro-organisms is higher than the fluid in which they are suspended. On average, these self-propelled swims in an upward direction. The upper surface of the suspension becomes unstable due to an increase in its density which creates hydrodynamic instability under certain conditions results in bioconvective flows. The bioconvection pattern was firstly observed by Platt [175] which is similar to Rayleigh-Benard convection. A deterministic mathematical model for hydrodynamics of bioconvection patterns due to motile micro-organisms was given by Pedley et al. [173], and Hill et al. [101], although without any consideration of engineering applications. The classification of micro-organisms as oxytactic, chemotactic, negative gravitactic, gyrotactic, magneto-tactic, or photo-tactic depending on the stimulus which induces motion was given by Pedley and Kessler [174]. Ghorai and Hill [82] investigated the development and stability of two-dimensional bioconvective plumes of gyrotactic micro-organisms using the continuum model of Pedley

et al. [173] in a tall narrow chamber. Kuznetsov and Avramenko [123] gave the pharmaceutical applications of bioconvection with the small-sized particles. They showed that if bioconvection develops, it enhances micro-scale mixing and helps slow down the settling of small-sized particles, which is important for pharmaceutical applications. Kuznetsov [124] did the linear stability analysis of the interaction between free convection and bioconvection by suspending gyrotactic micro-organisms in a heated horizontal fluid layer and gave the geophysical applications of bioconvection. Many other excellent studies have been conducted in recent years examining various combinations of nanoparticles and micro-organisms. This phenomenon of heat transfer has applications in the field of biotechnology and biological systems such as enzymes biosensors [129], chip-size micro-devices for evaluating nanoparticle toxicity [153]. The first attempt at developing a viscous fluid dynamic model for combined nanofluid bioconvection was presented by Kuznetsov [125] who analyzed with a perturbation method the stability of bioconvection in a horizontal layer filled with a base fluid containing both gyrotactic micro-organisms and also nanoparticles. Subsequently, many other studies have been communicated [20,61,118,120,128,131,156,207,236,240,247].

1.4.1.3 Radiation

Radiation is the form of heat transfer in which thermal energy is transmitted between two bodies in the form of electromagnetic waves. All materials (solid, liquid, or gas) at normal or higher temperatures emit or absorb thermal energy in the form of radiations. This means all the modes of heat transfer are accompanied by an exchange of energy by radiation. In almost all cases, heat transfer through radiation is less than the total amount of heat transfer through other processes, hence it can be neglected. However, in some cases, heat transfer through radiation is also significant; for example, solar radiations make the earth's surface hot, which is generated from extremely hot gases inside the sun. Radiation is the only mode of heat transfer where there is no material medium required to transfer heat. The transmission rate of radiative thermal energy per unit time per unit surface area depends on the type of material, temperature, and condition of the surface. For perfectly black bodies, the rate of transmission of radiative thermal energy is given by Stefan-Boltzmann law, and the relation is,

$$Q^{'} = \sigma^{'} T^4 \tag{1.4.5}$$

where $\sigma^{'}$ denotes the Stefan-Boltzmann constant and T is absolute temperature measured in Kelvin.

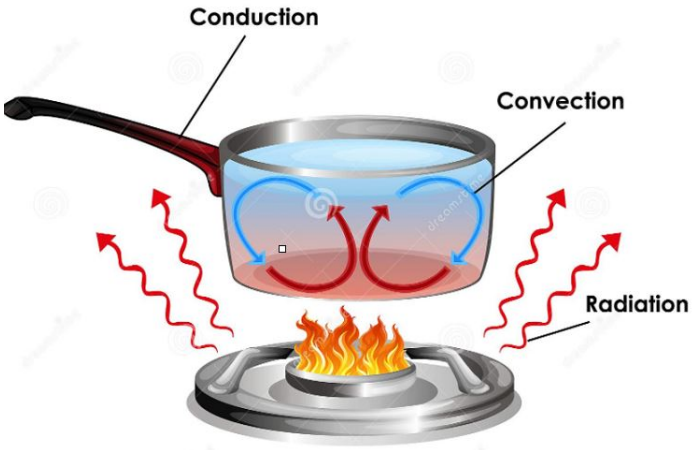

Figure 1.3: Modes of heat transfer (Ref: www.google/images.com)

1.5 Mass Transfer

The transfer of mass within a system takes place when it contains more than one component whose species varies in concentration at different parts. The constituents of matter move from a region of higher concentration to a lower concentration region until an equilibrium state is reached. Hence, we can say that the concentration gradient created by species in a mixture results in the transport of that species. For illustration, if we add sugar in the cup of tea eventually, it diffuses uniformly throughout in a cup of tea, the air becomes humid over the surface of ponds or lakes due to evaporation of water from its surface, the fragrance of the perfume is imparted throughout near its surroundings due to diffusion of its particles in the atmosphere.

1.5.1 Modes of mass transfer

There are two different modes of mass transfer, namely

- Diffusive mass transfer: The mass transfer due to the random motion of molecules is similar to conductive heat transfer. Mass transfer by diffusion occurs due to the concentration difference of species, resulting in the relative movement of molecules in a mixture. Separation of chemical species, transport of nutrients from blood vessels to the cells, purification of blood in the kidneys and liver are few examples of diffusive mass transfer. The rate of transfer of mass (flux) from the region of higher concentration to lower concentration is calculated by Fick's law, and the relation is:

$$J' = -D(\phi_1 - \phi_2). \tag{1.5.1}$$

where $J^{'}, D, \phi_1, \phi_2$ denotes the mass flux, diffusive mass transfer coefficient, concentration of species at different points, respectively.

- Convective mass transfer: The mass transfer by convection is similar to heat transfer by convection. Convective mass transfer occurs when mass is transported between fluid and a solid surface. Mass transfer by convection depends on transport properties and traits of flowing fluid. The rate of transfer of convective mass is calculated by a relation similar to Newton's law of cooling,

$$J^{'} = K^{'}(\phi_1 - \phi_2). \tag{1.5.2}$$

where $K^{'}$ denotes the coefficient of convective mass transfer.

The heat and mass transfer over a boundary layer flow due to stretching surface has influenced many researchers because of its use in several engineering processes, for instance, aerodynamics, materials manufactured by extrusion, paper production, and production of glass fiber, etc. One of the important industrial applications of stretching sheets is the extrusion of a polymer sheet from a die or the drawing of plastic films. During the process of making these sheets, the melt which comes out from the slit is stretched to get the desired thickness. Additionally, the rate of stretching and cooling significantly affects the quality of the final product. The linear stretching rate is not realistic, as the stretching rate changes during the process and causing non-linear stretching. The study of boundary layer flow over a continuous solid surface moving with constant speed for viscous fluids was initiated by Sakiadis [201]. After that, Crane [55] extended the idea of Sakiadis to two-dimensional flow through a stretching sheet. The heat and mass transfer on a stretching sheet with suction or blowing for viscous fluids was explored by Gupta and Gupta [84]. Elbashbeshy [66] studied heat transfer over a stretching surface with inconstant heat flux at the surface. Gorla and Sidawi [83] investigated the free convective heat transfer characteristics from a vertical stretching sheet with a surface mass transfer under the effect of blowing or suction. Chen and Char [44] examined the impact of power-law temperature and surface heat flux in the heat transfer process through a continuous linear stretching sheet. Later, Chiam [49], Hassanien and Gorla [89], Kelson and Desseaux [116], and few others have investigated the steady boundary layer flow due to permeable and non-permeable sheets. Later, various researchers analyzed the flow over a stretching surface in the directions of Newtonian and non-Newtonian fluid models under different situations [4, 12, 89, 116, 137, 139, 148, 150, 188]. Flow problems involve the exponential dependence of the similarity variables as the stretching velocity, and temperature distribution are presented by exponentially stretching surface. Mainly the researchers gave the solutions for two-dimensional exponentially stretching flows. Thermal boundary layer flow over

an exponentially stretching continuous surface with magnetic field effect was investigated numerically by Al-Odat et al. [6]. Analytical solutions of nanofluid flow over an exponential stretching surface were presented by Nadeem and Lee [158]. Heat transfer analysis over an exponentially shrinking surface by applying the shooting method was investigated by Bhattacharyya [27]. Heat transfer over a permeable stretching surface for a Casson fluid was studied by Mukhopadhyay et al. [152]. After that, three-dimensional viscous flow in the presence of heat transfer over an exponentially stretching surface is studied by Liu et al. [132]. Recently Ashraf et al. [10] extended the flow problem of Liu et al. by considering the viscoelastic fluid. Further, Rehman et al. [195] studied the three-dimensional flow over an exponential stretching sheet with water-based nanofluids.

1.6 Porous Medium

Porous medium may be defined as solid material having tiny pores uniformly distributed throughout the medium. Soil, sand, wood, limestone, and lungs, kidneys are natural examples of the porous medium, whereas fiberglass, cloth, and polymer are examples of the artificial porous medium. Flow through porous media has applications in almost every field of science and engineering, such as the production of float glass, air conditioning devices, processing of nuclear waste, scattering control of chemical waste and toxins, ceramic processing, medical, food industries, geothermal systems, and many more. The porous materials have many interconnected pores through which the fluid can flow. These curvy paths inside the porous media cause an incredibly high pressure drop. So here, we will discuss some common laws which relate velocity in the porous medium to the pressure drop.

1. ***Darcy's Law :*** The first momentum equation, which describes the flow through porous media, was obtained experimentally by Henry Darcy [57] in 1856, known as Darcys law. This law states that the volumetrically averaged velocity in any direction is proportional to the pressure gradient in that direction. Mathematically, it can be written as

$$\nabla P = -\frac{\mu}{\kappa V} \tag{1.6.1}$$

Here, V is volumetrically averaged velocity, κ is hydraulic conductivity (permeability) and P , μ are the pressure, and viscosity of the fluid, respectively.

Limitations of Darcy's Law

- Darcys law is restricted to fluid flow in which viscous forces dominate over the

inertia force.

- Darcys law is only valid for low velocity flows.

2. ***Forchheimer equation :*** Forchheimer's equation [73] is the earliest Non-Darcy model, also known as Dupuit-Forchheimer law. This equation comes into existence as Darcys law is applicable only when volumetric velocity is low. Forchheimer's equation accounts for the inertial effects in the flow, and as a result, an extra term is added to the Darcys law, known as Forchheimer term. Mathematically, it can be written as,

$$\nabla P = - \underbrace{\frac{\mu}{\kappa} V}_{Darcy\ term} - \underbrace{\frac{\rho_f b_f}{\sqrt{\kappa}} |V| V}_{Forchheimer\ term} \tag{1.6.2}$$

Here, b_f is inertia coefficient (Forchheimer coefficient or form drag constant).

3. ***Brinkmans equation:*** Brinkman's equation [34] removes the limitation of Darcy law in the sense that it is applicable to media with high permeability. Additionally, it can be applied for all boundary conditions at a solid interface or fluid interface.

$$\nabla P = - \underbrace{\frac{\mu}{\kappa} V}_{Darcy\ term} + \underbrace{\frac{\mu_{eff}}{\kappa} V^2}_{Brinkman\ term} . \tag{1.6.3}$$

Here, μ_{eff} is effective viscosity. Brinkman set $\mu = \mu_{eff}$ but generally this is not true. Several researchers investigated the relationship between effective and dynamic viscosity. The relationship $\frac{\mu_{eff}}{\mu} = \frac{1}{\epsilon'}$ is given by Ochoa-Tapia and Whitaker [167] in 1995, which has a greater value than unity and represents the porosity of the porous medium

4. ***Brinkman-Forchheimer extended Darcy model:*** This model incorporates both the viscous and inertial effects in the porous media. Basically, it combines it combines the above mentioned models in the single model. Mathematically, it can be written as

$$\rho_f \left[\frac{1}{\epsilon'} \frac{\partial V}{\partial t} + \underbrace{\frac{1}{\epsilon'} \nabla \left(\frac{V.V}{\epsilon'} \right)}_{Convective\ term} \right] = - \underbrace{\nabla P}_{Pressure\ term} + \underbrace{\frac{\mu}{\epsilon' \rho_f} \nabla^2 V}_{Brinkman\ term} - \underbrace{\frac{\mu}{\kappa} V}_{Darcy\ term} - \underbrace{\frac{\rho_f b_f}{\sqrt{\kappa}} |V| V}_{Forchheimer\ term} \tag{1.6.4}$$

Natural convective flow in porous cavities has gained much attention from researchers. This phenomenon has numerous applications such as fluid flow in geothermal reservoirs, processes involved in the chemical separation, removal of moisture from stored grain systems, production of crude oil, etc. Walker and Homsy [239] did the pioneer-

ing work in flow through differentially heated porous cavity. Prasad and Kulacki [181] investigated the free convective heat transfer through a rectangular porous cavity to study the effect of aspect ratio on flow and heat transfer. Trevisan and Bejan [232] examined the free convective heat and mass transfer characteristics of a fluid in a cavity filled with porous medium. Nithiarasu et al. [165] investigated the natural convection through a rectangular porous cavity of constant or variable porosity. They found that variable porosity significantly affects the flow patterns, which consequently affects the heat transfer traits. Also, the heat and mass characteristics in a multiporous cavity were examined by Saghir et al. [200]. He studied the impact of solutal Rayleigh number on double diffusion and found that salinity induces stronger convection than thermal ones. Baytas and Pop [16] investigated the natural convective flow in a cavity filled with porous medium using a non-equilibrium thermal model. They had considered a geometry in which side walls are at different temperatures whereas the top and bottom walls were thermally insulated and were helpful in designing thermal insulators. Heat and mass transfer in a cavity filled with partial porous matrix was studied by Gobin et al. [81]. Heat transfer in a square porous cavity under the effects of thermal radiation and viscous dissipation was investigated by Badruddin et al. [14]. Their results showed that the rate of heat transfer at the cold and hot walls enhances with an increase in radiation parameter. The flow and heat transfer in a porous cavity with sinusoidal heating of both the side walls was examined by Sivasankaran and Bhuvaneswari [222]. They obtained the solution of governing equations using FVM (finite volume method) and found that the rate of heat transfer enhances with an increase in porosity and permeability of the porous medium. The problem of combined heat and mass transfer in an inclined rectangular porous cavity was investigated by Farhany and Turan [5]. Their investigation showed that the coefficient of heat and mass transfer decreases with an increase in the angle of inclination. Apart from the literature mentioned above, various other researchers investigated flow in porous cavities by considering different situations [160, 212, 214, 217, 218]

Chapter 2

Mathematical Analysis of Bioconvective flow of nanofluids over a non-linear stretching sheet

In recent years there has been a concerted effort in fusing nano-technology and microbiology to develop more robust materials for engineering applications. For example, in solar coating materials, greater emphasis has been placed on designing sustainable, clean, durable, and ecologically friendly coating materials and inexpensive power systems. The presence of the nanoparticles has been confirmed to enhance durability, anti-corrosion, and anti-abrasion characteristics of coating materials. The parallel developments in biomimetics and exploiting biological phenomena for technological designs have also led to an interest in embedding micro-organisms in certain coatings. Bacterial micro-organisms have excellent anti-fouling properties and also protect engineering surfaces from environmental contamination. The resulting materials are sometimes called bio-functional materials [62]. The fundamental basis for nano-coatings (whether magnetic or biologically modified) is nanofluid science and technology. Introduced by Argonne energy laboratory pioneers, Choi and Eastman [51] in the 1990s, a nanofluid is a suspension of nano-sized particles (usually metallic) introduced into a base fluid (water, ethylene glycol, air, lubricant, etc) which boosts the effective thermal conductivity of the composite medium and even at relatively low volume fractions, the heat transfer enhancement is considerable. Via strategic dispersion of nanoparticles in the base fluid, it has been shown that the addition of less than 1% of nanoparticles doubles the heat conductivity of the nanofluid, as noted by Choi and Eastman [51] and Das et al. [58]. The boundary layer flow due to stretching surface has influenced many researchers because of its use in several engineering processes, for instance, materials manufactured by extrusion, paper production, glass fiber, etc. One of the essential industrial applications of stretching sheets is the extrusion of a polymer sheet from a die or plastic film drawing. During the process of making these sheets, the melt which comes out from the slit is stretched to get the desired thickness. Additionally, the rate of stretching and cooling significantly affects the quality of the final product. The linear stretching rate is not realistic, as the stretching rate changes during the process and causing non-linear stretching. Many authors investigated the flow within the boundary layer of

The content of this chapter has been published in *International Journal of Modern Physics B*

Newtonian or non-Newtonian fluids through stretching surfaces [44, 49, 66, 84, 89, 116, 201]. Out of these fluids, the potential significance of nanofluids in technology and engineering applications have inspired investigation in this direction. During these days, to provide stability to the nanoparticles in the base fluid, micro-organisms are infused. The concept of nanofluid bioconvection was firstly given by Kuznetsov [125, 127]. Bioconvection is a phenomenon that refers to the convectional flow of fluid due to density differences created by collective swimming of micro-organisms in a particular direction [102]. It has unique applications in biological systems and biotechnology such as chemical biosensors [129], chip-size small scale gadgets for assessing nanoparticle toxicity [104, 153]. The active mixers may damage the biological samples in these microfluidic devices due to the generation of ohmic (Joule heating) effects. The bioconvection enhances the mass transport and activates combinations in micro-volumes, and it helps to maintain the stable suspension of nanofluids. Moreover, bioconvection has a vital role in producing energy sources or mechanical power sources in mechanical engineering. The analysis of the development of bioconvection patterns due to motile micro-organisms was done by Pedley et al. [173]. The micro-organisms which cause bioconvection are categorized as oxytaxis, gravitaxis, and gyrotactic depend on the force causing their motion [79]. There is a dissimilarity between micro-organisms and nanoparticles. Micro-organisms are self-propelled whereas nanoparticles motion is due to Brownian motion and Thermophoresis. It is thus perceptible that micro-organisms move independently without affecting the movement of nanoparticles. Recently, numerous researchers explored the nanofluid bioconvection under different situations [22, 23, 38, 156, 186, 199].

In this transport phenomenon, the simultaneous effects of gyrotactic micro-organisms and non-uniform magneto-hydrodynamics over non-linear inclined stretching sheet is investigated. The inclination of the fabrication surface permits the scaling of gravity effects which provide a further mechanism of controlling the magnetic bio-nano-materials processing operations. Moreover, the benefits of including micro-organisms in the suspension incorporate micro-scale mixing and foreseen enhanced stability of nanofluid. Dissipation is a significant phenomenon even in low-speed incompressible heat transfer systems featuring buoyancy effects, as elucidated by Gebhart [76]. In the present work, the governing conservation equations (based on the Buongiorno-Kuznetsov gyrotactic nanofluid model) are converted from non-linear partial differential equations via similarity transformations to a third order, coupled, non-linear system of ordinary differential equations. The emerging boundary value problem is solved by an efficient variational finite element method. Numerical results for various physical parameters are expressed graphically and discussed. Validation with previous studies for two exceptional cases, i.e., negating bioconvection and viscous heating and sheet inclination, respectively, is conducted.

2.1 Mathematical Model

The present analysis intends to elaborate on the incompressible nanofluid flow through a non-linear stretching sheet in the presence of gyrotactic micro-organisms under steady-state conditions. The stretching sheet is inclined from the vertical with an acute angle of δ. The physical model of the problem and cartesian coordinates is shown in Fig 2.1. The x-direction is taken along the leading edge of the inclined stretching sheet, and the y-direction is normal to it. Following Mehyran et al. [144] and Chiam [50] the sheet is stretched with a power-law velocity, i.e., stretching velocity $u_w = ax^n$ where a is a positive constant and n is referred to as the non-linear stretching parameter. In the direction parallel to y-axis, a variable intense magnetic field $B(x) = B_o x^{(n-1)/2}$ is applied. Joule heating (Ohmic dissipation) is included. In comparison to the external magnetic field, however, the induced magnetic effect is negligible. The base fluid is taken as water for the survival of micro-organisms. The concentration of nanoparticles in the base fluid is chosen not to affect the velocity and swimming direction of micro-organisms in the flow. The Oberbeck-Boussinesq approximation is used for natural convection. Furthermore, the moving speeds of micro-organisms, base fluid, and nanoparticles are assumed to be similar. The governing equations of the flow problem under these approximations are as follows [144, 156]:

$$\frac{\partial u}{\partial x} + \frac{\partial v}{\partial y} = 0, \tag{2.1.1}$$

$$\rho\left(u\frac{\partial u}{\partial x} + v\frac{\partial u}{\partial y}\right) = \mu\left(\frac{\partial^2 u}{\partial x^2} + \frac{\partial^2 u}{\partial y^2}\right) - \sigma B^2(x)u + (\rho_f\beta(1-C_\infty)(T-T_\infty) - (\rho_p - \rho_f)(C-C_\infty))gcos\delta - g\gamma_e(\rho_m - \rho_f)(N-N_\infty)cos\delta, \tag{2.1.2}$$

$$u\frac{\partial T}{\partial x} + v\frac{\partial T}{\partial y} = \alpha\left(\frac{\partial^2 T}{\partial x^2} + \frac{\partial^2 T}{\partial y^2}\right) + \frac{\mu\alpha}{k}\left(\frac{\partial u}{\partial y}\right)^2 + \tau\left\{D_B\frac{\partial C}{\partial y}\frac{\partial T}{\partial y} + \frac{D_T}{T_\infty}\left(\left(\frac{\partial T}{\partial x}\right)^2 + \left(\frac{\partial T}{\partial y}\right)^2\right)\right\} + \frac{\sigma\alpha B^2(x)u^2}{k}, \tag{2.1.3}$$

$$u\frac{\partial C}{\partial x} + v\frac{\partial C}{\partial y} = D_B\left(\frac{\partial^2 C}{\partial x^2} + \frac{\partial^2 C}{\partial y^2}\right) + \frac{D_T}{T_\infty}\left(\frac{\partial^2 T}{\partial x^2} + \frac{\partial^2 T}{\partial y^2}\right), \tag{2.1.4}$$

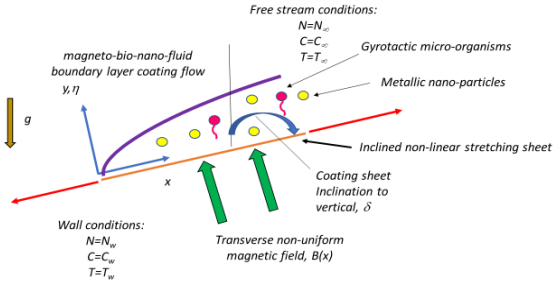

Figure 2.1: Schematic model and coordinates system

$$u\frac{\partial N}{\partial x}+v\frac{\partial N}{\partial y}+\frac{bW_c}{(C_w-C_\infty)}\left[\frac{\partial}{\partial x}\left(N\frac{\partial C}{\partial x}\right)+\frac{\partial}{\partial y}\left(N\frac{\partial C}{\partial y}\right)\right]=D_m\left(\frac{\partial^2 N}{\partial x^2}+\frac{\partial^2 N}{\partial y^2}+2\frac{\partial^2 N}{\partial x\partial y}\right). \quad (2.1.5)$$

The following physical boundary conditions are enforced for motile micro-organisms' velocity, temperature, nanoparticle concentration, and density:

$$\begin{aligned} &u=ax^n,\quad v=0,\quad T=T_w,\quad C=C_w,\quad N=N_w \quad \text{at}\quad y=0,\\ &u\to 0,\quad v\to 0,\quad T\to T_\infty,\quad C\to C_\infty,\quad N\to N_\infty \quad \text{at}\quad y\to\infty. \end{aligned} \quad (2.1.6)$$

To facilitate numerical solutions, the following similarity variables are introduced [156, 184]:

$$\eta=y\sqrt{\frac{a(n+1)}{2\nu}}x^{\frac{(n-1)}{2}},\ u=ax^n f'(\eta),\ v=-\sqrt{\frac{a(n+1)\nu}{2}}x^{\frac{(n-1)}{2}}\left(f(\eta)+\frac{(n-1)}{(n+1)}\eta f'(\eta)\right),$$
$$\theta(\eta)=\left(\frac{T-T_\infty}{T_w-T_\infty}\right),\ \phi(\eta)=\left(\frac{C-C_\infty}{C_w-C_\infty}\right),\ \chi(\eta)=\left(\frac{N-N_\infty}{N_w-N_\infty}\right).$$

The partial differential conservation equations are thereby converted into the following third-order system of non-linear, coupled and ordinary differential equations which take the form:

$$f'''+ff''-\left(\frac{2n}{n+1}\right)(f')^2-Mf'+\left(\frac{2}{n+1}\right)\left(\frac{Gr}{Re^2}\right)(\theta-Nr\phi-Rb\chi)cos\delta=0, \quad (2.1.7)$$

$$\frac{1}{Pr}\theta''+\theta'(f+Nb\phi')+Nt(\theta')^2+Ec[(f'')^2+M(f')^2]=0, \quad (2.1.8)$$

$$\phi^{''} + Lef\phi^{'} + \left(\frac{Nt}{Nb}\right)\theta^{''} = 0, \tag{2.1.9}$$

$$\chi^{''} + Lbf\chi^{'} - Pe[\phi^{''}(\Omega + \chi) + \phi^{'}\chi^{'}] = 0. \tag{2.1.10}$$

where $()^{'}$ designates differentiation with respect to the transformed transverse coordinate, η . The parameters arising in equations (2.1.7- 2.1.10) are defined as follows:

$Nb = \frac{\tau D_B(C_w - C_\infty)}{\alpha}$, $Nt = \frac{\tau D_T(T_w - T_\infty)}{\alpha T_\infty}$, $M = \frac{2\sigma B_o^2}{a\rho(n+1)}$, $\frac{Gr}{Re^2} = \frac{(g\beta(1-C_\infty)(T_w - T_\infty)x^3/\nu^2)}{u_w^2 x^2/\nu^2}$
$Nr = \frac{(\rho_p - \rho_f)(C_w - C_\infty)}{\rho\beta(1-C_\infty)(T_w - T_\infty)}$, $Rb = \frac{\gamma_e(\rho_m - \rho_f)(N_w - N_\infty)}{\rho\beta(1-C_\infty)(T_w - T_\infty)}$, $Pr = \frac{\nu}{\alpha}$, $Le = \frac{\nu}{D_B}$, $Lb = \frac{\nu}{D_m}$,
$Ec = \frac{u_w^2}{c_p(T_w - T_\infty)}$, $Pe = \frac{bW_c}{D_m}$, $\Omega = \frac{N_\infty}{(N_w - N_\infty)}$

The boundary conditions of equations in similarity space can be written as

$$f(0) = 0, \quad f^{'}(0) = 1, \quad \theta(0) = 1, \quad \phi(0) = 1, \quad \chi(0) = 1,$$

$$f^{'}(\infty) = 0, \quad \theta(\infty) = 0, \quad \phi(\infty) = 0, \quad \chi(\infty) = 0 \tag{2.1.11}$$

The key engineering design parameters [246] include the sheet surface shear stress, the heat flux, the mass flux, and the motile micro-organisms flux. In solar coating and other magnetic materials processing operations [246], key engineering design parameters include the sheet surface shear stress, the local heat flux, the local mass flux, and the motile micro-organisms flux. These are denoted as τ_w, q_w, q_m and q_n, respectively, and can be expressed mathematically as follows:

$$\tau_w = \mu\left(\frac{\partial u}{\partial y}\right)_{y=0}, \quad q_w = -k\left(\frac{\partial T}{\partial y}\right)_{y=0}, q_m = -D_B\left(\frac{\partial C}{\partial y}\right)_{y=0}, \quad q_n = -D_m\left(\frac{\partial N}{\partial y}\right)_{y=0} \tag{2.1.12}$$

In non-dimensional variables, these design quantities of physical interest are defined as the skin friction coefficient Cf_x, the Nusselt number Nu_x, the Sherwood number Sh_x and the density number of the motile micro-organisms Nn_x which take the form:

$$Cf_x = \frac{\tau_w}{\rho u_w^2}, \quad Nu_x = \frac{xq_w}{k(T_w - T_\infty)}, Sh_x = \frac{xq_m}{D_B(C_w - C_\infty)}, \quad Nn_x = \frac{xq_n}{D_m(N - N_\infty)}$$

Putting values of τ_w, q_w, q_m, q_n from 2.1.12 to 2.1.13, we obtain

$$Re_x^{1/2}Cf_x = \sqrt{\frac{n+1}{2}}f^{''}(0), \quad Re_x^{-1/2}Nu_x = -\sqrt{\frac{n+1}{2}}\theta^{'}(0),$$

$$Re_x^{-1/2} Sh_x = -\sqrt{\frac{n+1}{2}}\phi^{'}(0),\ Re_x^{-1/2} Nn_x = -\sqrt{\frac{n+1}{2}}\chi^{'}(0) \tag{2.1.13}$$

In the above equations, $Re_x = (U_0 x)/\nu$ refers to the Reynolds number.

2.2 Methodology

The finite element method was used to solve a system of non-linear ordinary differential equations (2.1.7-2.1.10) subjected to boundary conditions (2.1.11). The reduced momentum equation (2.1.7) is a third-order differential equation that is coupled with the heat and nanoparticle concentration equations through buoyancy terms as well as the motile microorganism density conservation number through advection-diffusion terms. As a result, it is beneficial to solve these equations in the coupled form. The finite element methodology is well-established and, therefore not elaborated here . For further elaboration of the interpolation weighting functions and stiffness matrix formulations, readers should consult Bhargava et al. [25, 26] work. In summary, firstly, the third-order momentum equation is reduced to second-order using a simple substitution:

$$f^{'} = h. \tag{2.2.1}$$

$$h^{''} + fh^{'} - \left(\frac{2n}{n+1}\right)(h)^2 - Mh + \left(\frac{2}{n+1}\right)\left(\frac{Gr}{Re^2}\right)(\theta - Nr\phi - Rb\chi)cos\delta = 0, \tag{2.2.2}$$

$$\frac{1}{Pr}\theta^{''} + \theta^{'}(f + Nb\phi^{'}) + Nt(\theta^{'})^2 + Ec[(h^{'})^2 + M(h)^2] = 0, \tag{2.2.3}$$

$$\phi^{''} + Lef\phi^{'} + \left(\frac{Nt}{Nb}\right)\theta^{''} = 0, \tag{2.2.4}$$

$$\chi^{''} + Lbf\chi^{'} - Pe[\phi^{''}(\Omega + \chi) + \phi^{'}\chi^{'}] = 0. \tag{2.2.5}$$

The corresponding boundary conditions (2.1.11) transformed to :

$$f(0) = 0,\quad h(0) = 1,\quad \theta(0) = 1,\quad \phi(0) = 1,\quad \chi(0) = 1, \tag{2.2.6}$$

$$h(\infty) = 0, \quad \theta(\infty) = 0, \phi(\infty) = 0, \quad \chi(\infty) = 0 \tag{2.2.7}$$

The whole finite element domain is divided into 80 two-noded line elements. Over each of the element, finite element equations are derived. The error tolerance has been considered to be 10^{-4}. The choice of $\eta_\infty = 7$ satisfies the boundary layer conditions, i.e., achieves asymptotically smooth results in the free stream. If η_∞ exceeds 7, all the unknown functions do not change up to the desired accuracy.

2.3 Validation With Published Studies

For the validation of code, careful comparison with special cases of the general model is conducted. Table 2.1 shows the benchmarking of the present finite element solutions for reduced Nusselt number with the earlier studies of Khan and Pop [119] for the case where bioconvection is ignored ($Rb = Pe = Lb = \Omega = Nr = 0$), the sheet is vertical ($\delta = 0^o$), linear sheet stretching velocity is assumed ($n = 1$), magnetic field and viscous heating and Joule dissipation terms vanish ($M = Ec = 0$) but nano-particle effects are retained ($Le = 10$) and $Nb \neq 0$ and $Nt \neq 0$. With these values prescribed in the general model, the boundary value problem reduced exactly to that studied by Khan and Pop [119]. Excellent correlation is achieved between the finite element code and the numerical shooting quadrature computations of Khan and Pop [119] for all values of Nb and Nt.

Table 2.1: Comparison of results for reduced Nusselt number $-\sqrt{((n+1)/2)}\theta'(0)$, for $Le = 10, n = 1, M = Ec = Nr = Rb = Pe = Lb = \Omega = 0, \delta = 0^o$ and different values for Nt and Nb

	$Nb = 0.1$		$Nb = 0.3$		$Nb = 0.3$	
Nt	Present Results	Khan and Pop [119]	Present Results	Khan and Pop [119]	Present Results	Khan and Pop [119]
0.1	0.956638	0.952493	0.256755	0.2522	0.05596	0.0543
0.2	0.69398	0.6932	0.181657	0.1816	0.0394372	0.0390
0.3	0.524139	0.5201	0.131437	0.1355	0.0299327	0.0291
0.4	0.408426	0.4026	0.100644	0.1046	0.0221499	0.0225
0.5	0.32752	0.3211	0.08291	0.0833	0.0175823	0.0179

The comparison of present results with the results obtained by Mehryan et al. [144] for the density gradient of motile micro-organisms is documented in Table 2.2. With $Ec = 0$ (negligible viscous heating effect and Ohmic dissipation term ignored in the energy equation (2.1.11)) and $\delta = 0^o$ (vertical sheet scenario) the present general model reduces exactly to that solved in [144]. The table shows that an excellent correlation is achieved with the finite element solutions and finite-difference solutions of Mehryan et al. [144].

Table 2.1 shows that reduced Nusselt decreases with an increase of Nb and Nt. The irregular motions of nanoparticles in fluid give rise to an increase in temperature (transfer

Table 2.2: Comparison of results for the density of motile micro-organisms $-\sqrt{((n+1)/2)}\chi^{'}(0)$ for $n = 1, M = Nb = 1, Ec = 0, Nr = Nt = Gr = 0.5, Lb = Le = 2, Rb = 0.3, \delta = 0^o$, $b = 1$, and different values for Ω and Pe

	$Pe = 0.3$		$Pe = 0.5$		$Pe = 0.5$	
Ω	Present Results	Mehryan et. al [144]	Present Results	Mehryan et. al [144]	Present Results	Mehryan et. al [144]
0.1	2.80479	2.819	3.20986	3.203	3.59853	3.598
0.2	2.84746	2.861	3.28579	3.275	3.70988	3.699
0.4	2.93298	2.945	3.43801	3.418	3.903	3.93266
0.6	3.01871	3.029	3.55134	3.561	4.15565	4.107
0.8	3.10416	3.114	3.70218	3.704	4.30139	4.311
1.0	3.18983	3.197	3.85296	3.847	4.515	4.52098

Table 2.3: Results for skin friction coefficient for $Gr = n = Pe = M = Lb = 1, Ec = Rb = \Omega = Nb = 0.1, Pr = 10, \delta = 0^o$ and different values for Nt and Nr

Nr	$Nt = 0.05$	$Nt = 0.1$	$Nt = 0.5$
0.3	1.22202	1.22392	1.224
0.5	1.28574	1.2979	1.3075
0.8	1.38412	1.41402	1.44224
0.4	1.45193	1.49629	1.54296
0.5	1.52195	1.58451	1.66415

of heat to the boundary layer from the wall), and hence heat transfer rates at the wall (sheet) decrease. From Table 2.2 it is evident that an increase in the motile micro-organism wall flux (density gradient at the sheet surface) accompanies an increment in Ω and Pe since both these parameters deplete the motile micro-organism's concentration within the boundary layer, as will be elucidated later. Table 2.3 shows that the skin friction coefficient increases with an increase in buoyancy ratio parameter (Nr) and thermophoresis parameter (Nt). Table 2.4 shows that Sherwood number increases with increasing Nb and Nt.

Table 2.4: Results for Sherwood number for $Le = Pe = 10$, $n = 1$, $\delta = 0^o, M = Ec = Nr = Rb = Pe = Lb = \Omega = 0$ and different values for Nt and Nb

Nb	$Nt = 0.1$	$Nt = 0.3$	$Nt = 0.5$
0.1	2.11927	2.40624	2.363477
0.2	2.27421	2.48186	2.43115
0.3	2.52916	2.57045	2.48106
0.4	2.78961	2.64549	2.5212
0.5	3.04169	2.70776	2.56326

2.4 Results & Discussion

The influence of various embedding parameters on flow velocity $f^{'}(\eta)$, temperature profile $\theta(\eta)$, nanoparticle concentration $\phi(\eta)$ and density of gyrotactic micro-organisms $\chi(\eta)$ are illustrated in figures 2.2-2.5. The data is carefully chosen based on industry recommendations and robust simulations.

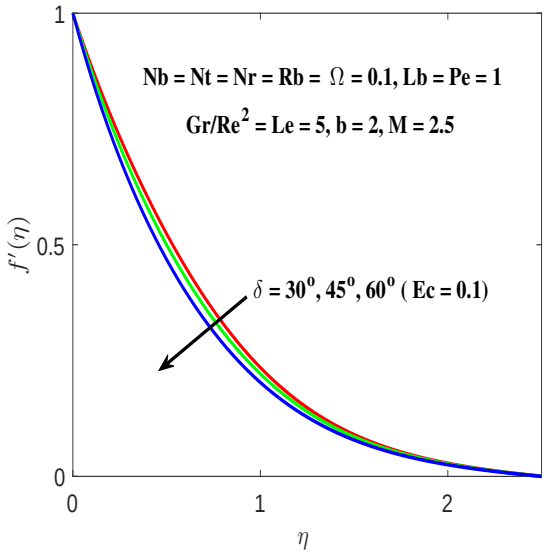

(a) Effect of δ

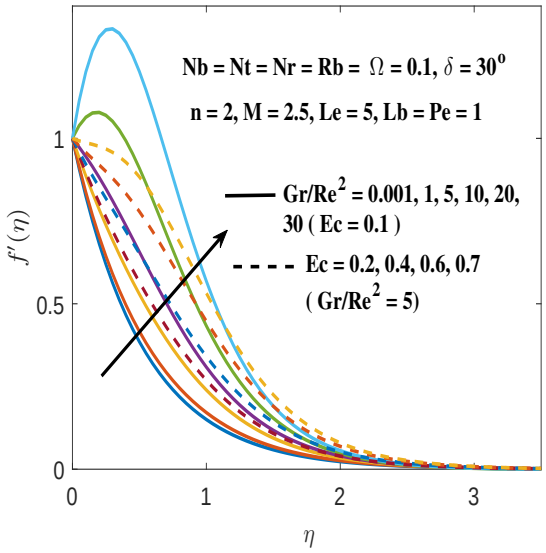

(b) Effect of Ec and $\frac{Gr}{Re^2}$

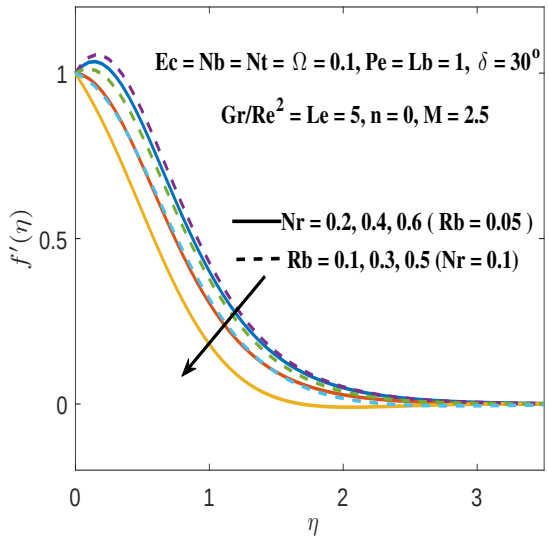

(c) Effect of Nr and Rb

Figure 2.2: Effect of varied thermophysical parameters on on velocity profiles

The effect of various thermophysical parameters on velocity profiles is depicted in figures 2.2a-c. It can be seen from the figure 2.2a that velocity decreases with an increase in the angle of inclination of the stretching sheet (δ). This is because buoyancy forces increase as the angle of inclination (δ) increases. Since, only the thermal buoyancy force, $(\frac{2}{(n+1)})(\frac{Gr}{Re^2})(\theta cos\delta)$, in equation (2.1.7), is positive. As a result, a greater inclination angle will aid momentum development. However, the contributions from nano-particle species buoyancy and motile microorganism species buoyancy forces are negative, as indicated by the terms $(\frac{2}{(n+1)})(\frac{Gr}{Re^2})(-Nr\phi cos\delta - Rb\phi cos\delta)$ in the momentum equation(2.1.7). They are increasingly opposing momentum development, resulting in flow deceleration, as shown in figure 2.2a. As a result, the thickness of the momentum (hydrodynamic) boundary layer will increase. The impact of $\frac{Gr}{Re^2}$ and Eckert number Ec on flow velocity is depicted in figure 2.2b. Generally natural convection is negligible when $\frac{Gr}{Re^2} < 0.1$ whereas forced convection is negligible when $\frac{Gr}{Re^2} > 10$. Both forced and free convection contribute when $0.1 < \frac{Gr}{Re^2} < 10$. Except in extremely low forced flow velocities, forced convection is always large relative to free convection. As the Richardson number increases, there is a significant rise in flow velocity. For high $\frac{Gr}{Re^2}$ values (> 10), a velocity overshoot is observed near the sheet surface. This overshoot is enhanced and displaced further from the sheet surface as $\frac{Gr}{Re^2}$ increases from 20 to 30. As a result of the strong accelerated flow, a significant reduction in momentum boundary layer thickness is induced with a higher Richardson number (stronger natural convection buoyancy effect). Figure 2.2b also shows that velocity increases with increasing Ec, especially near the wall. The Eckert number expresses the relative contribution of kinetic energy in the flow and the difference in enthalpy in the boundary layer. At very low Ec values, it represents the conversion of kinetic energy into thermal energy through work done against viscous fluid stresses, as elaborated by Gebhart [76]. Positive Eckert number (as studied here) implies cooling the wall and therefore a transfer of heat to the magnetized nanofluid. As noted by Ibrahim and Shankar [105], the presence of a strong magnetic field ($M=$ 2.5, i.e., magnetic Lorentz force is 250% greater than viscous hydrodynamic force) may also contribute to dissipation effects. On the other hand, the unusual response is most likely due to the presence of ohmic dissipation. Figure 2.2c shows that the velocity profile decreases with an increasing Rb values. The classical Rayleigh number is equal to the ratio of buoyancy forces to viscous forces multiplied by the momentum diffusivity to thermal diffusivity ratio. The bioconvection Rayleigh number is the modified form of the traditional Rayleigh number. The numerator of Rb consists of contribution from buoyancy effects of motile micro-organisms and the denominator, thermal buoyancy force. The primary outcome of increasing Rb is to decline fluid velocity for some distance away from the plate and effectively increase the momentum (velocity) boundary layer thickness. Figure 2.2c also shows that as Nr increases, the flow velocity de-

creases. Here Nr represents the relative contribution of buoyancy of nano-particle species to thermal buoyancy. Both contributions are the same when Nr equals unity. However, for $Nr < 1$ (as studied here), thermal buoyancy dominates nano-particle species buoyancy, resulting in accelerating flow within the boundary layer and increased momentum boundary layer thickness.

The temperature profiles computed for various thermophysical parameters are depicted in figures (2.3a-e). In figure 2.3a, it is noticeable that at a fixed value of other parameters, the heat transfer increases with an increase in δ. This is due to the greater overall increase in buoyancy effects with increasing sheet inclination. Furthermore, as shown in figure 2.3b, dimensionless temperature decreases with increasing $\frac{Gr}{Re^2}$ values. Consequently, the thermal boundary layer thickness is enhanced with an increase in the Richardson number. Figure 2.3c demonstrates that the temperature of the magnetic nanofluid strongly increases with a rise in Ec. For higher values of Ec, more mechanical energy is converted to thermal energy via internal friction, i.e., heat dissipation. This warms the boundary layer and accelerates heat transfer. In Figure 2.3d, it is shown that temperature is increased with greater values of Nb and Nt. This is because of Brownian motion and thermophoresis effects; additional heat is generated by the interaction of nanoparticles with the base fluid. Hence, as the value of Nb and Nt increases, the thermal boundary layer thickness decreases, causing temperature overshoots in the vicinity of the stretching sheet. In addition, as shown in figure 2.3e, there is a negligible increase in temperature with increasing Nr. With greater Nr, the nano-particle diffusion is elevated relative to the thermal diffusion, which boosts the buoyancy force of the nano-particle species while depleting the thermal buoyancy force. This causes the fluid to heat up and the thickness of the thermal boundary layer to decrease.

Figures 2.4a-d depicts the variation of nanoparticle concentration for different thermophysical parameters such as $(\frac{Gr}{Re^2})$, (Le), (Nb), (Nt) and δ. Figure 2.4a shows a slight increase in nanoparticle concentration as (δ) increases. The concentration of nanoparticles is low for the vertical sheet case, i.e., when the angle of inclination, $\delta = 0^0$, is encountered because this case has the greatest gravitational force resistance. The strength of gravitational force decreases as the angle of inclination increases. However, the magnitude of the nanoparticle buoyancy force increases as seen in the momentum equation (2.1.7), which aids in nano-particle species diffusion and thickens the nanoparticle concentration boundary layer. Figure 2.4b shows that as $\frac{Gr}{Re^2}$ increases, the concentration of nanoparticles within the boundary layer decreases. The nanoparticle concentration boundary layer also decreases with increasing Le. This parameter represents the ratio of thermal diffusivity of the nanofluid to species diffusivity of the nanoparticles. In the current calculations, $Le > 1$,

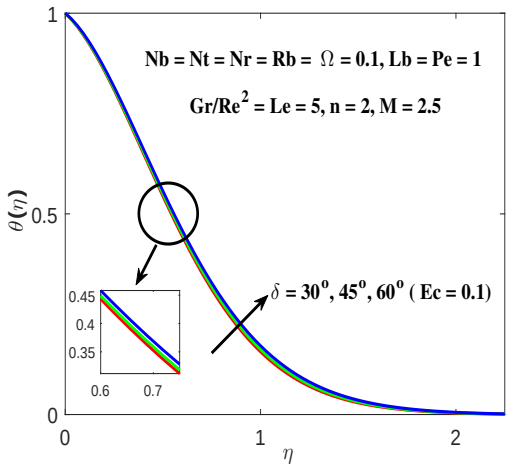

(a) Effect of δ

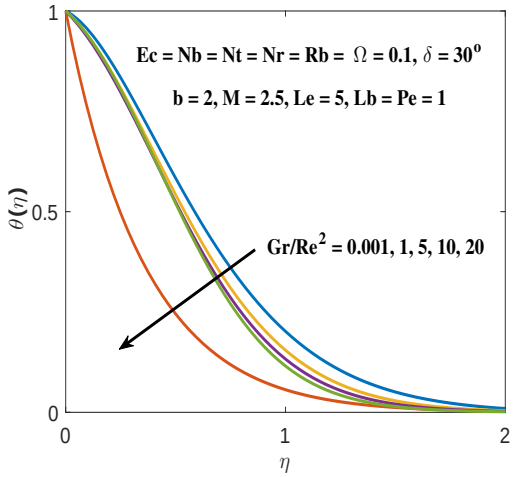

(b) Effect of $\frac{Gr}{Re^2}$

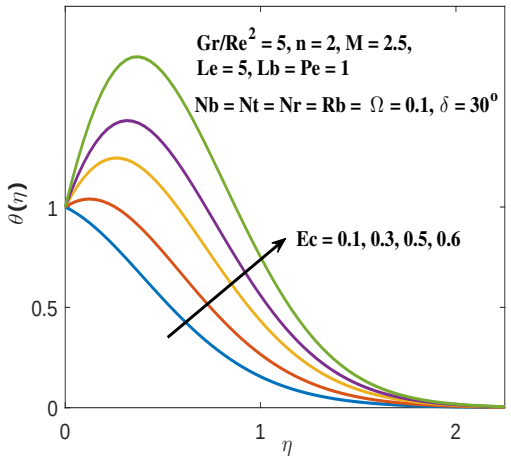

(c) Effect of Ec

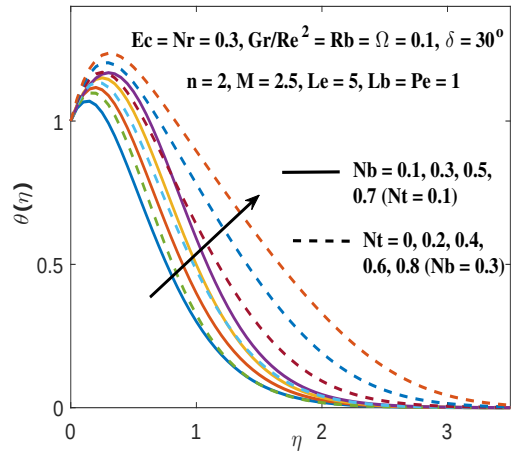

(d) Effect of Nb and Nt

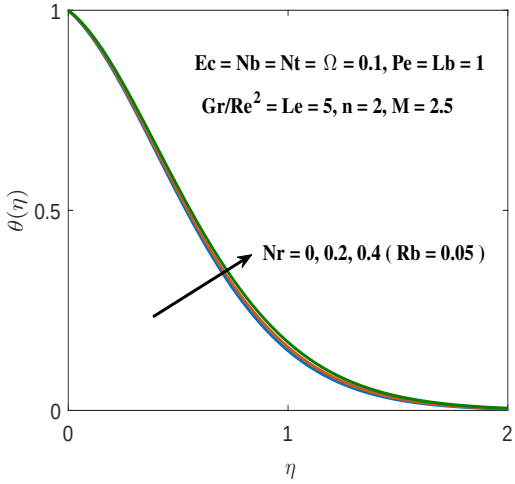

(e) Effect of Nr

Figure 2.3: Effect of varied thermophysical parameters on temperature profiles

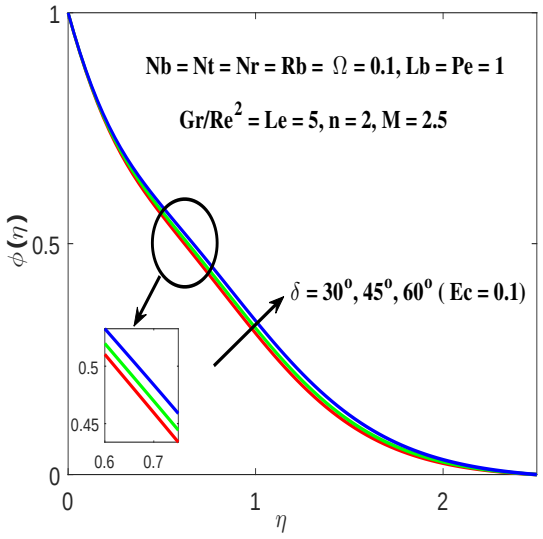

(a) Effect of δ

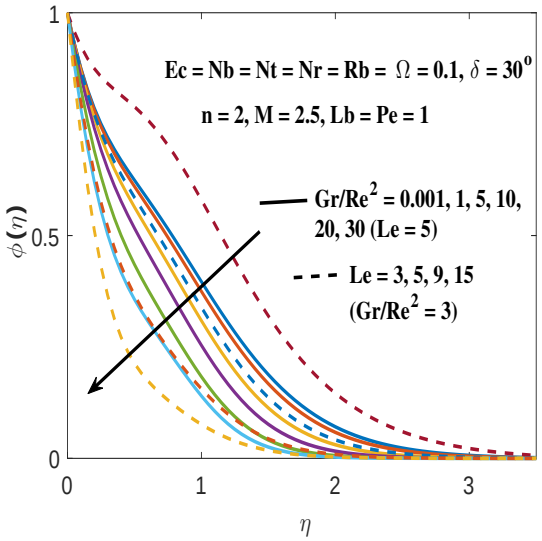

(b) Effect of $\frac{Gr}{Re^2}$ and Le

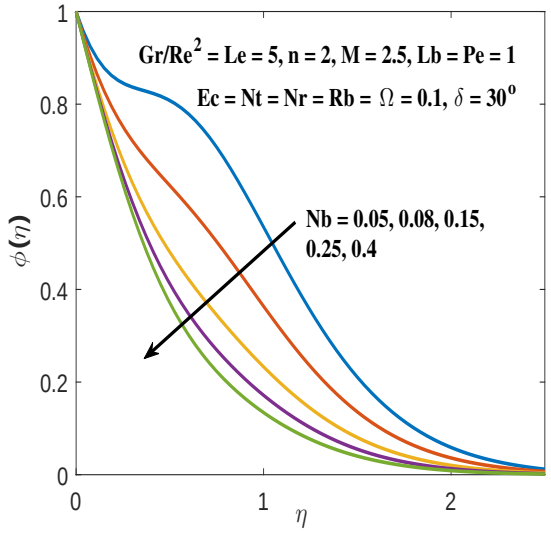

(c) Effect of Nb

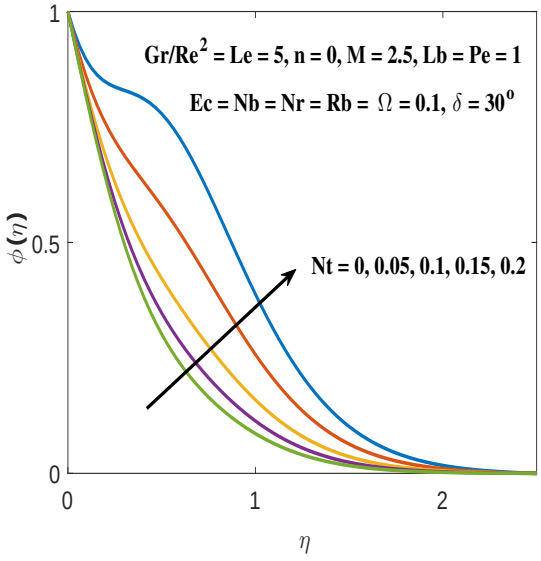

(d) Effect of Nt

Figure 2.4: Effect of varied thermophysical parameters on nanoparticle concentration

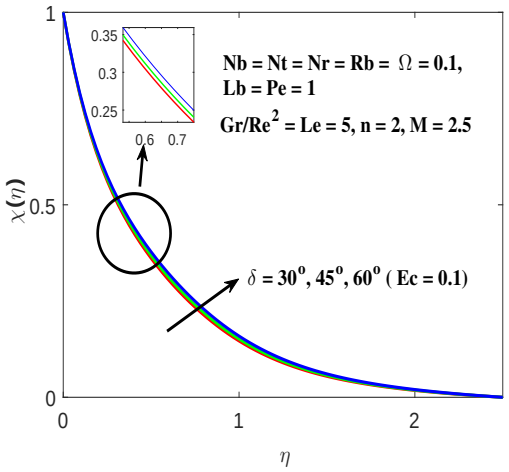

(a) Effect of (δ)

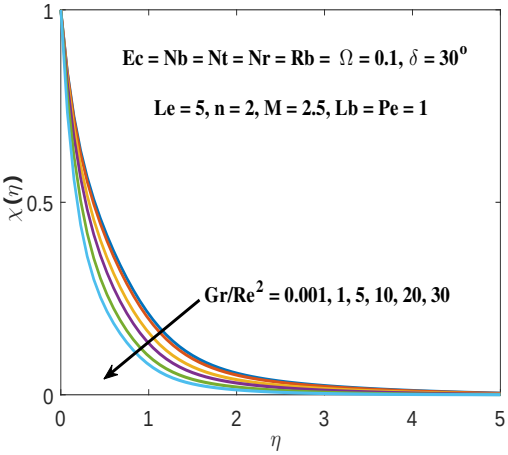

(b) Effect of $\frac{Gr}{Re^2}$

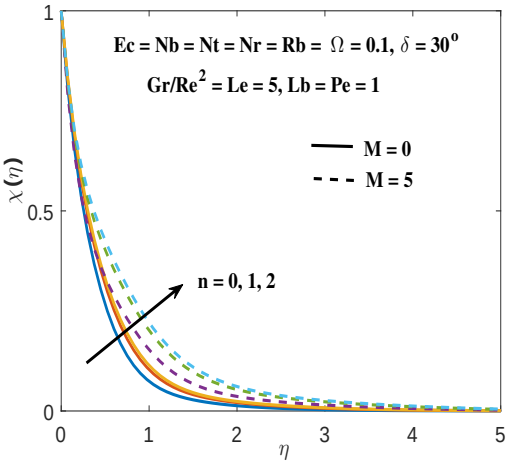

(c) Effect of M and n

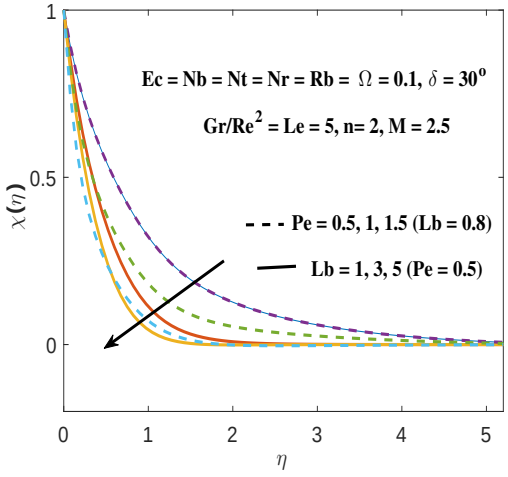

(d) Effect of Lb and Pe

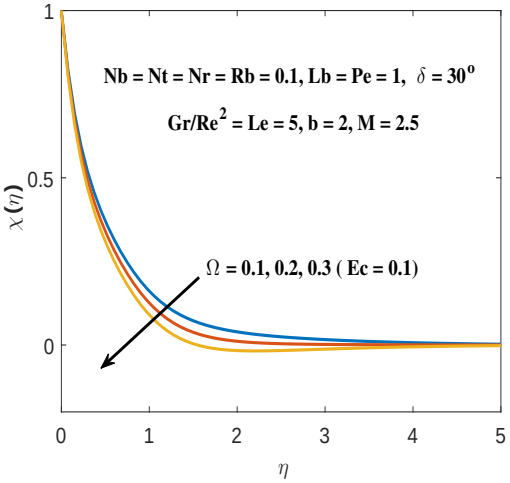

(e) Effect of Ω

Figure 2.5: Effect of varied thermophysical parameters on density of motile micro-organisms

implying that the thermal diffusivity of the nanofluid always exceeds the species diffusivity of the nanoparticles. As a result, the rate of nano-particle diffusion slows with increasing Lewis number, resulting in a significant decrease in nanoparticle concentration throughout the boundary layer regime transverse to the stretching sheet's surface. Figures 2.4c, d show the effect of the Brownian motion parameter and the thermophoresis parameter on the concentration of nanoparticles. Figure 2.4c shows that increasing (Nb) values result in a significant reduction of nanoparticle concentration magnitudes. Figure 2.4d shows that a higher (Nt) increases the concentration distribution of nanoparticles. This means that greater migration of hot nanoparticles in the direction of a decreasing temperature gradient results in thickening of nanoparticle concentration boundary layer thickness. Greater Brownian motion parameter, on the other hand, has the opposite effect.

The figures 2.5a-e show how bioconvection parameters, magnetic field, and nanofluid parameters affect the density of motile gyrotactic micro-organisms. Figure 2.5a and 2.5b show that increasing (δ) and $(\frac{Gr}{Re^2})$ have the same effect on the density variationof motile micro-organisms as they do on nanoparticle concentration. The density of motile micro-organisms increases as the angle of inclination increases, while forthe increase inRichardson number, itdecreases. Hence, species boundary layer thickness decreases with increasing sheet inclination and increases with increasing Richardson number. Figure 2.5c shows that as the magnetic parameter M is increased, the density of motile micro-organisms increases. The depletion of nanofluid momentum and deceleration in the flow with greater Lorentz magnetic drag force (featured in momentum (2.1.7)) aids in the propulsion of micro-organisms. The presence of Ohmic dissipation in the term $Ec[(f^{''})^2 + 2M(f^{'})^2]$ in the thermal boundary layer equation (2.1.8) also encourages micro-organism propulsion because it decelerates the boundary layer flow. Micro-organism density number is minimum for $M = 0$ and maximum for strong magnetic field effect with $M = 5$. Furthermore, figure 2.5d shows that increasing the non-linear stretching parameter n increases the density of motile micro-organisms within the boundary layer. Figure 2.5d shows that as Lb and Pe increase, the density of motile micro-organisms decreases significantly. These two parameters, in conjunction with the previously discussed bioconvection Rayleigh number Rb, govern the bioconvection phenomenon in the boundary layer. The Peclet number is defined as the ratio of advection to the diffusion of micro-organisms. Since $Pe = \frac{bW_c}{D_n}$, Pe is directly proportional to (constant maximum cell swimming speed) and inversely proportional to D_n for a given chemotaxis constant (the diffusivity of micro-organisms). At higher Pe values, the flow pattern of micro-organisms changes dramatically in biconvection. The internal energy of micro-organisms causes bioconvection. As Pe increases, the concentration of micro-organisms decreases as they move faster. Lower Pe values induce the opposite effect, i.e., motility of the micro-organisms is inhibited, and they move slower, resulting in

higher and significantly more homogeneous concentrations, as shown in figure 2.5d. Similarly, the bioconvection Lewis number contributes to a reduction in the thickness of the microorganism concentration layer. Physically, this is explained by the fact that as the bioconvection Lewis number increases, so does the viscous diffusion rate, which decreases the dimensionless velocity. As a result, the density of the micro-organisms decreases. The bioconvection Lewis number thus relates the viscous diffusion rate (fluid viscosity) to the motile microorganism diffusivity. The assisting effect of increasing Lb is due to a decrease in D_n relative to α. The motile micro-organism rescaled density boundary layer thickness increases as the Lb and Pe numbers increase. The decrease in density implies reduction in micro-organism settling due to increased bioconvection. In the nanofluid, this promotes mixing and species diffusion. The addition of nanoparticles to the bioconvection regime alters the distributions of motile micro-organisms. Both nanofluid and bioconvective mechanisms interact significantly (both nanoparticle and micro-organism species conservation equations are strongly coupled to each other), and careful selection can lead to optimized performance of potential magnetic bio-nanofluid devices. Figure 2.5e shows that increasing the value of the microorganism concentration difference parameter (Ω) results in a non-trivial increase in the density number of motile micro-organisms. This parameter appears only in the micro-organism conservation equation (2.1.13) and clearly serves to increase micro-organism concentration boundary layer thickness when increased.

2.5 Conclusions

A mathematical model is presented for incompressible, steady-state, boundary layer flow of a nanofluid containing motile gyrotactic micro-organisms over a non-linear inclined stretching sheet subjected to the non-uniform magnetic field. The Buongiorno-Kuznetsov nanofluid-bioconvection model is employed, and Ohmic dissipation (Joule heating) is incorporated. The finite element method is used to solve the emerging non-dimensional boundary value flow problem. A detailed parametric analysis of the impact of various thermophysical parameters is carried out. The following observations are noteworthy:

- Flow velocity declines with increasing angle of inclination of the stretching sheet, Eckert number, buoyancy ratio parameter, and bioconvection Rayleigh number. In contrast the velocity profile enhances with an increase in Richardson number and Eckert number.

- Increasing angle of inclination, Eckert number, Brownian motion parameter, Thermophoresis parameter, Buoyancy ratio parameter enhances the temperature near the

wall. In contrast, temperature decreases with a rise in the Richardson number.

- Nanoparticles concentration is boosted with an increment in the angle of inclination and thermophoresis parameter, whereas it is depressed with Richardson number, Lewis number, and Brownian motion parameter.
- Motile micro-organisms density number rises with enhancement in an angle of inclination, magnetic parameter, and non-linear stretching parameter whereas it is suppressed with increasing bioconvection Lewis number, bioconvection Peclet number, and Richardson number.
- Skin friction is increased with higher values of the Thermophoresis parameter and Buoyancy ratio parameter.
- Nusselt number reduces whereas Sherwood number enhances with an increment in Brownian motion and Thermophoresis parameters.
- Motile micro-organism density number elevates with an enhancement in both micro-organism concentration difference parameter and bioconvection Peclet number.

Chapter 3

Mathematical Analysis of Bioconvective flow of nanofluids using non-Fourier's heat flux and non-Fick's mass flux theory

The phenomenon of heat transfer is an active area of research due to its applications in engineering, sciences, and industries. As illustrations, electronic devices dissipate heat which aspires cooling, textile industries, cooling, and heating systems in the buildings, vehicles, phase change materials, etc. The heat transfer occurs when there is a temperature difference between the two bodies and within the same body at various parts. This is an extensive natural phenomenon occurring in many fields [9, 205]. Fourier gives us the primary equation for heat conduction [74]. This law is effectively executed in various engineering applications such as wire drawing, cooling of nuclear reactors, copper materials, heat pumps, energy production, refrigeration, and many more. The Fourier law of heat conduction is an empirical formula which says that initial disturbance felt throughout the domain in a flash of time. Thus this law does not have room for relaxation time. There are lot many applications in which heat is transported as a wave with finite speed which includes, bioheat transfer, biomedical technology (thermotherapy), design of garments for heating and cooling purposes [56]. Keeping in mind the fact mentioned above, different versions of Fourier's Law of heat conduction are suggested [35, 64]. Cattaneo [37] also adjusted the Fourier's law by adding relaxation time in the heat flux for getting a finite speed of propagation once the temperature gradient is imposed. To get the frame indifferent generalization of Catteneo's model, Christov [52] replaced the ordinary derivative with Oldroyd's upper-convected derivates and get the single temperature governing equation. This model is known as the Catteneo-Christov heat flux model. This innovative study has opened the door for the modern era of research mentioned in the refs [85, 86, 107, 155, 182, 223, 226, 230].

In today's era, the bioconvective nanofluid flow has many applications such as vehicle cooling, increased heat transfer in microchips, food processing, and applications in biotechnology (cancer treatment hypothesis, drug delivery at specific location), microbial increased oil recovery. Thus, the present research aims to study the heat and mass transfer due

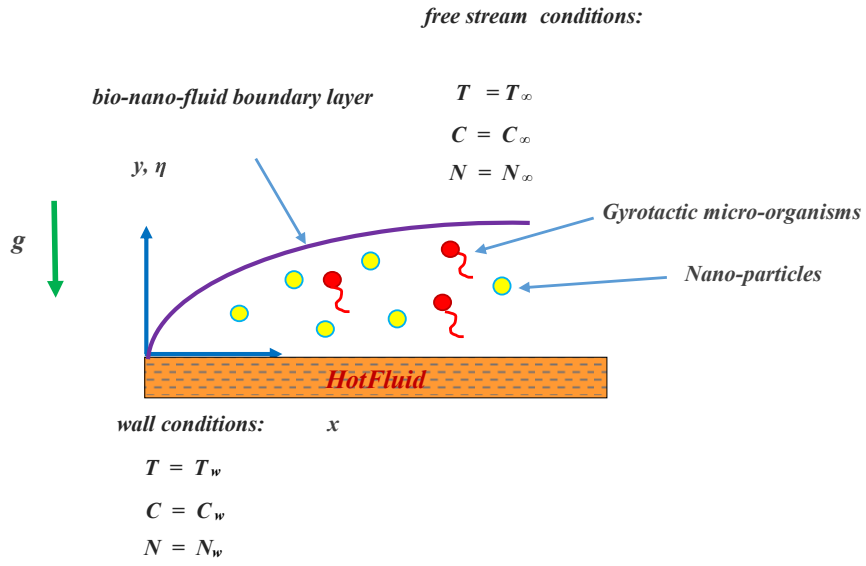

Figure 3.1: Schematic model and coordinates system

to moving gyrotactic micro-organisms and nanofluid over a heated surface. The addition of gyrotactic micro-organisms in the nanofluids provides stability to the suspension. The novelty of the problem is to investigate the Catteneo-Christov double diffusion model for the bioconvective flow of nanofluids, which have room for relaxation time for heat and mass transfer. The governing equations of the flow problem are non-linear coupled differential equations obtained after similarity transformations and are solved by Finite Element scheme [72,113,193]. The obtained results are thoroughly analyzed by plotting graphs with variations in involved parameters.

3.1 Mathematical Model

The present analysis intends to elaborate the incompressible nanofluid flow through a heated surface in the presence of gyrotactic micro-organisms under steady-state conditions. The configuration of the flow problem along with the co-ordinate axis is demonstrated in figure 3.1. It is taken into consideration that the surface is stretched with velocity $u_w = ax^n$ (a is constant, and n is the index with which surface is stretched). The base fluid is taken as water for the survival of micro-organisms. The nanoparticles concentration in the base fluid is considered in such a way that it does not affect the velocity and swimming direction of micro-organisms in the flow. For natural convection Oberbeck- Boussinesq approximation is used. Moreover, the velocities of moving micro-organisms, base fluid, and nanoparticles are assumed to be similar. Instead of Classical Fourier's Law for heat transfer, modern

heat flux ($q^{'}$) model [52] and modern mass flux ($J^{'}$) model [149] for mass transfer are used. The models for the case of incompressible flow are given below:

$$q^{'} + \lambda_e \left[\frac{\partial q^{'}}{\partial t} + V.\nabla q^{'} - q^{'}.\nabla V \right] = -K\nabla T. \tag{3.1.1}$$

$$J^{'} + \lambda_c \left[\frac{\partial J^{'}}{\partial t} + V.\nabla J^{'} - J^{'}.\nabla V \right] = -D_B \nabla C. \tag{3.1.2}$$

Here V, λ_e, λc, D_B and K denotes velocity, relaxation time for heat and mass flux, coefficient of Brownian diffusion, and fluid's thermal conductivity, respectively.

The governing equations of the flow problem under these assumptions are:

$$\frac{\partial u}{\partial x} + \frac{\partial v}{\partial y} = 0, \tag{3.1.3}$$

$$\rho\left(u\frac{\partial u}{\partial x} + v\frac{\partial u}{\partial y} \right) = \mu\frac{\partial^2 u}{\partial y^2} + \rho_f g\beta(1 - C_\infty)(T - T_\infty) - g(\rho_p - \rho_f)(C - C_\infty) - g\gamma_e(\rho_m - \rho_f)(N - N_\infty) \tag{3.1.4}$$

$$u\frac{\partial T}{\partial x} + v\frac{\partial T}{\partial y} + \delta_e\Lambda_e = \alpha\left(\frac{\partial^2 T}{\partial y^2} \right) + \tau\left(D_B\frac{\partial C}{\partial y}\frac{\partial T}{\partial y} + \frac{D_T}{T_\infty}\left(\frac{\partial T}{\partial y} \right)^2 \right) \tag{3.1.5}$$

$$u\frac{\partial C}{\partial x} + v\frac{\partial C}{\partial y} + \delta_c\Lambda_c = D_B\left(\frac{\partial^2 C}{\partial y^2} \right) + \frac{D_T}{T_\infty}\left(\frac{\partial^2 T}{\partial y^2} \right) \tag{3.1.6}$$

$$u\frac{\partial N}{\partial x} + v\frac{\partial N}{\partial y} + \frac{bW_c}{(C_w - C_\infty)}\left[\frac{\partial}{\partial y}\left(N\frac{\partial C}{\partial y} \right) \right] = D_m\left(\frac{\partial^2 N}{\partial y^2} \right). \tag{3.1.7}$$

The values of Λ_e and Λ_c in the above equations are interpreted as:

$$\Lambda_e = u\frac{\partial u}{\partial x}\frac{\partial T}{\partial x} + v\frac{\partial v}{\partial y}\frac{\partial T}{\partial y} + u\frac{\partial v}{\partial x}\frac{\partial T}{\partial y} + v\frac{\partial u}{\partial y}\frac{\partial T}{\partial x} + 2uv\frac{\partial^2 T}{\partial x\partial y} + u^2\frac{\partial^2 T}{\partial x^2} + v^2\frac{\partial^2 T}{\partial y^2} \tag{3.1.8}$$

$$\Lambda_c = u\frac{\partial u}{\partial x}\frac{\partial C}{\partial x} + v\frac{\partial v}{\partial y}\frac{\partial C}{\partial y} + u\frac{\partial v}{\partial x}\frac{\partial C}{\partial y} + v\frac{\partial u}{\partial y}\frac{\partial C}{\partial x} + 2uv\frac{\partial^2 C}{\partial x\partial y} + u^2\frac{\partial^2 C}{\partial x^2} + v^2\frac{\partial^2 C}{\partial y^2} \tag{3.1.9}$$

The corresponding boundary conditions are:

$$u(x,0) = ax^n, \quad v(x,0) = 0, \quad T(x,0) = T_w, \quad C(x,0) = C_w, \quad N(x,0) = N_w,$$

$$u \to 0, \quad v \to 0, \quad T \to T_\infty, \quad C \to C_\infty, \quad N \to N_\infty \quad \text{as} \quad y \to \infty \tag{3.1.10}$$

To examine the flow regime, the following similarity variables are introduced [134,156,184]

$$\eta = y\sqrt{\tfrac{a(n+1)}{2\nu}}x^{\frac{(n-1)}{2}}, \qquad u = ax^n f'(\eta), \qquad v = -\sqrt{\tfrac{a(n+1)\nu}{2}}x^{\frac{(n-1)}{2}}\left(f + \tfrac{(n-1)}{(n+1)}\eta f'\right),$$

$$\theta(\eta) = \left(\tfrac{T-T_\infty}{T_w-T_\infty}\right), \qquad \phi(\eta) = \left(\tfrac{C-C_\infty}{C_w-C_\infty}\right), \qquad \chi(\eta) = \left(\tfrac{N-N_\infty}{N_w-N_\infty}\right).$$

The equation of continuity (3.1.3) is satisfied by the above mentioned transformation and rest of the equations (3.1.4-3.1.7) are:

$$f''' + ff'' - \left(\frac{2n}{n+1}\right)(f')^2 + \left(\frac{2}{n+1}\right)\frac{Gr}{Re^2}(\theta - Nr\phi - Rb\chi) = 0, \tag{3.1.11}$$

$$\theta'' + Pr\theta'(f + Nb\phi') + Nt(\theta')^2 + \beta_e Pr\left(\left(\frac{n-3}{2}\right)\theta' ff' - \left(\frac{n+1}{2}\right)f^2\theta''\right) = 0 \tag{3.1.12}$$

$$\phi'' + Lef\phi' + \left(\frac{Nt}{Nb}\right)\theta'' + \beta_c Pr\left(\left(\frac{n-3}{2}\right)\phi' ff' - \left(\frac{n+1}{2}\right)f^2\phi''\right) = 0, \tag{3.1.13}$$

$$\chi'' + Lbf\chi' - Pe[\phi''(\Omega + \chi) + \phi'\chi'] = 0. \tag{3.1.14}$$

where,

$$\tfrac{Gr}{Re^2} = \tfrac{(g\beta(1-C_\infty)(T_w-T_\infty)x^3/\nu^2)}{u_w^2x^2/\nu^2}, \quad Nr = \tfrac{(\rho_p-\rho_f)(C_w-C_\infty)}{\rho\beta(1-C_\infty)(T_w-T_\infty)}, \quad Rb = \tfrac{\gamma_e(\rho_m-\rho_f)(N_w-N_\infty)}{\rho\beta(1-C_\infty)(T_w-T_\infty)},$$

$$Pr = \tfrac{\nu}{\alpha}, \quad Le = \tfrac{\nu}{D_B}, \quad Lb = \tfrac{\nu}{D_m}, \quad Pe = \tfrac{bW_c}{D_m}, \quad \Omega = \tfrac{N_\infty}{(N_w-N_\infty)},$$

$\beta_e = \delta_e a x^{b-1}$, $\beta_c = \delta_c a x^{n-1}$.

The prime denotes derivatives with respect to η. The dimensionless number obtained in the equations (3.1.11- 3.1.14) are listed in nomenclature.

The corresponding boundary conditions after normalization are:

$$f(0) = 0, \quad f'(0) = 1, \quad \theta(0) = 1, \quad \phi(0) = 1, \quad \chi(0) = 1,$$

$$f'(\infty) = 0, \quad \theta(\infty) = 0, \quad \phi(\infty) = 0, \quad \chi(\infty) = 0 \tag{3.1.15}$$

τ_w, q_w, q_m and q_n represents shear stress, heat flux, mass flux and motile micro-organisms flux at the wall, respectively. These are defined as

$$\tau_w = \mu\left(\frac{\partial u}{\partial y}\right)_{y=0}, q_w = -k\left(\frac{\partial T}{\partial y}\right)_{y=0}, q_m = -D_B\left(\frac{\partial C}{\partial y}\right)_{y=0}, q_n = -D_m\left(\frac{\partial N}{\partial y}\right)_{y=0}. \tag{3.1.16}$$

The quantities of interest for practical purpose are skin friction coefficient Cf_x, Nusselt number Nu_x, Sherwood number Sh_x and density number Nn_x. These quantities are defined as

$$Cf_x = \frac{\tau_w}{\rho u_w^2}, \quad Nu_x = \frac{xq_w}{k(T_w - T_\infty)}, \quad Sh_x = \frac{xq_m}{D_B(C_w - C_\infty)}, \quad Nn_x = \frac{xq_n}{D_m(N - N_\infty)}. \tag{3.1.17}$$

On combining the equations (3.1.16) and (3.1.17), we get

$$\begin{aligned} Re_x^{-1/2}Cf_x &= \sqrt{\frac{n+1}{2}}f''(0), \quad Re_x^{-1/2}Nu_x = -\sqrt{\frac{n+1}{2}}\theta'(0), \\ Re_x^{-1/2}Sh_x &= -\sqrt{\frac{n+1}{2}}\phi'(0), \quad Re_x^{-1/2}Nn_x = -\sqrt{\frac{n+1}{2}}\chi'(0) \end{aligned} \tag{3.1.18}$$

3.2 Methodology

The system of non-linear ordinary differential equation (3.1.11 - 3.1.14) subjected to boundary conditions 3.1.15 has been solved numerically by finite element method. Momentum equation 3.1.11 is third order equation and is coupled with energy, nanoparticles concentration and density of motile micro-organisms equations by buoyancy term. So, these equations are solved in the coupled form. In order to convert third order equation into second order, we assume:

$$f' = h, \tag{3.2.1}$$

$$h'' + fh' - \left(\frac{2n}{n+1}\right)(h)^2 + \left(\frac{2}{n+1}\right)\frac{Gr}{Re^2}(\theta - Nr\phi - Rb\chi) = 0, \tag{3.2.2}$$

$$\theta^{''} + Pr\theta^{'}(f + Nb\phi^{'}) + Nt(\theta^{'})^2 + \beta_e Pr\left(\left(\frac{n-3}{2}\right)\theta^{'}fh - \left(\frac{n+1}{2}\right)f^2\theta^{''}\right) = 0 \tag{3.2.3}$$

$$\phi^{''} + Lef\phi^{'} + \left(\frac{Nt}{Nb}\right)\theta^{''} + \beta_c Pr\left(\left(\frac{n-3}{2}\right)\phi^{'}fh - \left(\frac{n+1}{2}\right)f^2\phi^{''}\right) = 0, \tag{3.2.4}$$

$$\chi^{''} + Lbf\chi^{'} - Pe[\phi^{''}(\Omega + \chi) + \phi^{'}\chi^{'}] = 0. \tag{3.2.5}$$

The corresponding boundary conditions (3.1.15) transformed to:

$$f(0) = 0, \quad h(0) = 1, \quad \theta(0) = 1, \quad \phi(0) = 1, \quad \chi(0) = 1,$$

$$h(\infty) = 0, \quad \theta(\infty) = 0, \quad \phi(\infty) = 0, \quad \chi(\infty) = 0 \tag{3.2.6}$$

To derive the resulting finite element equations, the problem domain is divided into eighty two-noded line elements. The error tolerance has been considered to be 10^{-4}. The choice of $\eta_\infty = 7$ satisfies the boundary layer conditions. If η_∞ is more than 4, the desired accuracy of all the unknown functions remain unaltered.

3.3 Results & Discussion

The coupled non-linear differential Eqs (3.2.2 - 3.2.5) along with the boundary conditions (3.2.6) are solved by an efficient numerical technique i.e, finite element method. The impact of various key parameters such as $\frac{Gr}{Re^2}$, Nr, Rb, Le, Lb, Pe, Ω, β_e, β_c on flow behavior via velocity field $f^{'}(\eta)$, temperature profile $\theta(\eta)$, nanoparticle concentration $\phi(\eta)$ and density of gyrotactic micro-organisms $\chi(\eta)$ are presented in figures (3.2-3.6). The influence of varied Richardson number ($\frac{Gr}{Re^2}$) and constant values of other governing parameters on velocity field is depicted in figure 3.2a. Various analysts determined that convection due to density gradient is insignificant when $\frac{Gr}{Re^2} < 0.1$ though forced convection is irrelevant when $\frac{Gr}{Re^2} > 10$. Both free and forced convection play its role simultaneously for $0.1 < \frac{Gr}{Re^2} < 10$. In view of this fact, it is observed in figure 3.2a that velocity increases with an increase in $\frac{Gr}{Re^2}$. It is also found that there is a significant rise in flow speed accompanying an accentuation in natural convection. For high $\frac{Gr}{Re^2}$ values (>10), the monotonic decay of profiles morphs, and a speed overshoot is seen close to the heated surface. This overshoot in the velocity profile is more prominent when $\frac{Gr}{Re^2}$ increases from 20 to 30. As the flow is accelerated,

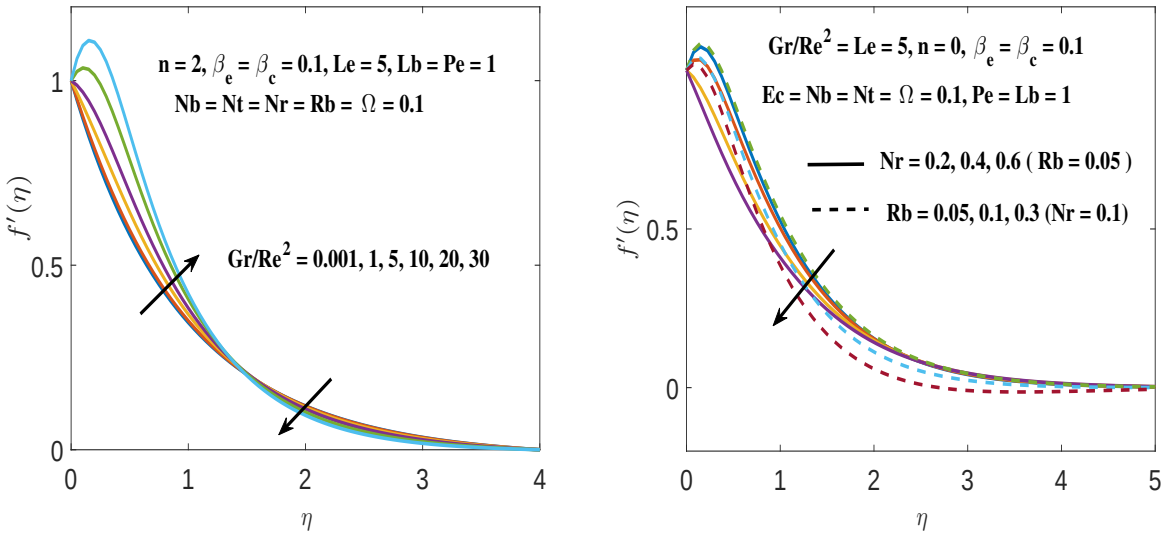

(a) Effect of $\frac{Gr}{Re^2}$ (b) Effect of Nr and Rb

Figure 3.2: Effect of varied thermophysical parameters on velocity profiles

momentum boundary layer thickness decreases with a higher Richardson number (stronger natural convection buoyancy effect). Figure 3.2b shows the effect of bioconvection Rayleigh number and buoyancy ratio parameter Nr on the velocity field. It can be seen in the figure that the overshoot in the velocity tends to decrease with an increase in Rb and Nr. The classical Rayleigh number is the ratio of buoyancy forces to the viscous forces multiplied by the ratio of momentum diffusivity to thermal diffusivity. The bioconvection Rayleigh number is the modified version of the traditional Rayleigh number. The numerator of Rb consists of contribution from buoyancy effects of motile micro-organisms and in the denominator, thermal buoyancy force. It is also found in figure 3.2b that flow speed declines with a rise in the buoyancy ratio parameter, Nr . It consolidates the relative contribution of nanoparticle species buoyancy to thermal buoyancy. The thermal buoyancy overwhelms the nanoparticle species buoyancy for Nr <1 (as studied here). This manifests in the enhancement of flow velocity and a decrease in the momentum boundary layer thickness. With an increase in values of Rb and Nr, velocity decreases. Figures 3.3a-b demonstrate the temperature profiles for different thermophysical parameters. In figure 3.3a, it is apparent that at the fixed value of other parameters, the temperature profile diminishes with higher values of thermal relaxation time parameter β_e. This is often inferable to the fact that if β_e is high, more time is taken by the fluid particles to transfer heat to the adjacent particles of the fluid due to this thickness of thermal boundary thickness increases. In figure 3.3b, the temperature profile for varying Richardson number is plotted. It is observed from the figure that there is no significant variation in the temperature field with higher

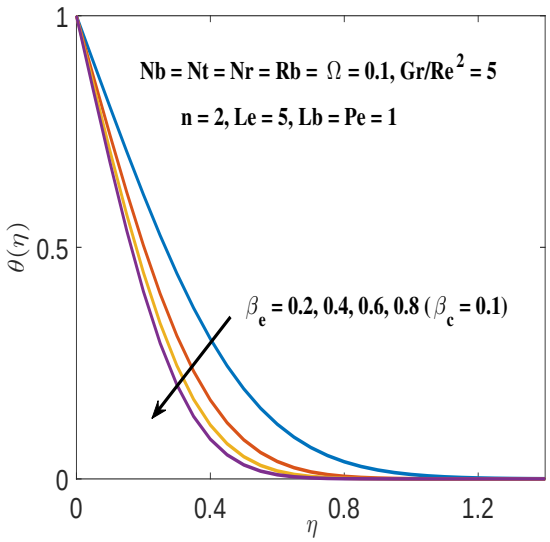

(a) Effect of β_e

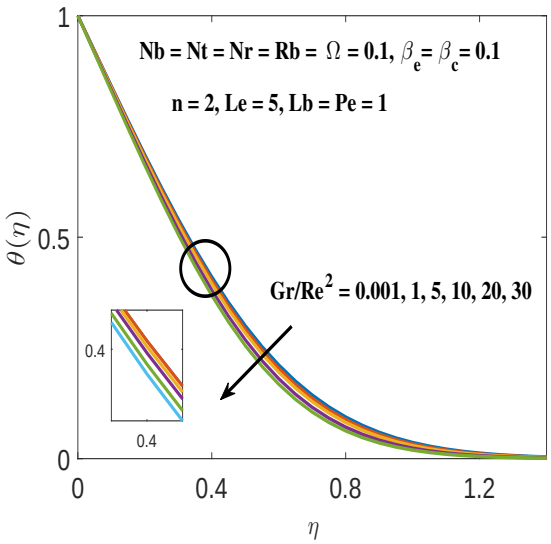

(b) Effect of $\frac{Gr}{Re^2}$

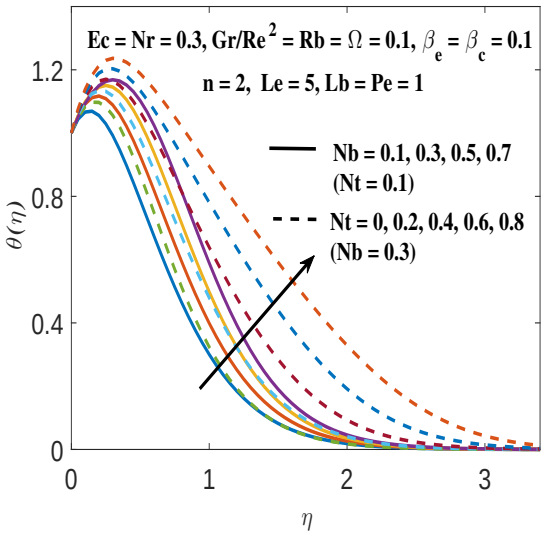

(c) Effect of Nb and Nt

Figure 3.3: Effect of varied thermophysical parameters on temperature profiles

values of Richardson number ($\frac{Gr}{Re^2}$). Consequently, the thickness of the boundary layer for temperature also does not show remarkable change with an increase in Richardson number. In figure 3.3c, it reveals that temperature is boosted with higher values of Brownian motion (Nb) and thermophoresis (Nt) numbers. This happened because supplementary heat is generated by the interaction of nanoparticles and the base fluid due to Brownian motion and thermophoresis effects. Consequently, the thermal boundary layer becomes thicker, and the effect is so prominent that temperature overshoots are observed in the vicinity of the heated surface for increasing values of Nb and Nt. Figures 3.4a-c visualize the conveyances of nanoparticle concentration for various estimations of parameters, for example, concentration relaxation time parameter β_c, Richardson number $\frac{Gr}{Re^2}$, Lewis number (Le). Influence of concentration relaxation time parameter (β_c) is depicted in fig 3.4a. Concentration distribution declines with higher values of concentration relaxation time parameter (β_c). This behavior is observed because as the (β_c) enhances, fluid particles diffuses gradually. Consequently, the concentration profile of nanoparticles decays. In figure 3.4b, it is apparent that nanoparticles fixation diminishes inside the boundary layer with an expansion in Richardson number (largely associated with the concomitant flow acceleration). It is disclosed in figure 3.4c, the concentration $\phi(\eta)$ also decreases with an increase in Lewis number (Le). In the present computations ($Le \geq 1$), which signifies physically that the thermal diffusivity of the nanofluid is higher than its species diffusivity. The increasing Lewis number manifests that there is a strong depression in nanoparticles concentration throughout the boundary layer regime transverse to the heated surface.

Figures 3.5a-b demonstrates the impact of bioconvection Lewis number Lb, Peclet number Pe, and concentration difference parameter on the density of motile gyrotactic micro-organisms. It can be seen from the figure 3.5a that density of motile micro-organisms is significantly diminshed with expanding (Lb) and (Pe). These two parameters dictate the bioconvection phenomenon in the boundary layer. The Peclet number in the bioconvection is the proportion of the rate of advection of micro-organisms to the rate of diffusion of micro-organisms under gyrotaxis. Customarily Peclet number is related to heat transfer processes due to convection. It is classically defined as the heat transport through convection to that by means of thermal conduction. In biconvection, adequately high values of this parameter drastically alter the flow patterns of motile micro-organisms. The internal energy of the micro-organisms is the source of bioconvection originates, as depicted in detail by Beg [21] and prior by Hill and Pedley [102]. With a more prominent Peclet number, the micro-organisms move with higher speed which reduces their concentration. At lower Pe the reverse effect is observed, i.e., the motion of the micro-organisms is hindered, and they move slower, as observed in figure 3.5a. This parameter can in this manner be controlled through the selection of various micro-organisms to achieve a different distribution in combination

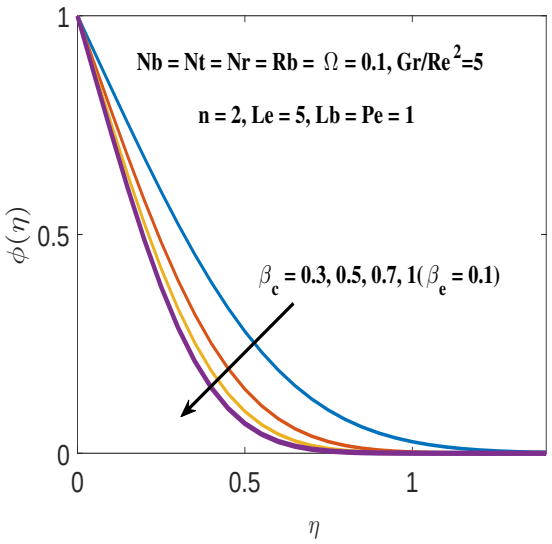

(a) Effect of β_c

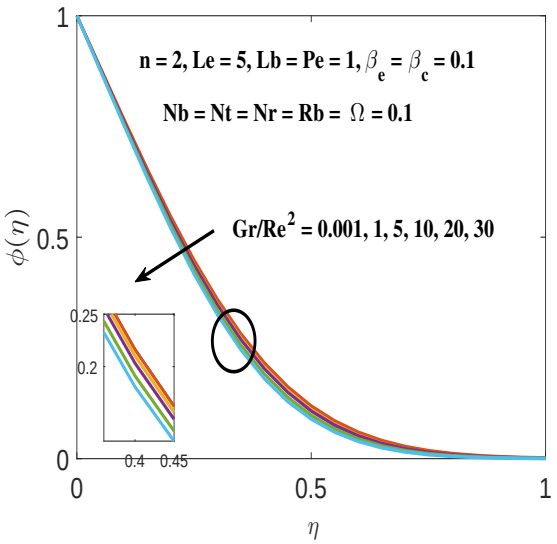

(b) Effect of $\frac{Gr}{Re^2}$

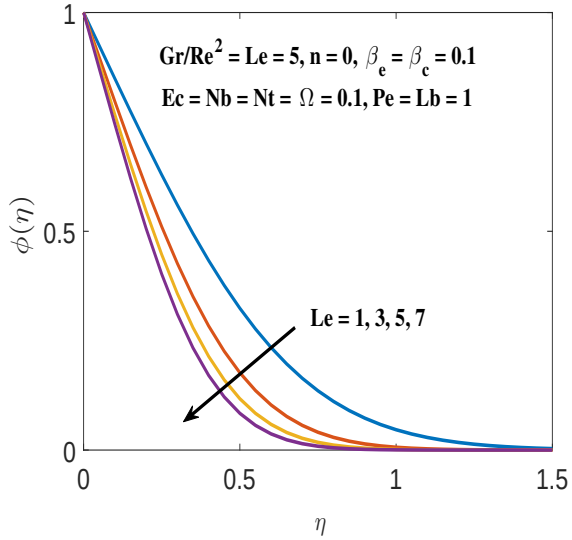

(c) Effect of Le

Figure 3.4: Effect of varied thermophysical parameters on concentration profiles

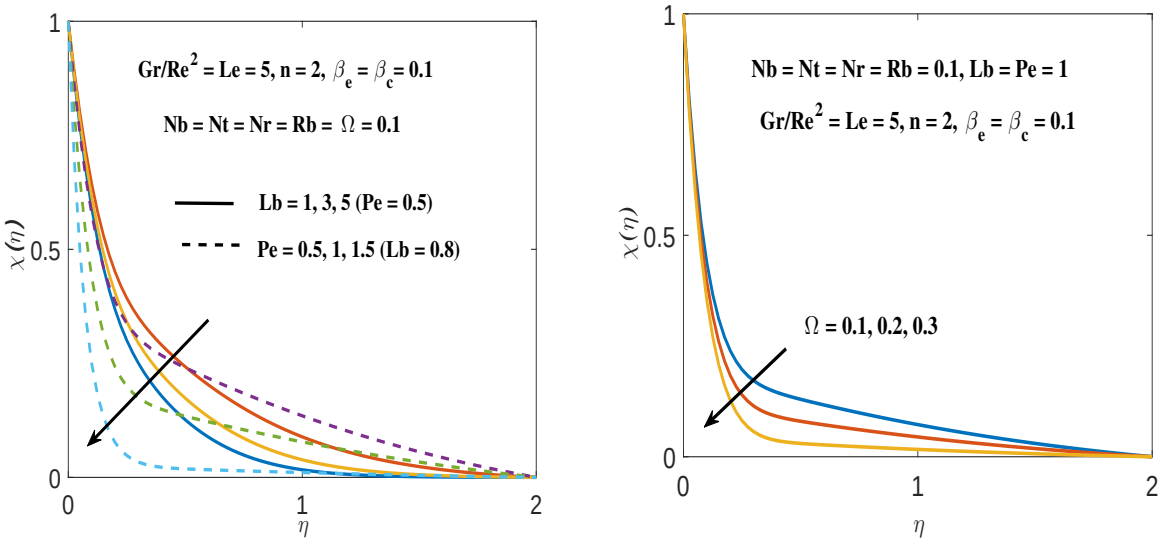

(a) Effect of Lb and Pe (b) Effect of Ω

Figure 3.5: Effect of varied thermophysical parameters on density profiles

with different nanoparticles. The bioconvection Lewis number (Lb) is connected with micro-organism concentration layer thickness. Physically, this is clarified by the way that as the Lb rises, the density of micro-organisms decreases due to decrease in velocity as the viscous diffusion rate increases. Bioconvection Lewis number in this way relates the viscosity of the fluid to the diffusivity of motile micro-organism. The aiding effect of increasing Lb is inferable to the decrease in D_n relative to α. The motile micro-organism rescaled density boundary layer thickness is diminished both with increasing Lb and Pe numbers. The decrease in density infers a reduction in the settling of micro-organisms with greater bioconvection. This encourages mixing and species diffusion in the nanofluid. The introduction of nanoparticles into the bioconvection regime additionally modifies the conveyances of motile micro-organisms. Figure 3.5b demonstrates that with increasing values of the micro-organism concentration difference parameter (Ω) there is a non-trivial enhancement in the motile micro-organisms density number. This parameter emerges only in the micro-organisms conservation equation (3.1.14) and clearly, when increased serves to boost the concentration of the micro-organism boundary layer thickness. The impact of Richard number $\frac{Gr}{Re^2}$, thermal relaxation time parameter (β_e) on skin friction and Nusselt number is depicted in figure 3.6a-b. Due to the presence of nanoparticles, motile micro-organisms push the fluid towards the heated surface, subsequently enhance the friction at the heated surface. Also, with an increase in thermal relaxation parameters, the skin friction coefficient increases. The rate of heat transfer increases with variation in $\frac{Gr}{Re^2}$ and β_e. It has been noticed in figure 3.6c that with an increase in Lewis number and

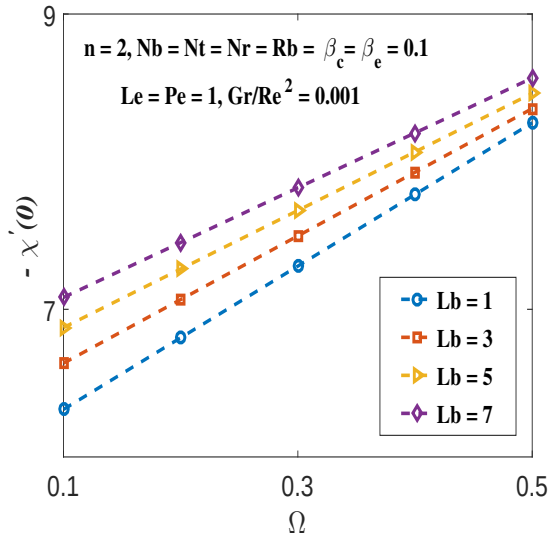

(a) Effect of β_e and $\frac{Gr}{Re^2}$

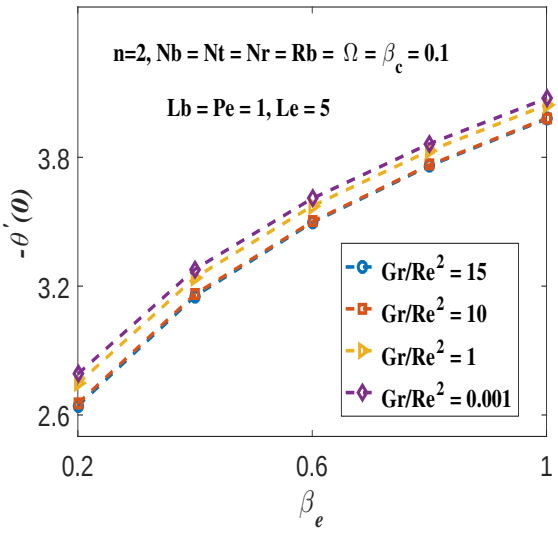

(b) Effect of β_e and $\frac{Gr}{Re^2}$

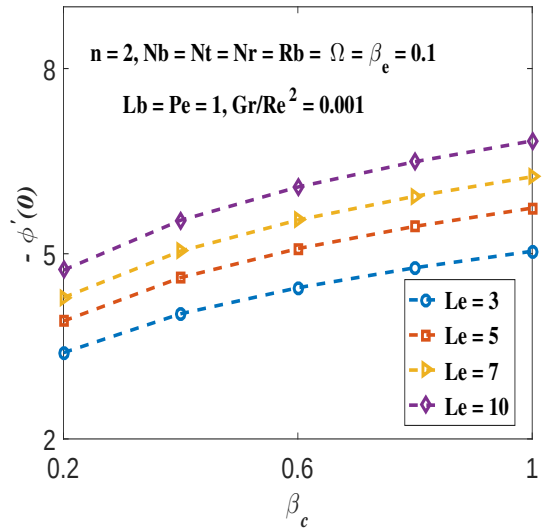

(c) Effect of β_c and $\frac{Gr}{Re^2}$

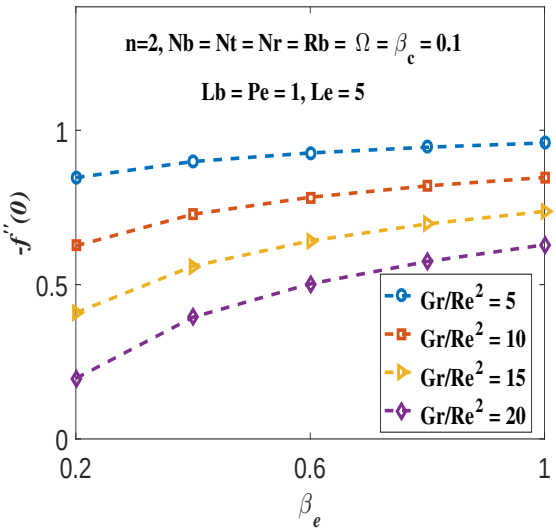

(d) Effect of Ω and Lb

Figure 3.6: Effect of varied thermophysical parameters on Skin Friction, Nusselt number, Sherwood number and Density number

concentration relaxation time parameter, Sherwood number also increases. It is observed in figure 3.6d density number enhances with Ω and Lb.

3.4 Conclusions

The influence of the Cattaneo-Christov heat flux and mass flux model on bioconvection over a continuous heated surface is investigated in the present study. A similarity solution is obtained, which depends upon various thermophysical parameters. The following observations are worth mentioning :

- The dimensionless velocity increases with increasing values of Richardson number while a reverse pattern is observed for bioconvection Rayleigh number and Buoyancy ratio parameter.
- Temperature varies insignificantly with a higher Richardson number. On the other hand, the temperature profile declines when the Cattaneo-Christov heat flux model is employed.
- The concentration profile shows similar behavior as shown by the temperature profile for a larger Richardson number and concentration relaxation time parameter and Lewis number.
- It is ascertained that the density of motile micro-organisms drops with improvement in bioconvection constant, bioconvection Lewis number, and Peclet number.
- Friction between fluid and heated surface increases with higher values of Richardson number and thermal relaxation time parameter.
- Both Nusselt number and Sherwood number rise with thermal relaxation time parameter, concentration relaxation time parameter, Richardson number, and Lewis number.
- Increasing bioconvection Lewis number and micro-organisms concentration difference parameter results in enhancement of density number of motile micro-organisms.

Chapter 4

Theoretical Analysis of flow of Eyring-Powell fluid over a Exponential Stretching Sheet by utilizing non-Fourier Heat Flux Model

4.1 Introduction

Recently, non-Newtonian fluids are found more appropriate for technical and engineering applications than Newtonian fluids. These fluids are having wide variety of applications in engineering and industries such as in the food processing industries, metallurgical processes, extraction of petroleum products from crude oil, drilling operations, and bio-engineering processes [77]. Thus researchers are more interested in the complex field of non-Newtonian fluids. The materials such as clay, mud, ketchup, blood, honey, paints, slurries, melted chocolates, egg whites, mayonnaise, etc., exhibit non-Newtonian behavior, i.e., their viscosity changes with applied stresses. There is no single model that demonstrate all the properties of non-Newtonian fluids due to the complex flow behavior. To understand the mechanism involved in the flow of these fluids, researchers proposed various flow models from time to time, such as power-law model [41, 42], Jeffrey fluid model [203], Maxwell fluid model [8], micropolar fluids [24] and Eyring-Powell model [180]. Out of these non-Newtonian fluid models, Eyring-Powell fluid model has special characteristics as this model was derived from the kinetic theory of gases instead of empirical relations. Moreover, this fluid model shows the behavior of Newtonian fluids at low and high shear rates but deviates at intermediate shear stresses. Various researchers investigate the flow behavior of Eyring-Powell fluid under different situations [2, 9, 78, 94, 95, 141, 161, 176].

Flow problems involve the exponential dependence of the similarity variables as the stretching velocity, and temperature distribution are presented by exponentially stretching surface. Mainly the researchers gave the solutions for two-dimensional exponentially stretching flows. Thermal boundary layer flow over an exponentially stretching continuous surface with magnetic field effect was investigated numerically by Al-Odat et al. [6]. Analytical solutions of nanofluid flow over an exponential stretching surface were presented by Nadeem

and Lee [158]. Heat transfer analysis over an exponentially shrinking surface by applying shooting method was investigated by Bhattacharyya [27]. Heat transfer over a permeable stretching surface for a Casson fluid was studied by Mukhopadhyay et al. [152]. After that, Three-dimensional viscous flow in the presence of heat transfer over an exponentially stretching surface is studied by Liu et al. [132]. Recently Ashraf et al. [10] extended the flow of Liu et al. [132] by considering the viscoelastic fluid. Many researchers focused on the magnetohydrodynamic flow of an electrically conducting fluid due to its numerous applications in the metallurgical industry, such as drawing, annealing, purification of molten metals from non-metallic inclusions electromagnetic pumps, MHD generators, and so on. The authors presented several studies in the presence of a transverse magnetic field over a stretching surface. Mukhopadhyay et al. [150] showed magnetohydrodynamic boundary layer flow with variable viscosity over a stretching surface. Using the successive Taylor series linearization method, Motsa et al. [148] obtained solutions for upper convected Maxwell fluid over a porous stretching sheet in the presence of the magnetic field. Rashidi and Erfani [187] investigated stagnation-point flow in porous media with a magnetic field.

Thus, the goal of this study is to investigate the three-dimensional flow of an Eyring Powell fluid with convective boundary conditions using the finite element method [193]. The problem's novelty is that it investigates for the Catteneo-Christov heat flux model for three-dimensional flow of Erying- Powell fluid. For different values of embedding parameters, numerical values of the skin-friction coefficient, Nusselt number, and Sherwood number are obtained and discussed.

4.2 Mathematical Model

We consider the three-dimensional boundary layer flow of Eyring Powell fluid over an exponential stretching surface. The surface coincides with the plane, $z = 0$ and the flow is restricted to the region $z > 0$. Figure 4.1 represents the flow problem configuration as well as the co-ordinate axis. Brownian motion and thermophoresis are taken into account. The Cauchy stress tensor T for an Eyring Powell Fluid can be written as [9]:

$$T = -pI + \tau_{ij} \tag{4.2.1}$$

$$\rho a_i = -\nabla p + \nabla.\tau_{ij} \tag{4.2.2}$$

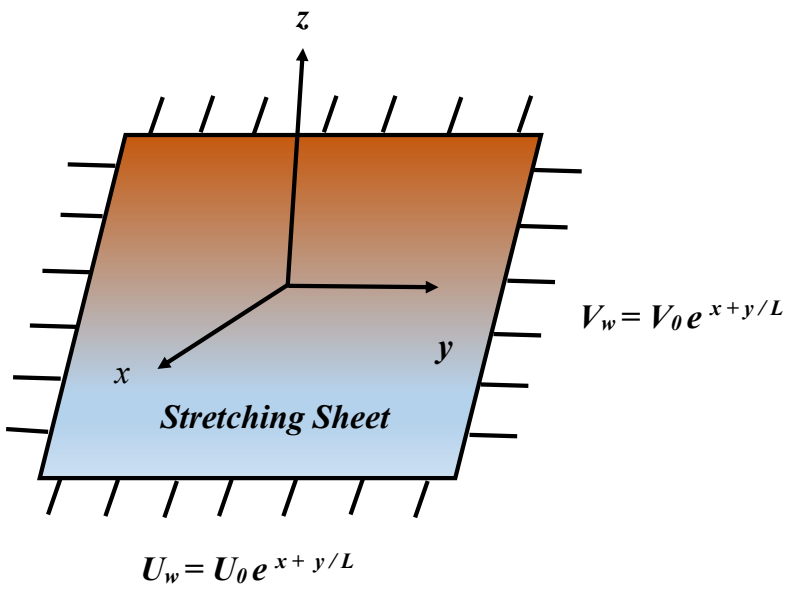

Figure 4.1: Schematic model and coordinates system

where extra stress tensor τ_{ij} is

$$\tau_{ij} = mu\frac{\partial u_i}{\partial x_j} + \frac{1}{\xi}sinh^{-1}\left(\frac{1}{c}\frac{\partial u_i}{\partial x_j}\right) \tag{4.2.3}$$

in which ξ and c are the Eyring-Powell fluid characterstics, p is the pressure and I is the identity tensor. Taking

$$sinh^{-1}\left(\frac{1}{c}\frac{\partial u_i}{\partial x_j}\right) \approx \frac{1}{c}\frac{\partial u_i}{\partial x_j} - \frac{1}{6}\left(\frac{1}{c}\frac{\partial u_i}{\partial x_j}\right)^3, \qquad \left|\frac{1}{c}\frac{\partial u_i}{\partial x_j}\right| < 1. \tag{4.2.4}$$

With these assumptions, the governing equations for the three-dimensional flow can be put into the form:

$$\frac{\partial u}{\partial x} + \frac{\partial v}{\partial y} + \frac{\partial w}{\partial z} = 0, \tag{4.2.5}$$

$$u\frac{\partial u}{\partial x} + v\frac{\partial u}{\partial y} + w\frac{\partial u}{\partial z} = \left(\nu + \frac{1}{\xi c\rho}\right)\frac{\partial^2 u}{\partial z^2} - \frac{1}{2\beta' c^3\rho}\left(\frac{\partial u}{\partial z}\right)^2\frac{\partial^2 u}{\partial z^2} - \frac{\sigma^* B_0^2}{\rho}u + g\beta(T - T_\infty) + g\beta_b(C - C_\infty), \tag{4.2.6}$$

$$u\frac{\partial v}{\partial x} + v\frac{\partial v}{\partial y} + w\frac{\partial v}{\partial z} = \left(\nu + \frac{1}{\xi c\rho}\right)\frac{\partial^2 v}{\partial z^2} - \frac{1}{2\beta' c^3\rho}\left(\frac{\partial v}{\partial z}\right)^2\frac{\partial^2 v}{\partial z^2} - \frac{\sigma^* B_0^2}{\rho}v, \tag{4.2.7}$$

$$(\rho c_p)\left(u\frac{\partial T}{\partial x}+v\frac{\partial T}{\partial y}+w\frac{\partial T}{\partial z}\right)=-\nabla.q^{'} \tag{4.2.8}$$

$$u\frac{\partial C}{\partial x}+v\frac{\partial C}{\partial y}+w\frac{\partial C}{\partial z}=D_B\frac{\partial^2 C}{\partial z^2}+\frac{D_T}{T_\infty}\frac{\partial^2 T}{\partial z^2}-k_1(C-C_\infty), \tag{4.2.9}$$

The heat flux $q^{'}$ is given by

$$q^{'}+\lambda_e\left[\frac{\partial q^{'}}{\partial t}+V.\nabla q^{'}+(\nabla.V)q^{'}-q^{'}.\nabla V\right]=-K\nabla T. \tag{4.2.10}$$

we eliminate $q^{'}$ from equations (4.2.8) and (4.2.10) to obtain the following:

$$u\frac{\partial T}{\partial x}+v\frac{\partial T}{\partial y}+w\frac{\partial T}{\partial z}=\frac{K}{\rho c_p}\frac{\partial^2 T}{\partial z^2}-\lambda_e\left(u^2\frac{\partial^2 T}{\partial x^2}+v^2\frac{\partial^2 T}{\partial y^2}+w^2\frac{\partial^2 T}{\partial z^2}+2uv\frac{\partial^2 T}{\partial x\partial_y}+2vw\frac{\partial^2 T}{\partial y\partial_z}+\right.$$
$$2wu\frac{\partial^2 T}{\partial z\partial_x}+\left(u\frac{\partial u}{\partial x}+v\frac{\partial u}{\partial y}+w\frac{\partial u}{\partial z}\right)\frac{\partial T}{\partial y}+\left(u\frac{\partial u}{\partial x}+v\frac{\partial u}{\partial y}+w\frac{\partial u}{\partial z}\right)\frac{\partial T}{\partial x}+$$
$$\left.\left(u\frac{\partial u}{\partial x}+v\frac{\partial u}{\partial y}+w\frac{\partial u}{\partial z}\right)\frac{\partial T}{\partial z}\right) \tag{4.2.11}$$

The boundary conditions can be expressed in the form

$$u=U_w,\quad v=V_w,\quad w=0,\quad -k\frac{\partial T}{\partial z}=h(T_{f'}-T),\quad -D\frac{\partial T}{\partial z}=h^*(C_{f'}-C)$$

$$\text{at}\ \ z=0\ \ \text{and}\ \ u\to 0,\quad v\to 0,\quad T\to T_\infty,\quad C\to C_\infty\ \ \text{as}\ \ z\to\infty \tag{4.2.12}$$

where subscript w corresponds to the wall condition, h is the heat transfer coefficient, h^* is the concentration transfer coefficient, $T_{f'}$ is the ambient fluid temperature and $C_{f'}$ is the ambient fluid concentration. At wall the velocities and temperature are

$$U_w=U_0e^{\frac{x+y}{L}},\quad V_w=V_0e^{\frac{x+y}{L}},\quad T_w=T_\infty+T_0e^{\frac{A(x+y)}{2L}},\quad C_w=C_\infty+C_0e^{\frac{B(x+y)}{2L}} \tag{4.2.13}$$

Following transformations are used to convert the governing equations into non-dimensional form:

$$u=U_0e^{\frac{x+y}{L}}f^{'}(\eta),\quad v=U_0e^{\frac{x+y}{L}}g^{'}(\eta),\quad w=-\left(\frac{\nu U_0}{2L}\right)^{1/2}e^{\frac{x+y}{2L}}(f+\eta f^{'}+g+\eta g^{'}),$$
$$T=T_\infty+T_0e^{\frac{A(x+y)}{2L}}\theta(\eta),\quad C=C_\infty+C_0e^{\frac{B(x+y)}{2L}}\phi(\eta),\quad \eta=\left(\frac{U_0}{2\nu L}\right)^{1/2}e^{\frac{x+y}{2L}}z. \tag{4.2.14}$$

Now equation (4.2.5) is identically satisfied and equations(4.2.6) - (4.2.11) yield

$$(1+\epsilon)f^{'''}+(f+g)f^{''}-2(f^{'}+g^{'})f^{'}-\epsilon\varsigma(f^{''})^2f^{'''}-Haf^{'}+\lambda_e\theta+\lambda_c\phi=0, \tag{4.2.15}$$

$$(1+\epsilon)g^{'''}+(f+g)g^{''}-2(f^{'}+g^{'})g^{'}-\epsilon\varsigma(g^{''})^2g^{'''}-Hag^{'}=0, \tag{4.2.16}$$

$$\frac{1}{Pr}\theta^{''}+\frac{\beta_e}{2}(A\theta(f+g)(f^{''}+g^{''})-A\theta(2+A)(f^{'}+g^{'})^2+(1+2A)(f^{'}+g^{'})(f+g)\theta^{'}-$$
$$(f+g)^2\theta^{''})-A\theta(f^{'}+g^{'})+\theta^{'}(f+g)=0 \tag{4.2.17}$$

$$\phi^{''}+Sc(f+g)\phi^{'}-ScB(f^{'}+g^{'})\phi+\frac{Nt}{Nb}\theta^{''}-Sck\phi=0. \tag{4.2.18}$$

The corresponding boundary conditions after normalization are as follows:

$$f=0,\quad g=0,\quad f^{'}=1,\quad g^{'}=\alpha,\quad \theta^{'}=-\gamma_1(1-\theta(0)),\quad \phi^{'}=-\gamma_2(1-\phi(0)),$$

$$\text{at}\ \ \eta=0,\ \ \text{and}\ \ f^{'}\to 0,\ \ g^{'}\to 0,\ \ \theta\to 0,\ \ \phi\to 0\ \ \text{as}\ \ \eta\to\infty, \tag{4.2.19}$$

$$\epsilon=\frac{1}{\mu\beta^{'}c},\quad \varsigma=\frac{U_0^3e^{\frac{3(x+y)}{L}}}{2\nu c^2l},\quad Pr=\frac{\nu}{\alpha},\quad Nb=\frac{\rho c_pD_B(C_w-C_\infty)}{\rho c\nu},\quad k=\frac{k_1}{U_0},$$

$$Ha=\frac{\sigma}{B_0^2}\rho, Nt=\frac{\rho c_pD_T(T_w-T_\infty)}{\rho cT_\infty\nu},\quad Sc=\frac{\nu}{D_B}, \alpha^{'}=\frac{V_0}{U_0},\quad \gamma_1=\frac{h}{k}\sqrt{\frac{\nu}{a}},$$

$$\gamma_2=\frac{h^*}{D}\sqrt{\frac{\nu}{a}},\quad \gamma=\frac{\lambda_1U_0e^{\frac{x+y}{L}}}{L}. \tag{4.2.20}$$

4.3 Methodology

The system of non-linear ordinary differential equations (4.2.15 - 4.2.18) subjected to boundary conditions (4.2.19) has been solved numerically by finite element method. Momentum equations (4.2.15, 4.2.16) is third-order coupled equations. So, these equations are solved in the coupled form. To convert third order equation into second order, we

assume:

$$f^{'} = h, \tag{4.3.1}$$

$$g^{'} = l, \tag{4.3.2}$$

$$(1+\epsilon)h^{''} + (f+g)h^{'} - 2(f^{'}+g^{'})f^{'} - \epsilon\varsigma(h^{'})^2 h^{''} - Mf^{'} + \lambda_e\theta + \lambda_c\phi = 0, \tag{4.3.3}$$

$$(1+\epsilon)l^{''} + (f+g)l^{'} - 2(f^{'}+g^{'})g^{'} - \epsilon\varsigma(l^{'})^2 l^{''} - Hag^{'} = 0, \tag{4.3.4}$$

$$\frac{1}{Pr}\theta^{''} + \frac{\gamma}{2}(A\theta(f+g)(h^{'}+l^{'}) - A\theta(2+A)(f^{'}+g^{'})^2 + (1+2A)(f^{'}+g^{'})(f+g)\theta^{'} - (f+g)^2\theta^{''}) - A\theta(f^{'}+g^{'}) + \theta^{'}(f+g) = 0 \tag{4.3.5}$$

$$\phi^{''} + Sc(f+g)\phi^{'} - ScB(f^{'}+g^{'})\phi + \frac{Nt}{Nb}\theta^{''} - Sck\phi = 0. \tag{4.3.6}$$

The corresponding boundary conditions takes the form:

$$f = 0, \quad g = 0, \quad h = 1, \quad l = \alpha, \quad \theta^{'} = -\gamma_1(1-\theta(0)), \quad \phi^{'} = -\gamma_2(1-\phi(0)),$$

$$\text{at} \quad \eta = 0, \quad \text{and} \quad h \to 0, \quad l \to 0, \quad \theta \to 0, \quad \phi \to 0 \quad \text{as} \quad \eta \to \infty, \tag{4.3.7}$$

4.4 Validation of Results

The results has been validated with previous obtained results by Bilal et al. [9] by considering special case in which thermal relaxation time $\beta_e = 0$ and is presented in figure 4.2.

4.5 Results & Discussion

The non-linear, coupled ordinary differential equations (4.2.14 - 4.2.17) with boundary conditions (4.2.18) has been analyzed numerically using finite element method. The in-

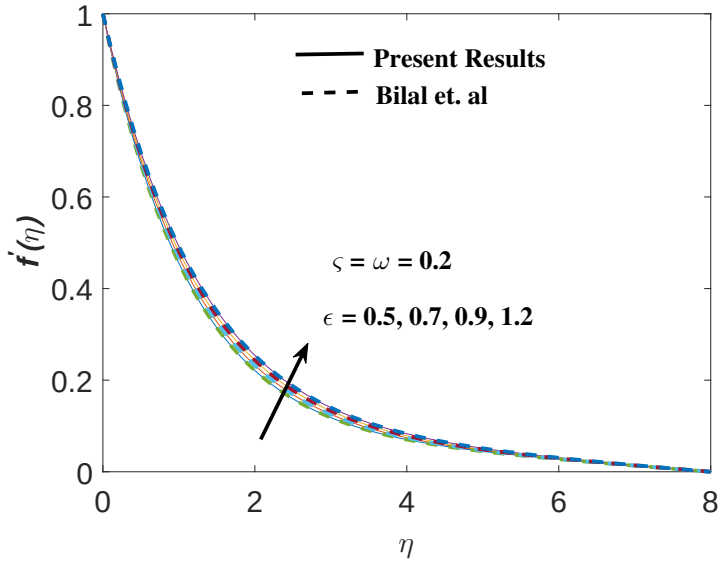

Figure 4.2: Validation of Results with previous work

fluence of important parameters such as Eyring-Powell fluid parameters ϵ, ς, relaxation time for heat flux β_e, heat and mass transfer Biot number γ_1 and γ_2, Prandtl number Pr, Brownian motion parameter Nb, Thermophoresis parameter Nt are analyzed on velocity profile, temperature profile, concentration profile graphically.

Figure 4.3a describes that velocity profile for different values of ϵ. Since $\epsilon = \frac{1}{\rho\beta' c}$, so by increasing ϵ viscosity of fluid decreases, which causes increases in velocity. Figure 4.3b reflects the effect of ς on velocity profile. It is depicted that velocity decreases with an increase in ς. This is because that the viscosity of the fluid increases with an increase in ς, which causes a decrease in the velocity profile.

Figures 4.4a-e show the variation of temperature field $\theta(\eta)$ for different values of Brownian motion parameter Nb, thermophoresis parameter Nt, relaxation time for heat flux β_e, heat transfer Biot number γ_1, Prandtl number Pr. Figure 4.4a depicts the variation of the temperature profile and boundary layer thickness as Nb increases. An increase in the Brownian motion parameter Nb leads to an increase in the random motion of the fluid. As a result, fluid particles frequently collide, producing more heat and raising the temperature. Figure 4.4b depicts the effect of thermophoresis parameter Nt on a temperature profile. Thermophoresis is a mechanism that pulls small particles away from a hot surface and pushed them towards a cold surface. The temperature of the fluid rises as a result of this transportation. This has happened because additional heat is generated due to the interaction of nanoparticles with the base fluid due to brownian motion and thermophoresis effects. This results in depletion of thermal boundary layer thickness, and hence the temperature overshoots are observed in the vicinity of the stretching sheet for increasing

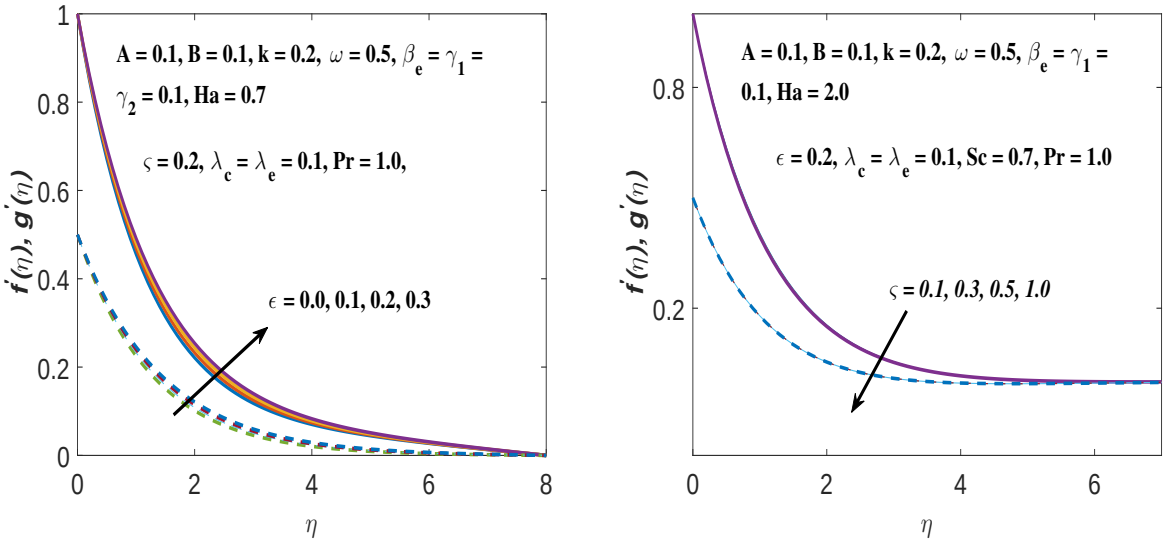

(a) Effect of ϵ (b) Effect of ς

Figure 4.3: Effect of varied thermophysical parameters on on velocity profiles

value of Nb and Nt. Figure 4.4c depicts that temperature reduces when thermal relaxation time for heat flux increases β_e. Physically when β_e increases the material particles need extra time to transfer heat to their adjacent particles, thus temperature reduces. Figure 4.4d shows that a pronounced increase in the temperature and corresponding boundary layer thickness when there is an increase in heat transfer Biot number γ_1. Figure 4.4e depicts the effect of the Prandtl number Pr on the temperature profile. Because $Pr = \frac{\nu}{\alpha}$, increasing the Prandtl number Pr reduces the thermal conductivity of the fluid, resulting in a lower temperature profile. Furthermore, increasing the Prandtl number reduces the thickness of the thermal boundary layer. As a result, heat transfers quickly, causing a drop in fluid temperature.

Figures 4.5a-c shows the variation in concentration profile for different values of Schmidt number Sc, chemical reaction parameter k and mass transfer Biot number γ_2. Figure 4.5a reveals that when Schmidt number increases, it causes a decrease in concentration. A higher value of Schmidt number lowers the mass diffusivity. Due to this thickness of the concentration boundary layer declines. Figure 4.5b reveals the influence of chemical reaction parameter k on concentration profile. It shows that concentration decreases with the increase in parameter k. This is because the higher the reaction rate, the thicker the concentration boundary layer. It is observed in figure 4.5c that concentration profile rises when mass transfer Biot number γ_2 increases.

Impacts of parameters ϵ and ς, Brownian motion parameter Nb, Thermophoresis parameter Nt on Nusselt number $-\theta'(0)$ are depicted in figures 4.6a, b. Figure 4.6 a is drawn to

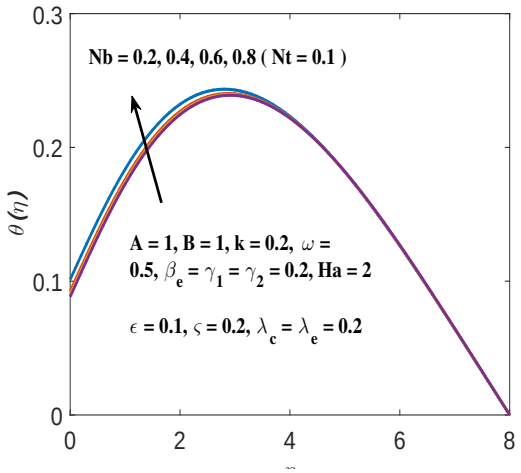

(a) Effect of Nb

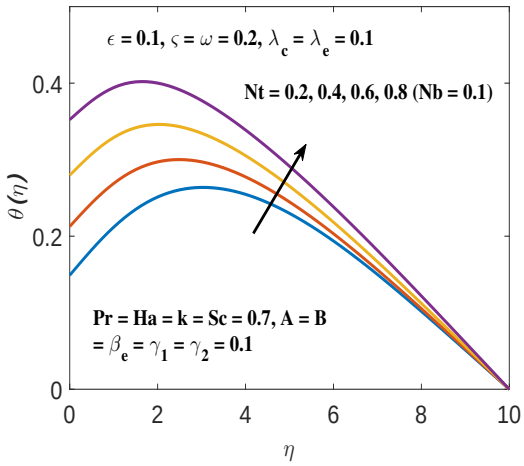

(b) Effect of Nt

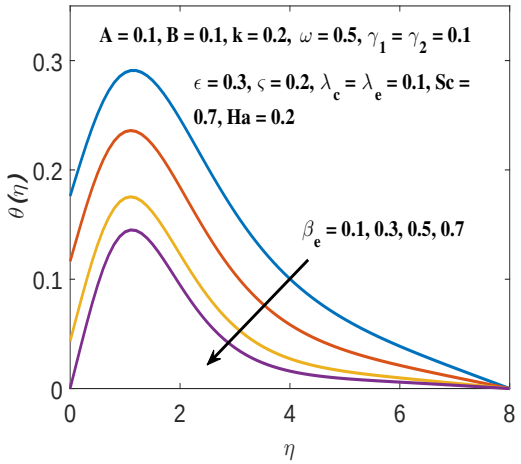

(c) Effect of β_e

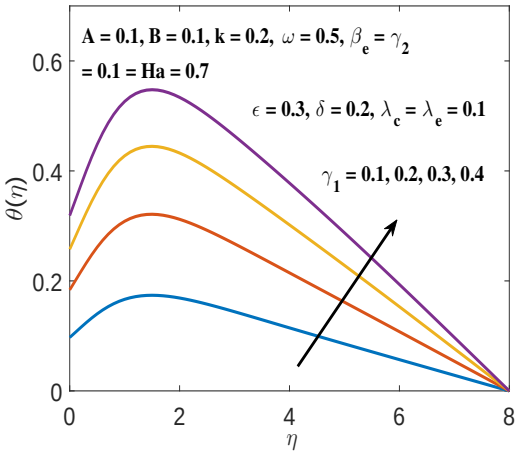

(d) Effect of γ_1

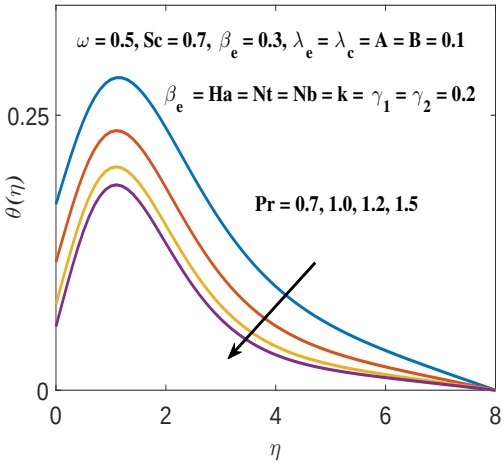

(e) Effect of Pr

Figure 4.4: Effect of varied thermophysical parameters on temperature profiles

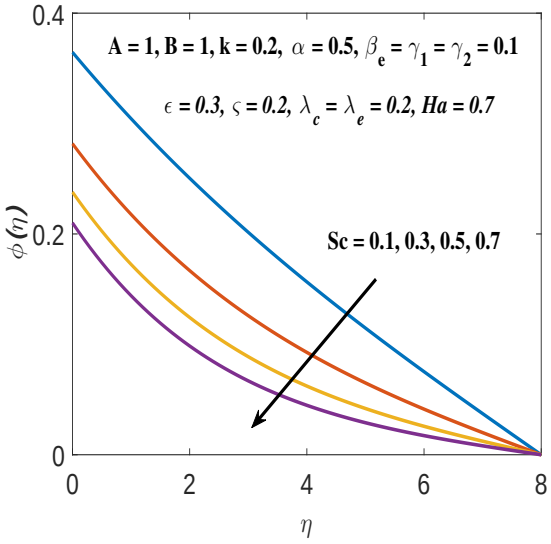

(a) Effect of Sc

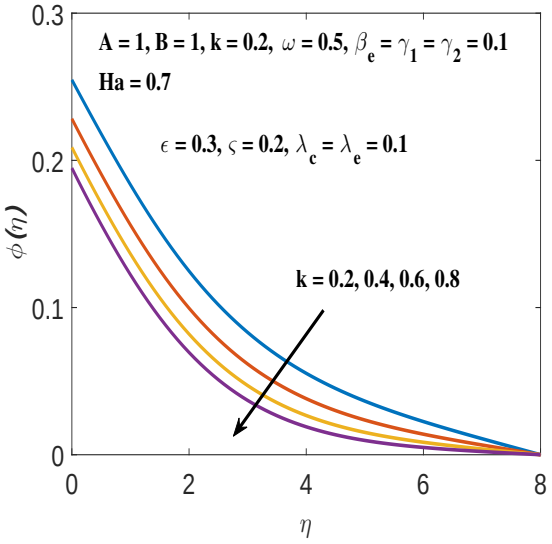

(b) Effect of k

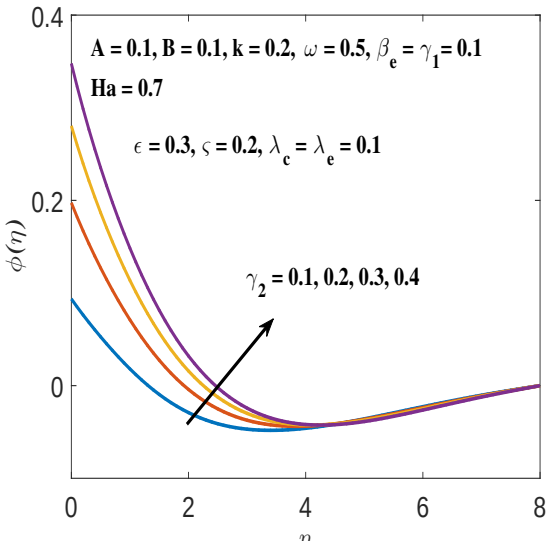

(c) Effect of γ_2

Figure 4.5: Effect of varied thermophysical parameters on concentration profiles

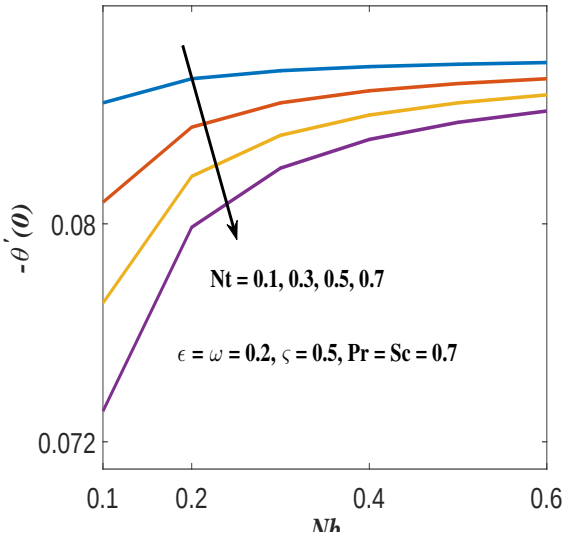

(a) Effect of Nb and Nt

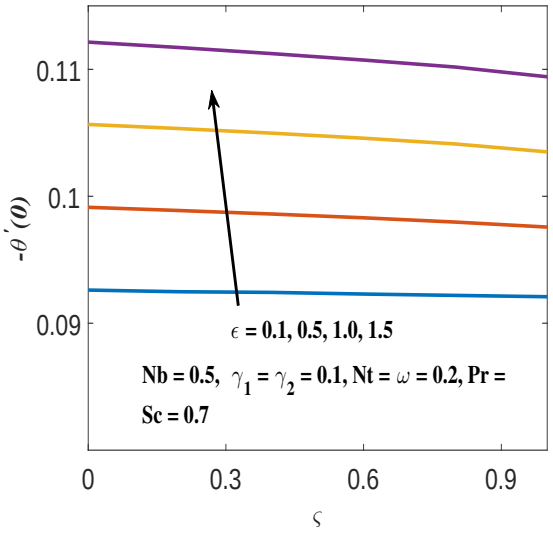

(b) Effect of ϵ and ς

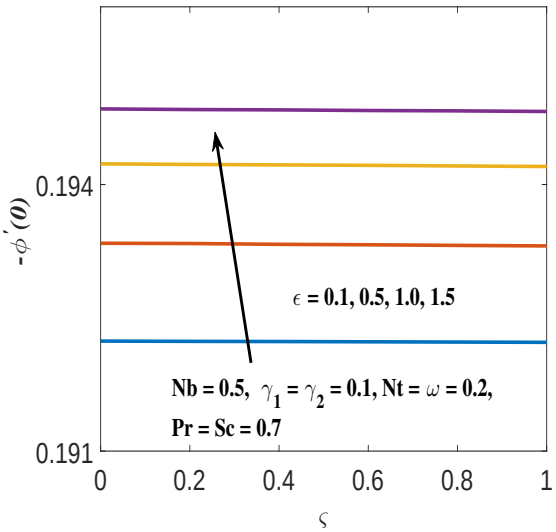

(c) Effect of ϵ and ς

Figure 4.6: Effect of varied thermophysical parameters on Nusselt number and Sherwood number

examine the variations of ϵ and ς on Nusselt number $-\theta^{'}(0)$. Nusselt number increases with an increase in ϵ while Nusselt reduces with an enhancement in ς. It is shown in figure 4.6b that with variations in Nb and Nt Nusselt number increases. Figure 4.6c shows the variation of parameters ϵ and ς on Sherwood number $-\phi^{'}(0)$. It is analyzed that Sherwood number rises with an increase in ϵ while it reduces with ς.

4.6 Conclusions

In the present study non-Fourier (Catteneo-Christov) heat flux model is considered for the three-dimensional flow of Erying-Powell fluid. The following observations in the current study are worth mentioning:

- Velocity profile in x and y direction increases with increase in ϵ while reverse pattern is observed for increasing value of ς.
- Temperature rises with enhancement in Nb, Nt and γ_1 while it decreases with increment in thermal relaxation time β_e.
- Concentration profile decreases with increase in Sc (Schmidt number) and k (chemical reaction parameter). On the other it enhances with mass transfer biot number γ_2.
- Rate of heat transfer i.e., Nusselt number decreases with Nt and it increases with ϵ.
- Rate of mass transfer i.e., Sherwood number remains almost constant for different values of ς while it rises with ϵ.

Chapter 5

Mathematical Analysis of flow of Casson fluid in a Partially Heated Porous Cavity

5.1 Introduction

The heat transport phenomenon is an important topic of research due to its wide variety of applications in the field of science, engineering and industries. As illustrations, electronic devices dissipates heat which aspires cooling, textile industries, cooling and heating systems in the buildings, vehicles, phase change materials, etc. The above-said applications have gained the interest of researchers to examine the heat transport processes via means of experiments and theoretical investigations which saves time as well as expenditure. In this context, the process of transfer of heat via Newtonian and non-Newtonian fluids in various geometries through efficient methods has gained the focus of the research community [11, 88, 93, 210, 244].

The heat transfer in cavities has become an attractive topic of research and industrial usages. This is because, in cavities, no external source such as electric power is required for induction of convectional heat transfer. Due to the absence of power sources, convectional heat transfer in cavities is free from magnetic noise, fee, and sound. In most of the industrial and engineering applications such as air conditioning devices, food processing industries, float glass production, disposal of nuclear waste, ceramic processing, geothermal systems, and many more [45, 47, 109, 110, 114, 162, 172, 178, 211, 235]. cavities filled with porous media are used. Beavers and Joseph [17] investigated the influence of various boundary conditions for the flow through porous media. Natural convection at high Rayleigh number in a porous bed by incorporating the Darcy model is studied by Poulikakos et al. [179]. Heat transfer due to steady-state natural convection in a rectangular enclosure saturated with porosity was experimentally and numerically investigated by Beckermann et al. [18]. Their key findings showed that for a low value of Da and Ra, fluid flow and heat transfer in the porous layer was due to conduction only. Moreover, Beckermann et al. [19] also discussed the free convective heat and mass transfer in a vertical rectangular enclosure

This chapter has been published in *International Communications in Heat & Mass Transfer*

by considering simultaneous fluid and the porous layer. On the other hand, Singh and Thorpe [206] studied the natural convection of a fluid in a porous layer by considering different fluid models. In this context, Sheikholeslami et al. [213,215] studied the influence of electric/magnetic field on the free convective flow of a nanofluid in a porous cavity.

Viscoplastic fluids are a special type of non-Newtonian materials that flows only when applied stresses are more than a critical value known as yield stress. Once the applied stress exceeds the value above the yield stress, it flows like a liquid. The rheological models like the inelastic Bingham model [30], Herschel-Bulkley [100], and Casson models [36] are developed to describe the flow behavior of viscoplastic fluids. Out of these models, Hurschel-Bulkley or Casson fluid models are frequently used as most of the materials behave as shear-thinning fluids. In present days, the Casson fluid model is adopted by food industries. The Cocoa and Chocolate making industries used the Casson fluid model to illustrate the rheological behavior of chocolates. Moreover, these days the Casson model is also used for developing the rheological model for human blood [32, 39, 202, 234]. The detailed analysis of Casson fluid flow through various geometries under different situations are available in the literature [1, 80, 136, 157, 177, 183, 189, 237]

This type of problem has efficient potential due to its applications as mentioned earlier in the food industry, like the processing of mayonnaise, jam, and chocolate. The behavior of these fluids is similar to that of Casson fluids and is cooled by natural convection. Since the natural convective flow in cavities arises in many engineering processes, the results obtained in the present study may apply to other fields of interest. Thus, the current investigation aims to analyze Casson fluid's steady-state natural convective heat transfer characteristics in a porous square cavity.

5.2 Mathematical Model

In the existing problem of natural convection, Casson fluid is filled in the square porous cavity ($L \times L$). The geometrical visualization of the cavity along with the coordinate system is demonstrated in figure 5.1. The bottom wall is maintained at a higher temperature T_h compared to other walls. The length of the heated portion of the wall has been varied to study the effect of a heated zone on fluid flow and heat transfer characteristics. The side walls of the cavity are kept cooled to a constant temperature (T_c). On the other hand, the upper wall and portion of the bottom wall are taken to be adiabatic. The physical-chemical properties of the fluid and porous medium are assumed to be constant except the density in the buoyancy term, which is satisfied by Boussinesq's approximation. Further,

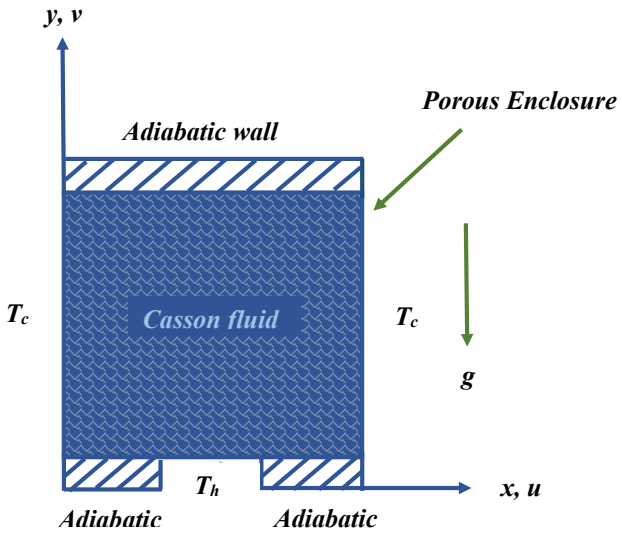

Figure 5.1: Physical Description and Cartesian Co-ordinates

the properties of the fluid and porous medium are homogeneous. For the momentum transfer in the porous medium Darcy-Forchheimer model is applied without considering inertial term.

The rheological condition of state for the stress tensor [159] of Casson fluid is given by

$$\tau_{ij} = \begin{cases} 2(\mu_B + p_y/\sqrt{2\pi})e_{ij}, & \pi > \pi_c \\ 2(\mu_B + p_y/\sqrt{2\pi_c})e_{ij}, & \pi < \pi_c \end{cases} \tag{5.2.1}$$

Here $\pi = e_{ij}e_{ij}$ and e_{ij} are the (i,j)th component of the deformation rate, π denotes the product of the component of deformation rate itself, π_c designates the critical value based on the type of non-Newtonian model, μ_B represents the dynamic viscosity of viscoplastic fluids, and p_y is the yield stress.

The governing equations for the given model are:

$$\frac{\partial U}{\partial X} + \frac{\partial V}{\partial Y} = 0, \tag{5.2.2}$$

$$U\frac{\partial U}{\partial X} + V\frac{\partial U}{\partial Y} = -\frac{\partial P}{\partial X} + Pr(1+\frac{1}{\gamma})\left(\frac{\partial^2 U}{\partial X^2} + \frac{\partial^2 U}{\partial Y^2}\right) - \frac{Pr}{Da}U, \tag{5.2.3}$$

$$U\frac{\partial V}{\partial X} + V\frac{\partial V}{\partial Y} = -\frac{\partial P}{\partial Y} + Pr(1+\frac{1}{\gamma})\left(\frac{\partial^2 V}{\partial X^2} + \frac{\partial^2 V}{\partial Y^2}\right) - \frac{Pr}{Da}V - RaPr\theta, \tag{5.2.4}$$

$$U\frac{\partial\theta}{\partial X}+V\frac{\partial\theta}{\partial Y}=\frac{\partial^2\theta}{\partial X^2}+\frac{\partial^2\theta}{\partial Y^2}. \tag{5.2.5}$$

Boundary conditions:

$\theta=0,\ \ U=V=0 \quad \text{at} \quad X=0 \quad \text{and} \quad 0<Y<1$

$\theta=0,\ \ U=V=0 \quad \text{at} \quad X=1 \quad \text{and} \quad 0<Y<1$

$\theta=1,\ \ U=V=0 \quad \text{at} \quad Y=0 \quad \text{and} \quad \dfrac{1-\varepsilon}{2}\leqslant X\leqslant\dfrac{1+\varepsilon}{2}$

$$\frac{\partial\theta}{\partial Y}=0,\ \ U=V=0 \quad \text{at} \quad Y=0,\ 0<X<\frac{1-\varepsilon}{2} \quad \text{and} \quad \frac{1+\varepsilon}{2}<X<1,$$

$$\frac{\partial\theta}{\partial Y}=0,\ \ U=V=0 \quad \text{at} \quad Y=1,\ 0<X<1. \tag{5.2.6}$$

The following transformations are used for getting the dimensionless governing equations:

$$X=\frac{x}{L},\ \ Y=\frac{y}{L},\ \ U=\frac{uL}{\alpha},\ \ V=\frac{vL}{\alpha},\theta=\frac{T-T_c}{T_h-T_c},\ \ Pr=\frac{\nu}{\alpha},\ \ \gamma=\mu_B\sqrt{2\pi_c}\Big/\frac{\partial p}{\partial y},$$

$$Da=\frac{\kappa}{L^2},\ \ Ra=\frac{g\beta(T_h-T_c)L^3Pr}{\nu^2} \tag{5.2.7}$$

The variation of the the plastic dynamic viscosity μ_B and yield stress p_y as a function of temperature and pressure are not studied earlier and no experimental data is available to address this issue. It is not trivial to incorporate the variation of temperature and pressure in the absence of relevant model and data [43, 70, 164, 233]. For the simplification of governing equations, the above mentioned factors are assumed to be constant throughout the study.

The average Nusselt number for the heated portion of the bottom wall is given by

$$\overline{Nu}=\int_{\frac{1-\varepsilon}{2}}^{\frac{1+\varepsilon}{2}}Nu(X)dX \tag{5.2.8}$$

where $Nu(X) = -\left(\frac{\partial \theta}{\partial Y}\right)_{Y=0}$ is the local Nusselt number.

5.3 Methodology

The penalty finite element method [103, 190, 192] is used to solve the governing equations (5.2.2-5.2.5). In this method, an incompressibility criteria and a penalty parameter Γ is used to accomodate the pressure in the momentum equations, which results as $P = -\Gamma\left(\frac{\partial U}{\partial X} + \frac{\partial V}{\partial Y}\right)$. The continuity equation is satisfied automatically for large values of Γ and Γ is taken as 10^7 for stable solution [15]. By using the above definition of P, we have eliminated the pressure from momentum equations (5.2.3 & 5.2.4) and reduce the equations in the following form:

$$U\frac{\partial U}{\partial X} + V\frac{\partial U}{\partial Y} = \Gamma\frac{\partial}{\partial X}\left(\frac{\partial U}{\partial X} + \frac{\partial V}{\partial Y}\right) + Pr(1+\frac{1}{\gamma})\left(\frac{\partial^2 U}{\partial X^2} + \frac{\partial^2 U}{\partial Y^2}\right) - \frac{Pr}{Da}U, \tag{5.3.1}$$

$$U\frac{\partial V}{\partial X} + V\frac{\partial V}{\partial Y} = \Gamma\frac{\partial}{\partial Y}\left(\frac{\partial U}{\partial X} + \frac{\partial V}{\partial Y}\right) + Pr(1+\frac{1}{\gamma})\left(\frac{\partial^2 V}{\partial X^2} + \frac{\partial^2 V}{\partial Y^2}\right) - \frac{Pr}{Da}V, \tag{5.3.2}$$

The finite element based commercial software freefem++ [97] is used to solve the governing equations. The tolerance for the study is considered is upto 10^{-6}.

5.3.1 Validation of the Results

To validate our numerical scheme, the study of Basak et al. [15] has been considered. The results for natural convection in a square porous cavity filled with Newtonian fluids have been reproduced and compared with Basak et al.. It is noted that, as the value of $\gamma \to \infty$, the Casson fluid model tends to Newtonian fluid (Eqns 5.2.3 & 5.2.4). The obtained results and literature value are presented in figure 5.2, and it shows a good agreement of the produced results with Basak et al.

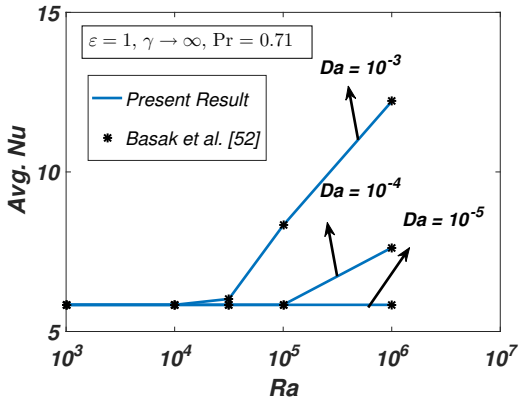

Figure 5.2: Comparison of average Nusselt number with literature value for $Pr = 0.71$

5.4 Results & Discussion

The present work is aimed to analyze the natural convective heat transfer characteristics of Casson fluid in a square porous cavity with a partially heated bottom wall. The heating zone is kept at a constant temperature, and vertical side walls are maintained at a lower temperature to provide cooling effects. The top wall of the square cavity is taken as an adiabatic wall. The two-dimensional situation is assumed to simplify numerical calculation problems due to higher simulation time and effort. The numerical results are obtained for the ranges of parameters as $\gamma = 0.1 - 5, Ra = 10^2 - 10^6, Da = 10^{-5} - 100, \varepsilon = 0.2, 0.5, 0.8$. The numerical results are presented as streamlines and isotherm profiles, average Nusselt number for the given ranges of parameters.

5.4.1 Streamlines & Isotherms Profile

The streamlines and isotherms for our study are shown in figures (5.3-5.10). The non-dimensional values of the temperature are taken here to present isotherms as a function of other parameters. The two counter-rotating symmetric vortices are seen along the vertical mid-plane of the cavity. The positive and negative signs for the streamlines are used to present counter-rotating streamlines. The local fluids get heated in the vicinity of the partial heating zone. The buoyancy forces are developed due to the reduced density of the local fluid. This density difference allows the heated fluid to move upward and replaced by nearby fluid. Then the cooled side wall absorbs the heat from the moving fluid became cold (higher density fluid). The simultaneous heating and cooling effect made the fluid in motion.

The streamlines and isotherms are plotted for all governing parameters that are Da, Ra, γ

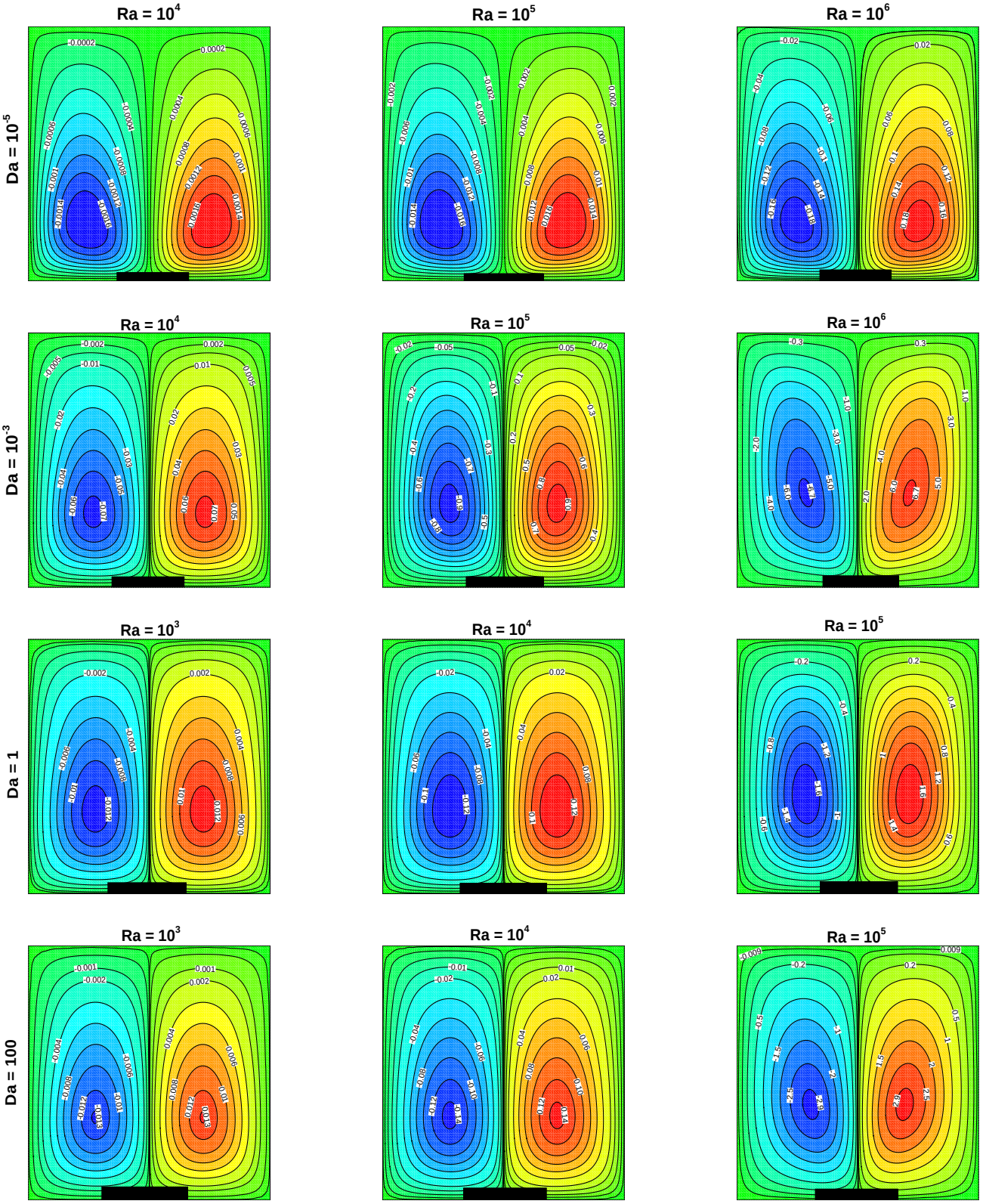

Figure 5.3: Streamlines plots for varying Ra, Da at fixed value of $\gamma = 0.1, \varepsilon = 0.2, Pr = 7$

and ε. In figure 5.3, the streamline profiles are shown for varying values of Da and Ra at $\gamma = 0.1, \varepsilon = 0.2$. The figure shows that as the Darcy number increases from 10^{-5} to 100, the flow circulation increases at any constant value of Ra. This phenomenon is seen more prominent at $Ra = 10^6$ than $Ra = 10^4$. As we go on increasing the value of Ra from 10^4 to 10^6, again circulation increases because of an increase in natural convective forces at the constant value of other parameters. It is also seen that this change in the flow characteristics is much higher (up to two orders of magnitude) for the extreme value of Ra. The center of circulation is also observed, and it is seen that as the value of Da increases, it moves upward, and it shows complex variation with respect to increase in Ra and all these effects are clearly seen in figure 5.3. Similarly, in figure 5.4, the streamlines are plotted for increased value of Casson fluid parameter as $\gamma = 1$. The observations of figure 5.4 show that the circulation increases as compared to figure 5.3 and a similar trend is observed with the variation of Ra and Da. It is noted that the change in magnitude of the streamline function changes sharper than figure 5.3 because of the influence of the Casson fluid parameter. This can also be explained as with an increase in γ from 0.1 to 1, the effective viscosity of the fluid decreases. Hence the inertial forces increases and the increased inertial forces lead to shifting of the center of circulation in the upward direction. Further, in figure 5.5, similar streamline profiles for $\gamma = 5$ are observed. The above explained phenomenon further enhances at this value of Casson fluid parameter, i.e., the highest circulation is seen at extreme value of Da, Ra and γ.

In figure 5.6, the streamlines for low and extreme values of parameters are shown with varying length of heating zone to see its influence on flow structure (streamline profile). As the value of governing parameters increases, the recirculation increases, and the center of circulation shifted upward. In contrast, the heating zone changes from 0.2 to 0.8, the flow structure changes, and the center of circulation shifted horizontally towards cold walls. Further, as the length of the heated zone increases at fixed values of Ra, Da and γ flow circulation enhances. It is also noticed in figure 5.6 that center of circulation showing complex behavior with increasing values of all the governing parameters. Further, in figure 5.6 as the heating zone length changes the circulation zone shifted downwards (vertically) and moved towards cold walls (horizontally). Thus, overall the figure 5.6 shows very complex behavior of flow structure by changing the heating zone length.

The isotherms profile corresponding to streamlines profile (figures 5.3-5.5) are shown in figures (5.7-5.9) depict the temperature distribution inside the cavity with varying value of Da, Ra, γ and at fixed value of $\varepsilon = 0.2$. In figure 5.7, isotherms are demonstrated for $\gamma = 0.1$ with varying values of Da, Ra. It can be seen from the figure that the temperature contours are more concentrated near the bottom wall than the side walls due to the heating

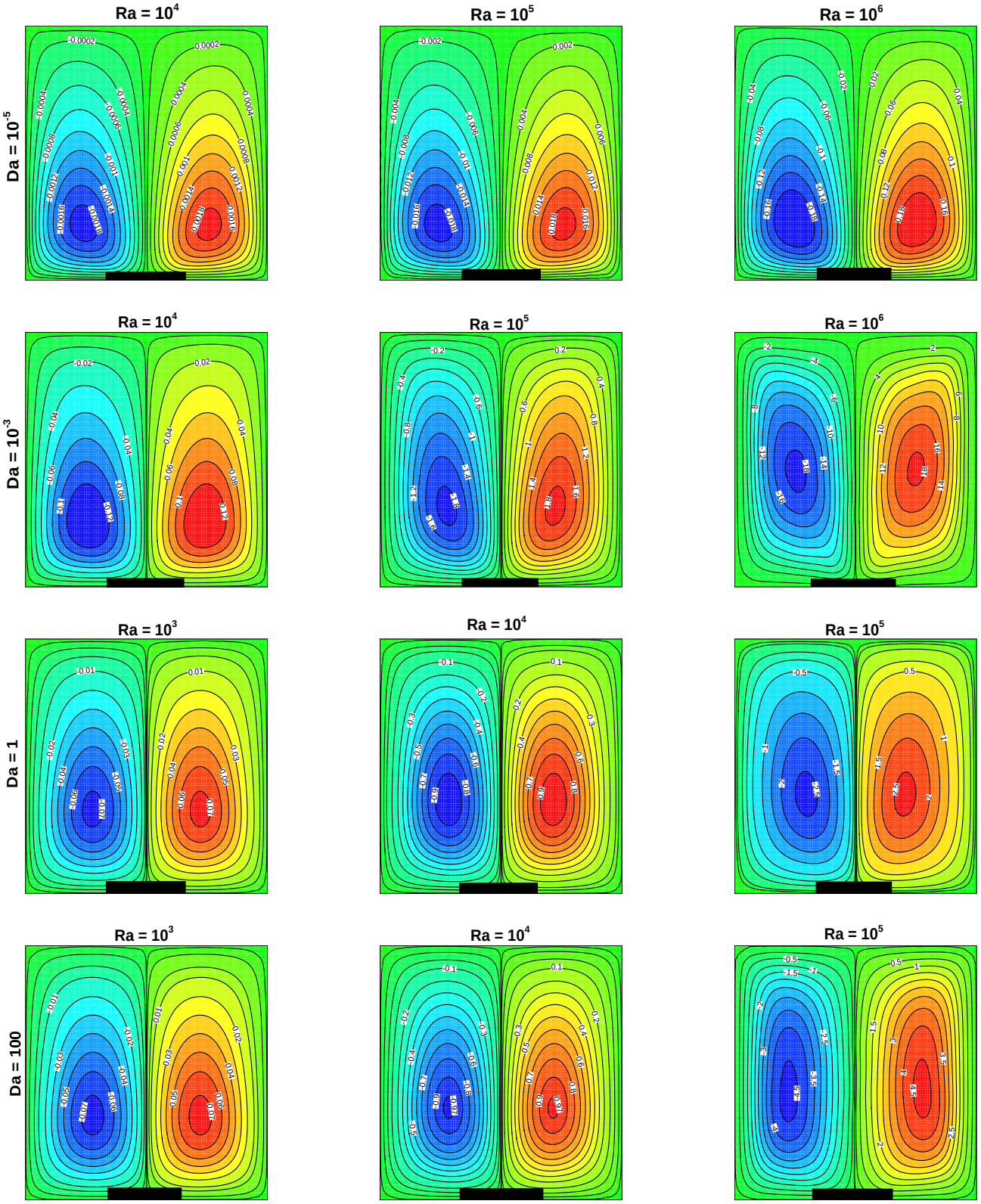

Figure 5.4: Streamlines plots for varying Ra, Da at fixed value of $\gamma = 1, \varepsilon = 0.2, Pr = 7$

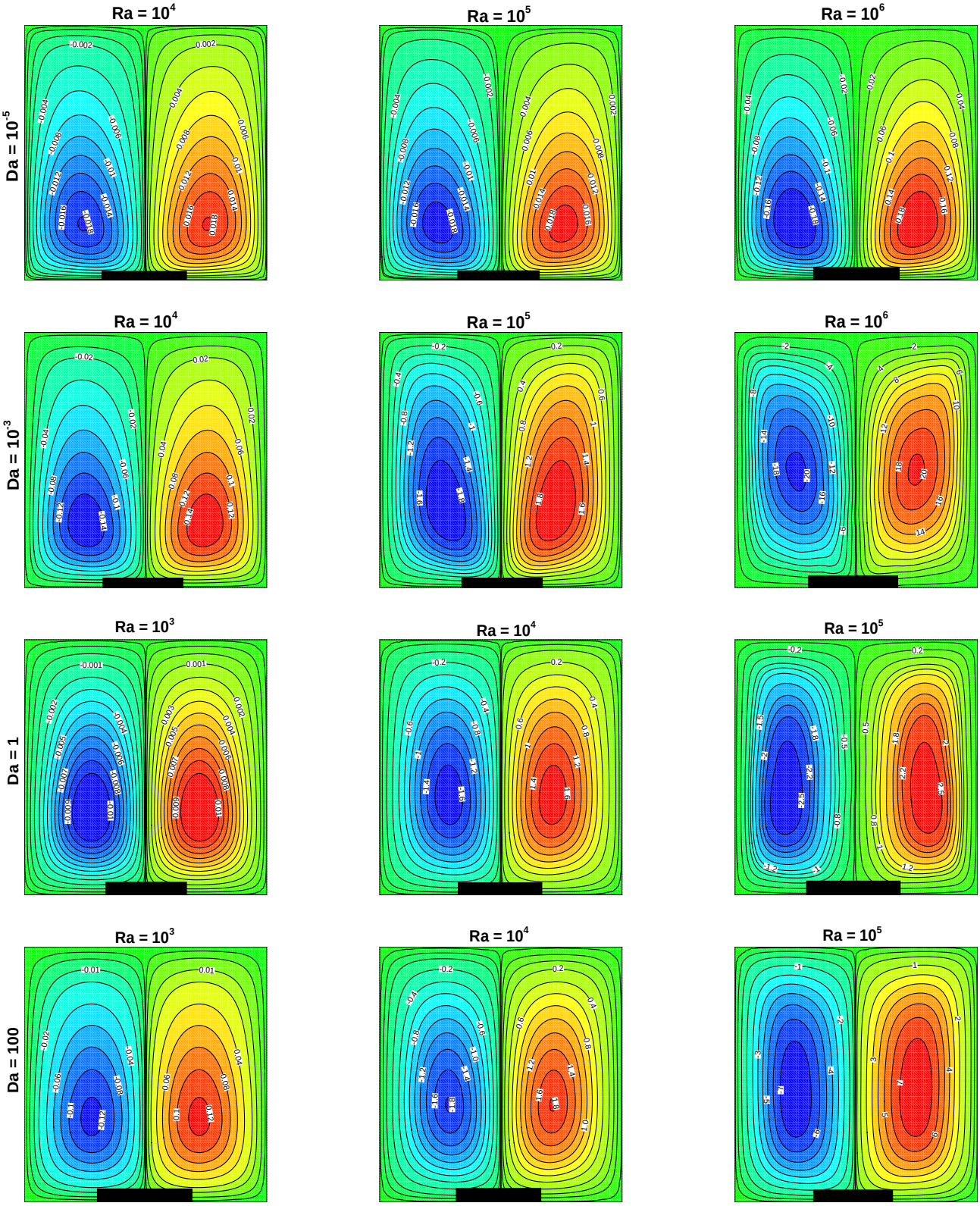

Figure 5.5: Streamlines plots for varying Ra, Da at fixed value of $\gamma = 5, \varepsilon = 0.2, Pr = 7$

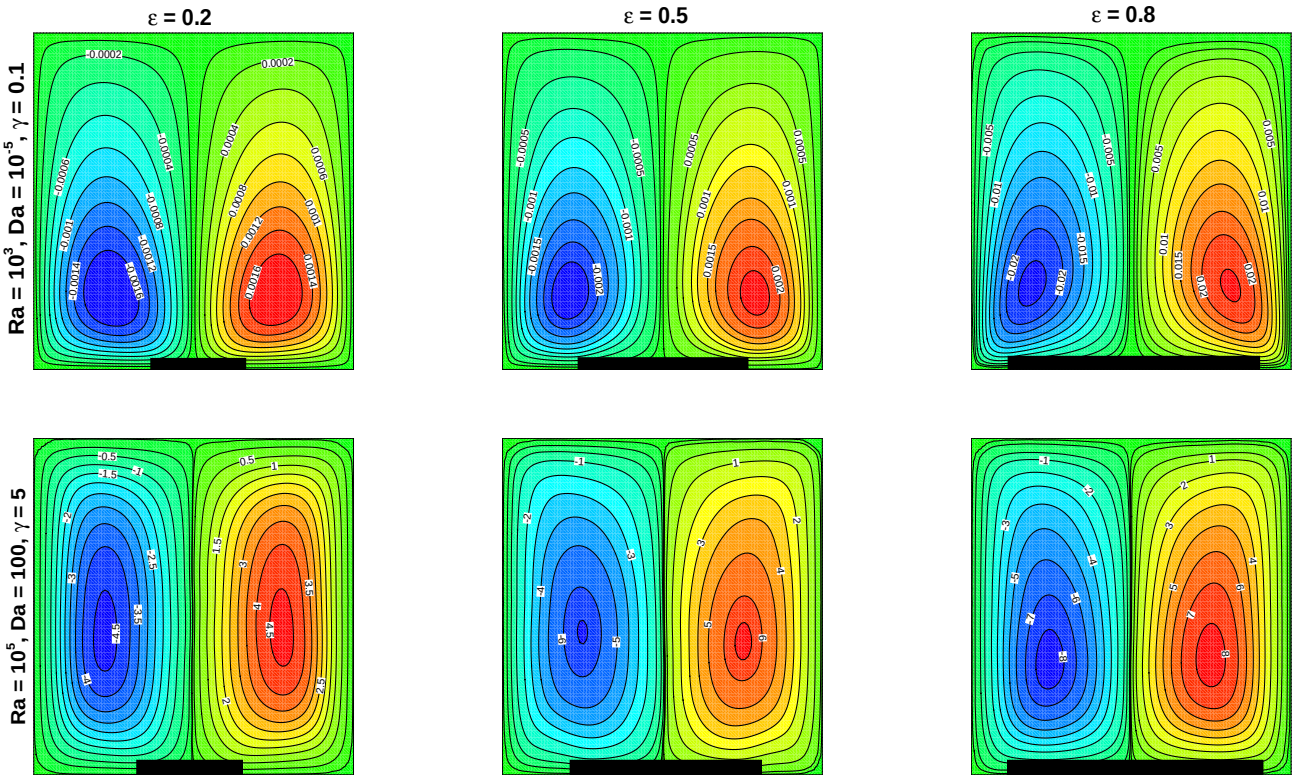

Figure 5.6: Streamline plots for varying ε at fixed value of $Pr = 7$

at the bottom wall. The streamlines and isotherm profiles show that the conductive heat transfer dominates in the whole cavity because of low momentum and thermal gradients. A symmetric behavior along the center line is also seen. Further, with an increase in value of Ra from 10^4 to 10^6, the thermal gradient increases, and this increment in thermal gradient cause the increase in the value of momentum gradient (velocity gradient). Hence, recirculation increases. Thus the structure of isotherms changes, and it starts getting shifted towards the cold walls. At extreme values of Ra, more circulations of the fluid took away heat from the bottom wall, and transferred it to the cold vertical walls and hence the more noteworthy heat exchange between the side walls and bottom wall is observed. Further, the observation of figure 5.8 shows the isotherms profile for $\gamma = 1$ and other parameter are same as figure 5.7. It is already known that the viscosity of the fluid decreases with increasing the value of γ and this decrease in the viscosity is being lead to increased heat transfer and similarly it continues for $\gamma = 5$ (figure 5.9). The presented isotherms shows very complex behavior with the governing parameters and it becomes more complex at the values of governing parameters as $\gamma = 5, Da = 10^{-3}, Ra = 10^6$ (figure 5.9).

Furthermore, figure 5.10, represents the influence of heating zone length on isotherms pro-

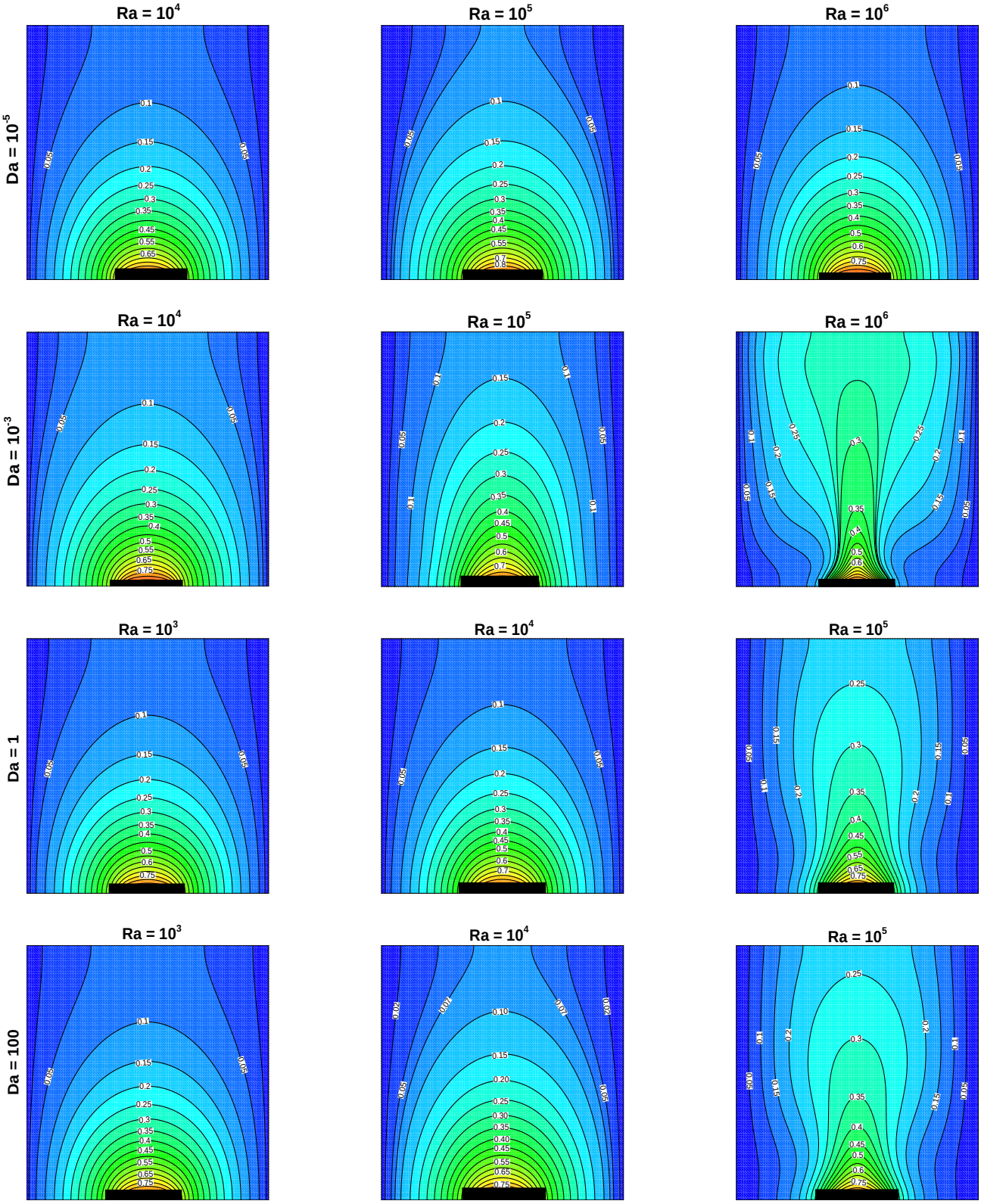

Figure 5.7: Isotherms plots for varying Ra, Da at fixed value of $\gamma = 0.1, \varepsilon = 0.2, Pr = 7$

file, as the length of the heating zone increases, the isotherms are occupying most of the cavity, and the isotherm structure is getting more complex. In other words, it can be concluded that for low values of governing parameters, the heat transfer is less in comparison to extreme values of parameters. Isotherm profiles are displayed for ($Da = 100$) with varying values of other governing parameters. It has been noticed that almost all the isotherms are smooth curves occupying most parts of the cavity at low values of all governing parameters. As the values of governing parameter increase, isotherms start getting deformed and moved towards the cold side walls. More heat exchange occurs between the cold vertical walls and bottom wall at extreme values of all the parameters.

The centers of rotation illustrated in figure 5.11 shows variation with all the governing parameters. In figure 5.11a, center co-ordinates of recirculating zone are plotted for varying γ with three different values of Da. As γ increases, flow circulation increases thus the center of rotations shifted upwards. Similarly, in figure 5.11b center co-ordinates versus Rayleigh number for varied values of Da is presented. It is found from the figure that the center of rotation shifted vertically upward for $Ra > 10^4$ and $Da = 10^{-3}$, but horizontally it is not showing significant variation with an increase in Da and Ra. In figure 5.11c and 5.11d, center co-ordinates are shown for varying heated length zone with Casson fluid parameter. It is depicted from the figures that the center of circulations is shifted vertically more than horizontally with increasing values of governing parameters.

5.4.2 Average Nusselt number

The heat transfer coefficient in the form of non-dimensionalized value (Nusselt number) has been plotted in figures (5.12-5.13) for the chosen range of operating conditions. The influence of operating conditions on the value of the average Nusselt number depicts that it increases with an increase in γ, Ra, Pr, Da and ε. The magnitude of the coefficient of heat transfer is higher at the hot wall than at the cold walls. Figure 5.12a demonstrates the impact of γ on average Nusselt number with varying Darcy number. It is observed from the figures that the rate of heat transfer for both the walls remains constant irrespective of the Casson fluid parameter at $Da = 10^{-5}$. For low Darcy number, fluid moves slowly inside the cavity and hence, conduction dominant heat transfer occurs. The overall rate of heat transfer increases prominently with all values of Casson fluid parameter at $Da = 10^{-3}$. Figure 5.12b displays the average Nusselt number versus Rayleigh number, and it also shows that heat transfer rate does not show significant change at all values of Ra at $Da = 10^{-5}$ as conduction is the dominant heat transfer mode. At $Da = 10^{-4}$, heat transfer rate increases for $Ra > 10^5$ and it further increases at $Da = 10^{-3}$ for $10^4 < Ra < 10^6$.

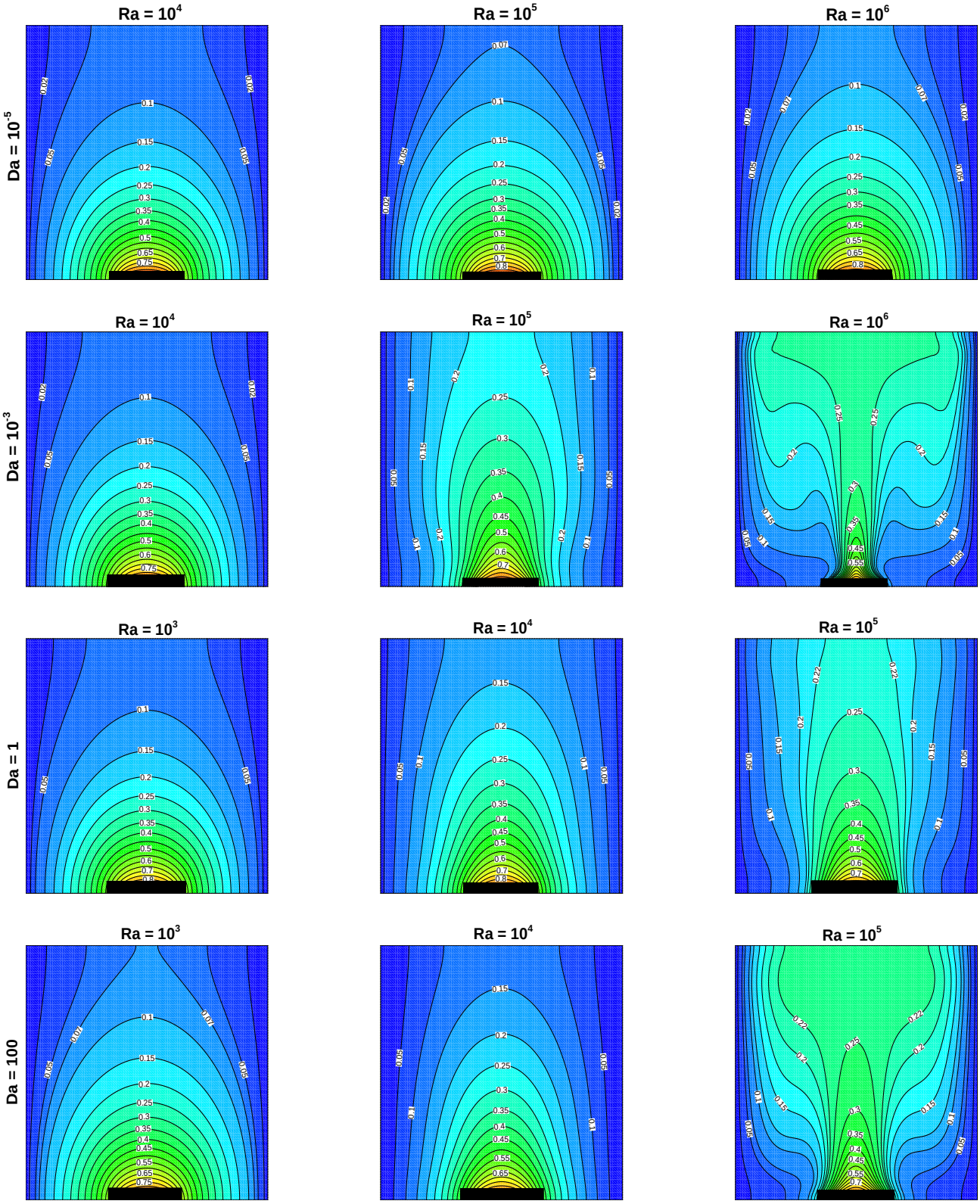

Figure 5.8: Isotherms plots for varying Ra, Da at fixed value of $\gamma = 1, \varepsilon = 0.2, Pr = 7$

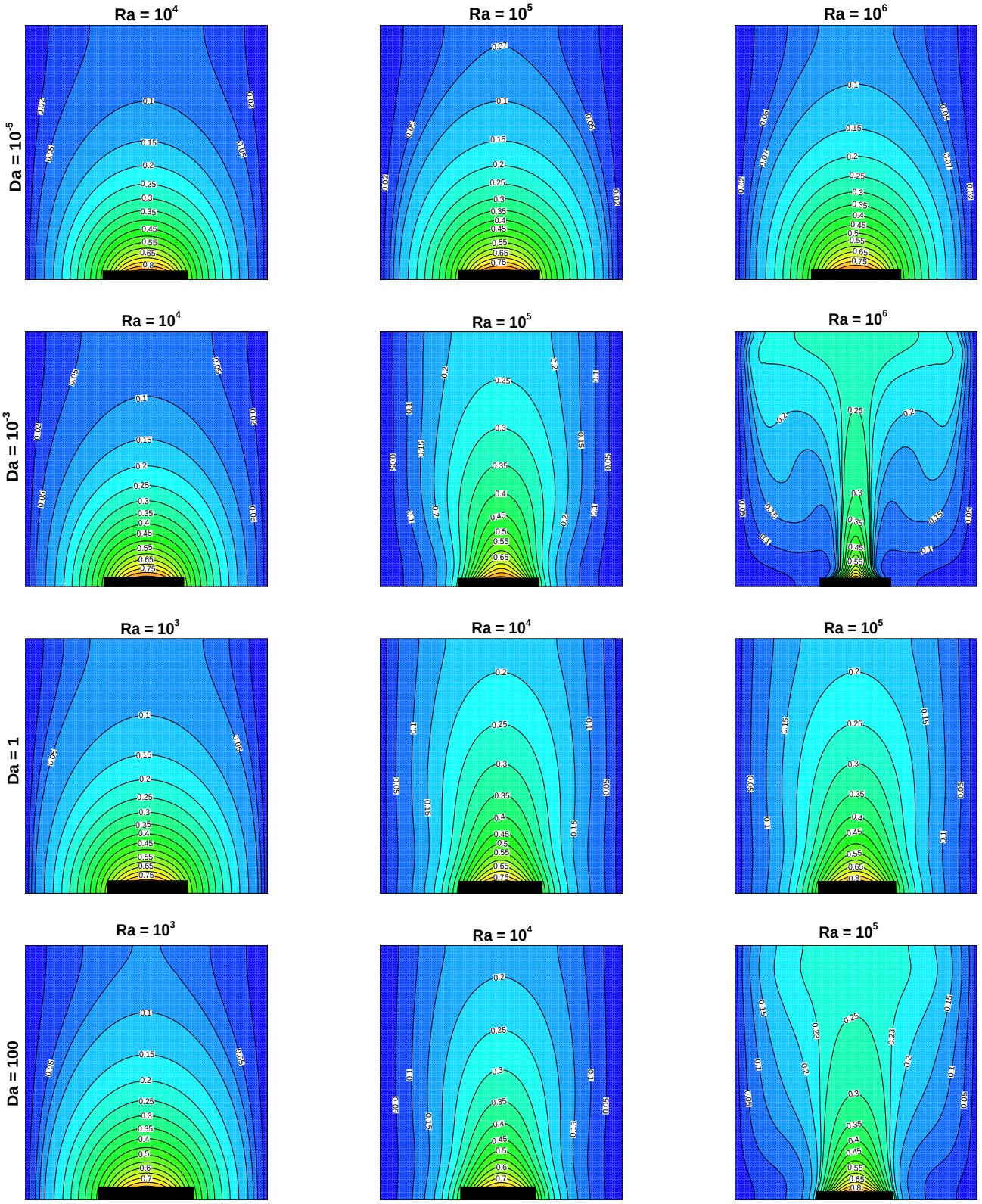

Figure 5.9: Isotherms plots for varying Ra, Da at fixed value of $\gamma = 5, \varepsilon = 0.2, Pr = 7$

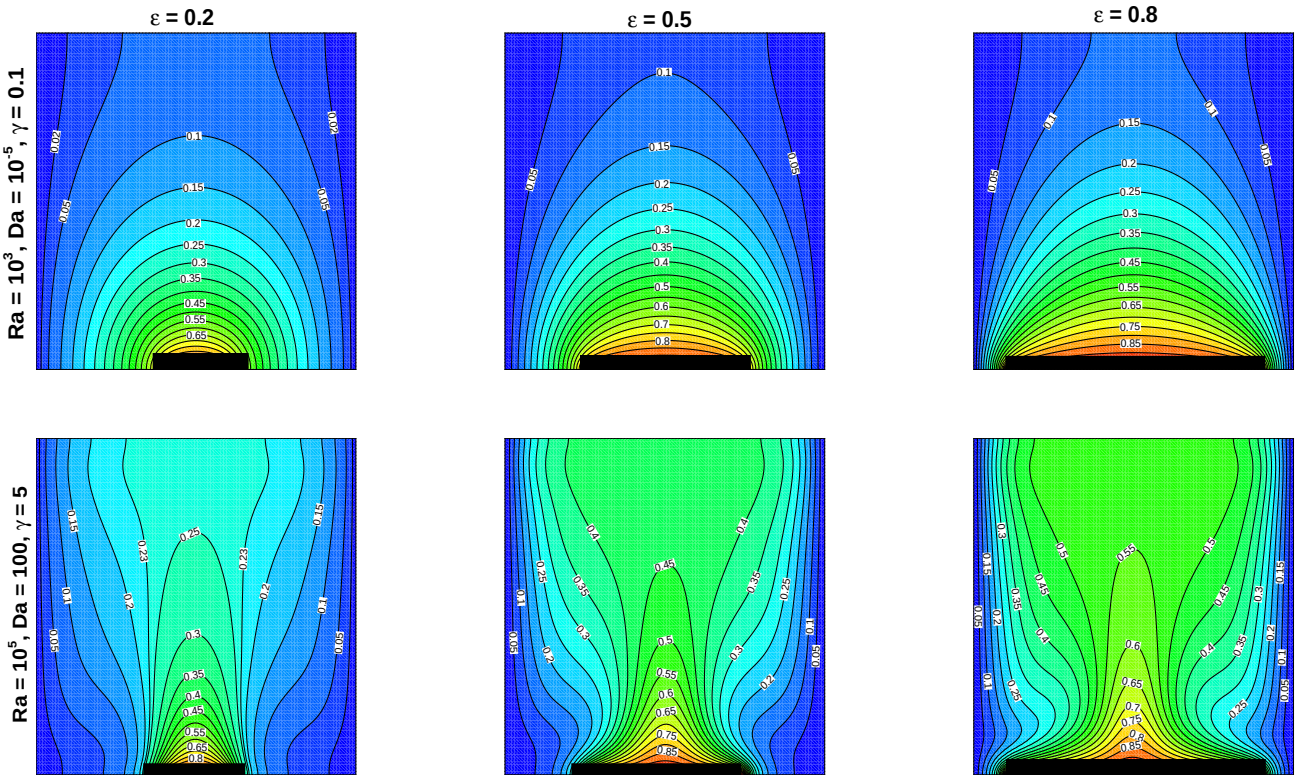

Figure 5.10: Isotherms plots for varying ε at fixed value of $Pr = 7$

At these values of Ra and Da, buoyancy driven convection starts to play its dominant role. For $Da = 1$, the coefficient of heat transfer increases when $Ra > 10^4$ for the partial heated bottom wall as well as for the cold wall whereas, it remains almost constant up to $Ra = 10^4$. On the other hand, at $Da = 100$, the average Nusselt number remains constant till $Ra = 10^3$ and it starts increasing for $Ra > 10^3$. Variation of the rate of heat transfer with Pr for the hot and cold wall is manifested in figure 5.12c. It is observed from the figure that heat transfer rate increases with Pr for $Da \geq 10^{-4}$. It is also noted from the figure that the average Nusselt number shows typical variation with Pr. At the hot wall, the average Nusselt number increases significantly up to $Pr < 60$ and then it becomes almost constant for a higher Prandtl number. At the cold wall, a similar kind of variation in the average Nusselt number is observed. The variation of average Nusselt with heated length zone and other governing parameters are shown in figure 5.13. The heat transfer rate with varied heated zone length ε and Casson parameter γ is presented in figure 5.13a. It is noticed from the figure that the average Nusselt number increases with an increase in heated zone length. Further, it is depicted from the figure that there is a significant rise in heat transfer rate at $\varepsilon = 0.8$ for all values of the Casson fluid parameter. The variation of average Nusselt number for varied Ra and ε is demonstrated in figure 5.13 b. For $\varepsilon = 0.2$ and $\varepsilon = 0.5$, the average Nusselt number remains almost constant for $Ra < 10^5$ and then

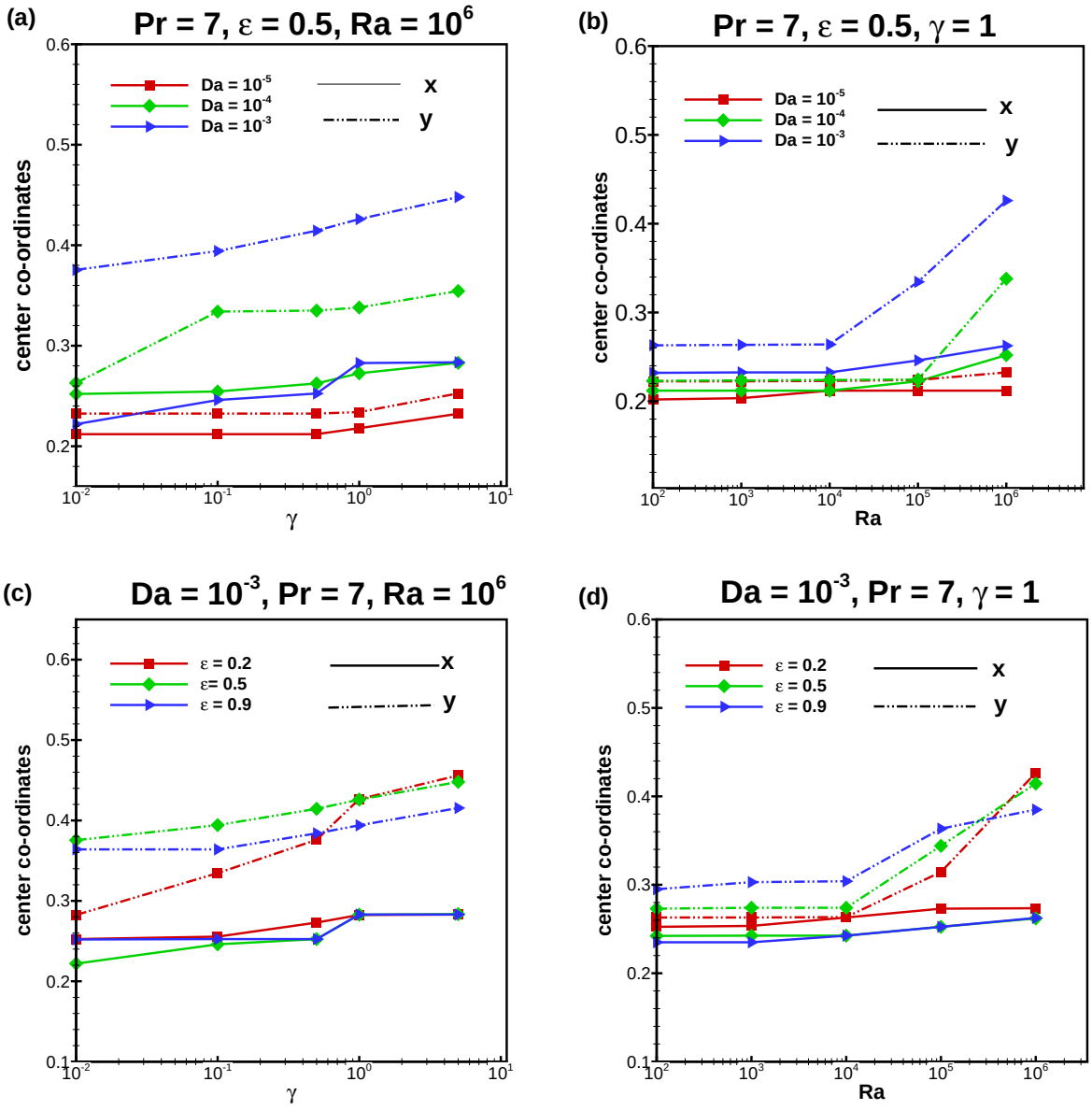

Figure 5.11: center co-ordinates plots for varying values of $Da, Ra, \gamma, \varepsilon$

it increases for $Ra = 10^5$ but at $\varepsilon = 0.8$, the average Nusselt number shows significant variation for $Ra > 10^4$. Figure 5.13c shows the variation of average Nusselt number with different heated zone lengths and Prandtl number. It is found that at the fixed of other governing parameters, there is a significant rise in coefficient of heat transfer for all values of Pr at the hot wall. This variation is seen less prominent at the cold wall as compared to the hot wall. In figure 5.13d, the average Nusselt number versus Casson fluid parameter is demonstrated for $Ra = 10^5, Da = 100, Pr = 7$. It shows that the value of the coefficient of heat transfer enhances significantly for higher value ε as compared to lower lengths of the heated zone. It is concluded that whenever the length of the partial heated zone increases, more heat is transferred from the bottom wall toward the cold vertical walls.

Concluding Remarks

The numerical simulations of steady-state buoyancy-driven convection in a partially heated square porous cavity filled with Casson fluid have been done. The penalty finite element method is used to obtain the smooth solutions of the governing equations. The influence of various pertinent parameters like Darcy number, Rayleigh number, Casson fluid parameter, and heated zone length on flow and thermal field were obtained. Following observations of the above said analysis are summarized below:

- It is found that with an increase in Casson fluid parameter, the flow circulation and heat transfer increases. The center of flow circulations is also obtained to get a detailed analysis of flow dynamics.
- Further, for higher values of Darcy number and Rayleigh number, buoyancy driven convection increases. Thus the increase in flow circulation due to convection at extreme values of Da and Ra cause the isotherms get more distorted, occupying most of the cavity.
- The flow circulation also increases with the increasing heated zone length and its influence is more prominent at extreme values of all the governing parameters.
- The average Nusselt number exhibit increasing behavior under the influence of Rayleigh number, Darcy number, and Casson fluid parameter. At a low Darcy number, the heat transfer is dominated by conduction irrespective of other parameters.

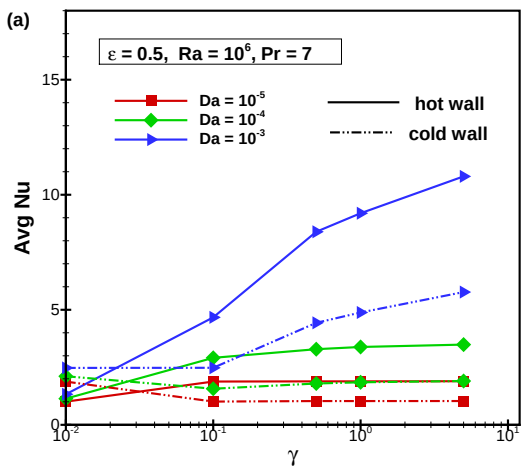

(a)

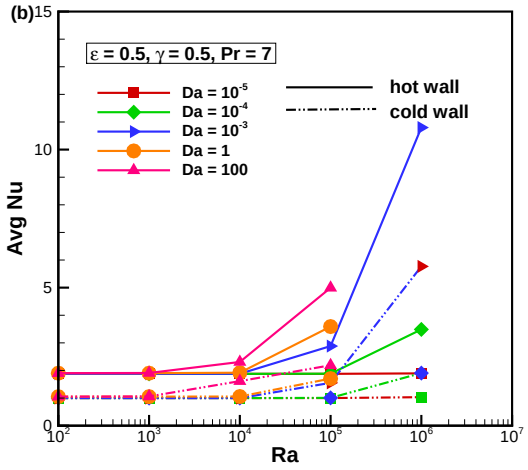

(b)

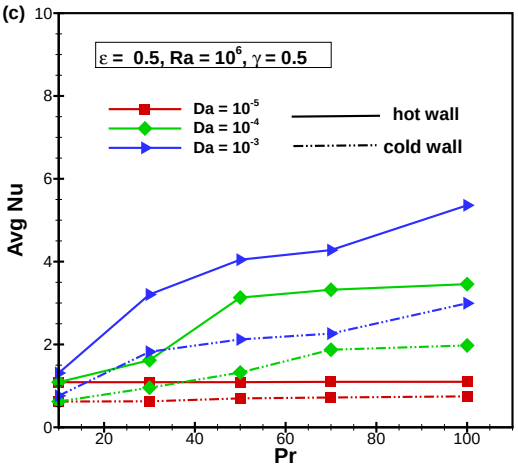

(c)

Figure 5.12: Average Nusselt number at hot and cold wall for varying Darcy number with Ra, γ, Pr (a) $\varepsilon = 0.5, Ra = 10^6, Pr = 7$ (b) $\varepsilon = 0.5, \gamma = 0.5, Pr = 7$ (c) $\varepsilon = 0.5, Ra = 10^6, \gamma = 0.5$

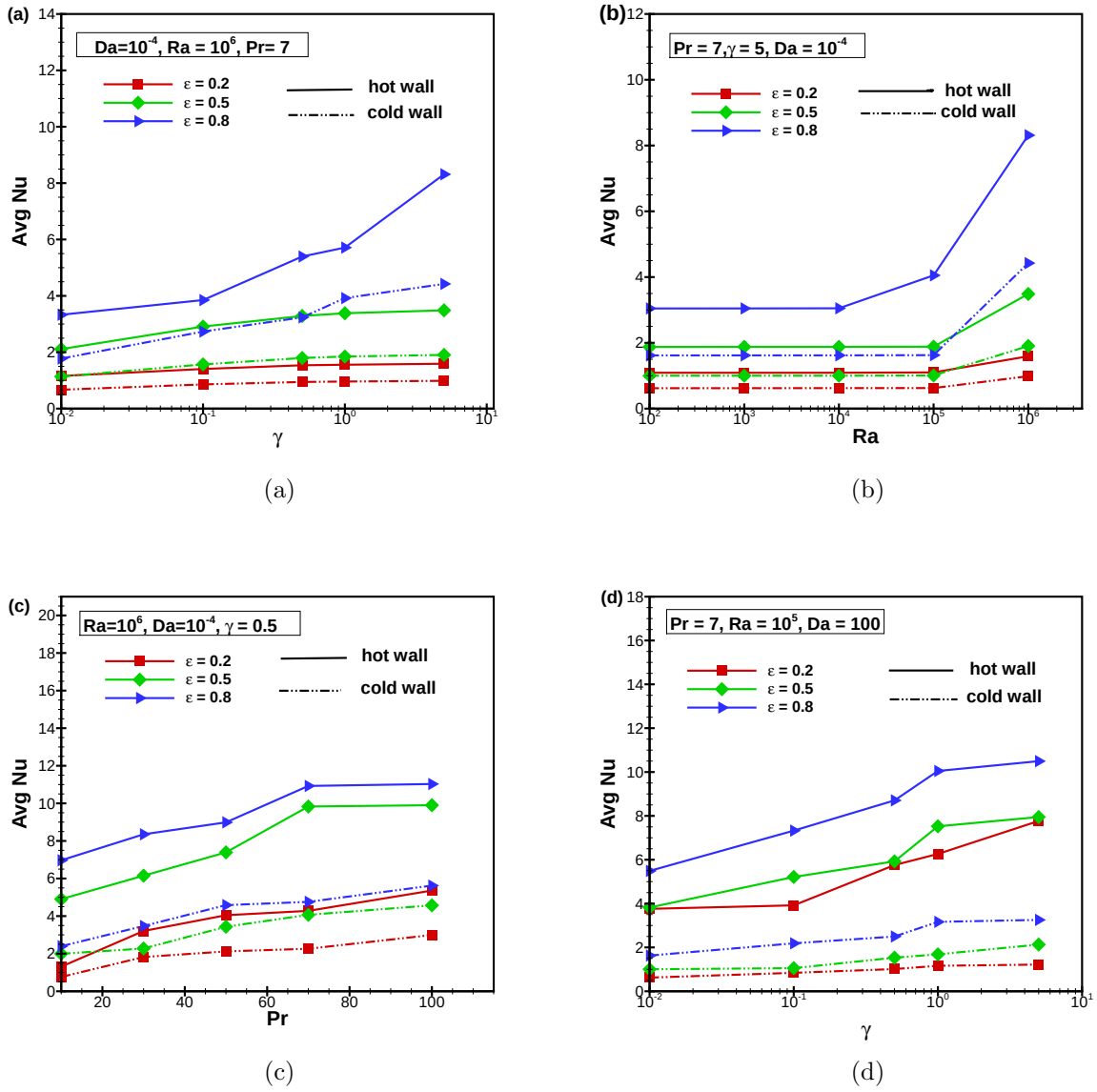

Figure 5.13: Average Nusselt number at hot and cold wall for varying ε with Ra, γ, Pr (a) $Ra = 10^6, Da = 10^{-4}, Pr = 7$ (b) $Da = 10^{-4}, \gamma = 5, Pr = 7$ (c) $Da = 10^{-4}, Ra = 10^6, \gamma = 0.5$ (d) $Da = 100, Ra = 10^5, Pr = 7$

Chapter 6

Numerical Analysis of flow of $Al_2O_3-SiO_2$/water Hybrid in a Porous Cavity

Pure fluid, oil, ethylene glycol are used as conventionally heat transfer fluid. These fluids have a low thermal conductivity which affects the heat transfer rate. For improving the thermal characteristics of these fluids, the idea of adding tiny particles of size microns or millimeters was introduced in the past few decades [143]. In practical applications, these large-sized particles cause problems such as abrasion and obstruction in the flow of fluid. After that, in the late twentieth century, Choi and Eastman [51] gave us the idea of using nanosized particles instead of large-sized particles in the host fluid to enhance the heat transfer rate. The base fluids which contain nanosized particles of high thermal conductivity are named as nanofluids. Mostly, the nanoparticles considered with the base fluids are metals (Cu, Ag, Au), metals in their oxide form (Al_2O_3, CuO), semiconductors (TiO_2, SiO_2), non-metals (graphite, carbon nanotubes), carbides (SiC) and nitrides (SiN). It is found that the addition of even a small amount of nanoparticles in the base fluid can enhance its thermophysical properties (viscosity, thermal conductivity, heat transfer rate). Nanofluids have lot many applications which include nanofluids as coolants [166], antimicrobial agent [245], bionanofluids, environmental nanofluids [138], nanowires [65], and others. Due to potential applications of nanofluids, researchers have done a study on heat transfer aspects of nanofluids, theoretically, experimentally, or numerically [3, 13, 29, 63, 99, 169, 170, 196, 210, 241, 242].

In recent years, scientists are eagerly doing research on further improving the thermophysical properties of nanofluids. They come up with the idea of hybridizing two different nanofluids in a single base fluid with better physical and chemical properties. The metallic nanofluids have high thermal conductivity, but their usage is restrictive due to instability and reactivity. On the other hand, non-metallic nanoparticles are chemically inert and stable in the suspension but have low thermal conductivity. Similarly, metal oxides also have low thermal conductivity compared to metallic nanoparticles. Therefore, to get the desired thermal conductivity, more volume fraction ($> 5\%$) of these nanoparticles must be taken in the base fluid. Thus, it is beneficial to combine these nanoparticles' properties to get nanofluids with high thermal conductivity, high heat transfer rate, less concentration,

low cost, high stability, and flexibility. The advanced class of nanofluids is called hybrid nanofluids which contain nanoparticles of different nature in a single host fluid. Due to synergistic effects, hybrid nanofluids have more heat transfer rate compared to regular nanofluids. This innovative class of nanofluids has applications in almost every field such as bionanofluids for the treatment of cancer, power generation, coolant for various machinery (computers or CPUs, microelectronics), aeronautics, refrigeration, cooling of nuclear reactors, chemical processes, and many more. Thus, in the last few decades, scientist have shown keen interest to work on hybrid nanofluids which include modeling, composition, experimental verification, and applications [40, 68, 111, 122, 130, 135, 204, 224, 227, 228, 243]. In the present investigation, Al_2O_3/SiO_2 water-based nanofluid model is adopted as a case study for heat transfer.

6.1 Mathematical Model

In the existing natural convection problem, a Al_2O_3/SiO_2 water-based hybrid nanofluid is filled in the square porous cavity of side L . Figure 1 depicts the geometrical visualization of the cavity as well as the coordinate system. The vertical walls of the cavity are at a lower temperature T_c while the portion of the bottom wall is kept at a higher temperature T_h. To investigate the effect of a heated zone on fluid flow and heat transfer characteristics, the length of the heated part of the wall was varied. The physical-chemical properties of the hybrid nanofluid (Table 1) and porous medium are assumed to be constant, with the exception of the density in the buoyancy term, which is satisfied by Boussinesq's approximation. Further, it is assumed that the two-dimensional flow circulation caused by buoyancy forces due to temperature differences is steady-state, laminar, and incompressible. The Darcy-Forchheimer model is used to calculate momentum transfer in a porous medium. Making use of these assumptions, the governing equations of the flow problem are as follows:

$$\frac{\partial u}{\partial x} + \frac{\partial v}{\partial y} = 0, \tag{6.1.1}$$

$$u\frac{\partial u}{\partial x} + v\frac{\partial u}{\partial y} = \frac{1}{\rho_{hnf}}\left[-\frac{\partial p}{\partial x} + \mu_{hnf}\left(\frac{\partial^2 u}{\partial x^2} + \frac{\partial^2 u}{\partial y^2}\right) - \frac{\mu_{hnf}}{K}u\right] \tag{6.1.2}$$

$$u\frac{\partial v}{\partial x} + v\frac{\partial v}{\partial y} = \frac{1}{\rho_{hnf}}\left[-\frac{\partial p}{\partial y} + \mu_{hnf}\left(\frac{\partial^2 v}{\partial x^2} + \frac{\partial^2 v}{\partial y^2}\right) - \frac{\mu_{hnf}}{K}v\right] + (\rho\beta)_{hnf} g(T - T_c) \tag{6.1.3}$$

$$u\frac{\partial T}{\partial x}+v\frac{\partial T}{\partial y}=\alpha_{hnf}\left(\frac{\partial^2 T}{\partial x^2}+\frac{\partial^2 T}{\partial y^2}\right) \tag{6.1.4}$$

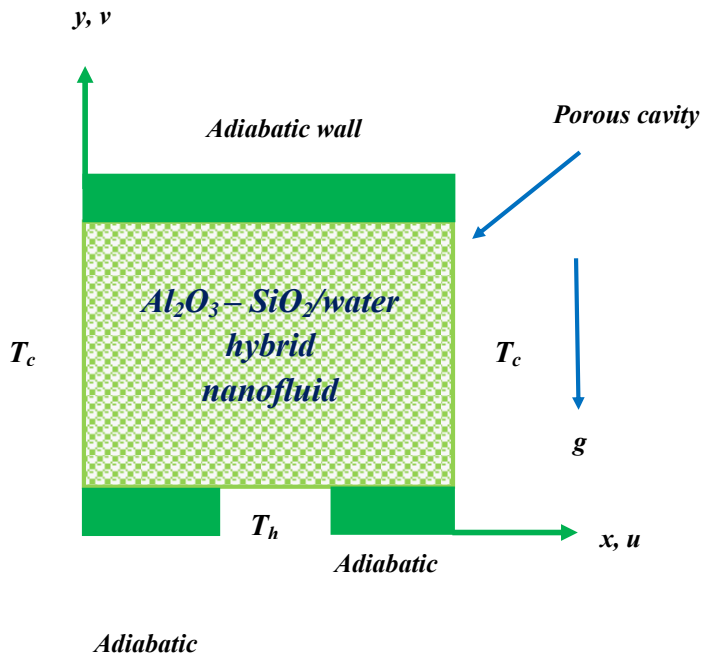

Figure 6.1: Physical Description and Cartesian Co-ordinates

To convert the variables of governing equations into non-dimensional form, following transformations are utilized [243]:

$$X=\frac{x}{L},\quad Y=\frac{y}{L},\quad U=\frac{uL}{a_f},\quad V=\frac{vL}{a_f},\quad P=\frac{pL^2}{\rho_{nf}a_f^2},\quad \theta=\frac{T-T_c}{T_h-T_c}$$

$$Ra=\frac{g\beta_f L^3(T_h-T_c)}{a_f\nu_f},\quad Pr=\frac{\nu_f}{a_f},\quad Da=\frac{\kappa}{L^2} \tag{6.1.5}$$

By using above mentioned transformations, the non-dimensional continuity, momentum and energy equations are as follows:

$$\frac{\partial U}{\partial X}+\frac{\partial V}{\partial Y}=0, \tag{6.1.6}$$

$$U\frac{\partial U}{\partial X}+V\frac{\partial U}{\partial Y}=-\frac{\partial P}{\partial X}+\frac{\mu_{hnf}}{\rho_{hnf}a_f}\left(\frac{\partial^2 U}{\partial X^2}+\frac{\partial^2 U}{\partial Y^2}\right)-\frac{\mu_{hnf}}{\rho_{hnf}a_f}\frac{1}{Da}U, \tag{6.1.7}$$

$$U\frac{\partial V}{\partial X}+V\frac{\partial V}{\partial Y}=-\frac{\partial P}{\partial Y}+\frac{\mu_{hnf}}{\rho_{hnf}a_f}\left(\frac{\partial^2 V}{\partial X^2}+\frac{\partial^2 V}{\partial Y^2}\right)-\frac{\mu_{hnf}}{\rho_{hnf}a_f}\frac{1}{Da}V+\frac{(\rho\beta)_{hnf}}{\rho_{hnf}\beta_f}RaPr\theta, \tag{6.1.8}$$

$$U\frac{\partial \theta}{\partial X}+V\frac{\partial \theta}{\partial Y}=\frac{\alpha_{hnf}}{a_f}\left(\frac{\partial^2 \theta}{\partial X^2}+\frac{\partial^2 \theta}{\partial Y^2}\right). \tag{6.1.9}$$

The corresponding boundary conditions in non-dimensionalized form are given below:

$\theta=0,\quad U=V=0\quad \text{at}\quad X=0\quad \text{and}\quad 0<Y<1$

$\theta=0, U=V=0\quad \text{at}\quad X=1\quad \text{and}\quad 0<Y<1$

$\theta=1, U=V=0\quad \text{at}\quad Y=0\quad \text{and}\quad \frac{1-\varepsilon}{2}\leqslant X\leqslant\frac{1+\varepsilon}{2}$

$\frac{\partial\theta}{\partial Y}=0, U=V=0\quad \text{at}\quad Y=0,\ 0<X<\frac{1-\varepsilon}{2}\quad \text{and}\quad \frac{1+\varepsilon}{2}<X<1,$

$$\frac{\partial\theta}{\partial Y}=0, U=V=0\quad \text{at}\quad Y=1,\ 0<X<1. \tag{6.1.10}$$

Table 6.1: Thermophysical properties of fluid and nanoparticles at room temperature [7, 140]

Physical properties	Fluid phase (water)	SiO_2	Al_2O_3
$C_p(J/kgK)$	4179	703	765
$\rho(kg/m^3)$	997.1	2200	3970
$k(W/mK)$	0.613	1.2	40.0
$\beta\times10^{-5}(1/K)$	21.0	0.55	0.58
Pr	6.2	–	–

The correlations established for the density, specific heat and thermal expansion coefficients of hybrid nanofluid are:

$$\rho_{hnf}=\varphi_1\rho_1+\varphi_2\rho_2+(1-\varphi_{tot})\rho_{bf} \tag{6.1.11}$$

$$(\rho c_p)_{hnf}=\varphi_1(\rho c_p)_1+(1-\varphi_{tot})\rho_{bf} \tag{6.1.12}$$

$$(\rho\beta)_{hnf} = \varphi_1(\rho\beta)_1 + \varphi_2(\rho\beta)_2 + (1-\varphi_{tot})(\rho\beta)_{bf} \tag{6.1.13}$$

For the estimation of effective thermal conductivity of the hydrid nanofluid Maxwell's model for effective thermal conductivity model is rewritten for two different nanoparticles are as follows [142]:

$$k_{hnf} = k_{bf}\frac{\left(\frac{(\varphi_1 k_1+\varphi_2 k_2)}{\varphi} + 2k_{bf} + 2(\varphi_1 k_1 + \varphi_2 k_2) - 2\varphi k_{bf}\right)}{\left(\frac{(\varphi_1 k_1+\varphi_2 k_2)}{\varphi} + 2k_{bf} - (\varphi_1 k_1 + \varphi_2 k_2) + \varphi_{tot} k_{bf}\right)} \tag{6.1.14}$$

The effective visocity of the hybrid nanofluid is estimated by generalizing Brinkman model which is widely applicable model in the case of numerical studies [142, 147].

$$\mu_{hnf} = \frac{\mu_{bf}}{(1-(\varphi_1+\varphi_2)^{2.5})} \tag{6.1.15}$$

where $\varphi = \varphi_1 + \varphi_2$

The subscripts bf, hnf refer to the base fluid and hybrid nanofluid. Also φ_1, φ_2 denotes the volume fractions of Al_2O_3 particles and SiO_2 particles in the hybrid nanofluid.

The average Nusselt number for the heated portion of the bottom wall is given by

$$\overline{Nu} = \int_{\frac{1-\varepsilon}{2}}^{\frac{1+\varepsilon}{2}} Nu(X)dX \tag{6.1.16}$$

where $Nu(X) = -\frac{k_{hnf}}{k_{bf}}\left(\frac{\partial\theta}{\partial Y}\right)_{Y=0}$ is the local Nusselt number

6.2 Methodology & Validation of Results

The governing equations of the flow problem are coupled non-linear partial differential equations. These equations cannot be solved by an analytic approach. Instead, a numerical technique has to be applied. In the present investigation, penalty finite element method [103, 190, 192] is employed for solving the above-said equations. In this method, pressure term in the momentum equations is accommodated by a penalty parameter Γ and an incompressibility criteria, which results as $P = -\Gamma\left(\frac{\partial U}{\partial X} + \frac{\partial V}{\partial Y}\right)$. The value of penalty parameter is taken as $\Gamma = 10^7$ to get the stable solution [15]. For this large value of Γ,

the continuity equation is automatically satisfied. The pressure term is eliminated from momentum equations by using the above definition of P, and reduced equations take the following form:

$$U\frac{\partial U}{\partial X}+V\frac{\partial U}{\partial Y}=\Gamma\frac{\partial}{\partial X}\left(\frac{\partial U}{\partial X}+\frac{\partial V}{\partial Y}\right)+\frac{\mu_{hnf}}{\rho_{hnf}a_f}+\left(\frac{\partial^2 U}{\partial X^2}+\frac{\partial^2 U}{\partial Y^2}\right)-\frac{\mu_{hnf}}{\rho_{hnf}a_f}\frac{1}{Da}U \tag{6.2.1}$$

$$U\frac{\partial U}{\partial X}+V\frac{\partial U}{\partial Y}=\Gamma\frac{\partial}{\partial X}\left(\frac{\partial U}{\partial X}+\frac{\partial V}{\partial Y}\right)+\frac{\mu_{hnf}}{\rho_{hnf}a_f}\left(\frac{\partial^2 V}{\partial X^2}+\frac{\partial^2 V}{\partial Y^2}\right)-\frac{\mu_{hnf}}{\rho_{hnf}a_f}\frac{1}{Da}V \tag{6.2.2}$$

To solve the governing equations, the commercial software freefem++ [97] is used. The study allows for a tolerance of up to 10^{-6}. The study of Basak et al. [15] has been considered for validation of our numerical scheme. Figure 6.2 shows that the isotherm lines obtained in this study are consistent with those obtained in Basak et al. study's for two different values of the Darcy number ($Da = 10^{-4}, 10^{-3}$) while keeping the others constant as $Pr = 0.71, \varepsilon = 1, Ra = 10^6$. Furthermore, under similar thermal conditions and flow characteristics, average Nusselt number values (figure 3) show good agreement with Basak et al.'s work.

6.3 Results & Discussion

The current research is aimed to analyze the hydrodynamic and thermal characteristics of $Al_2O_3 - SiO_2$/water hybrid nanofluid in a square porous cavity. The bottom wall of the porous cavity has been partially heated at the center, while the temperature at the vertical side walls is low for providing cooling effects. The remaining portion of the bottom and the top wall have been considered to be adiabatic. The outcomes of the present investigation are represented in terms of vertical component of velocity profiles, isolines of stream function, and temperature, average Nusselt number for the ranges of parameter as $\varphi = 1\% - 3\%, Ra = 10^3 - 10^6, Da = 10^{-5} - 10^{-3}, \varepsilon = 0.2, 0.5, 0.8$ and for fixed value of $Pr = 6.2$.

6.3.1 Streamlines & Isotherms Profile

The streamlines and isotherms for the present study are shown in figures (6.3-6.9). It can be seen in the figures that both the streamlines and isotherm contours are symmetric

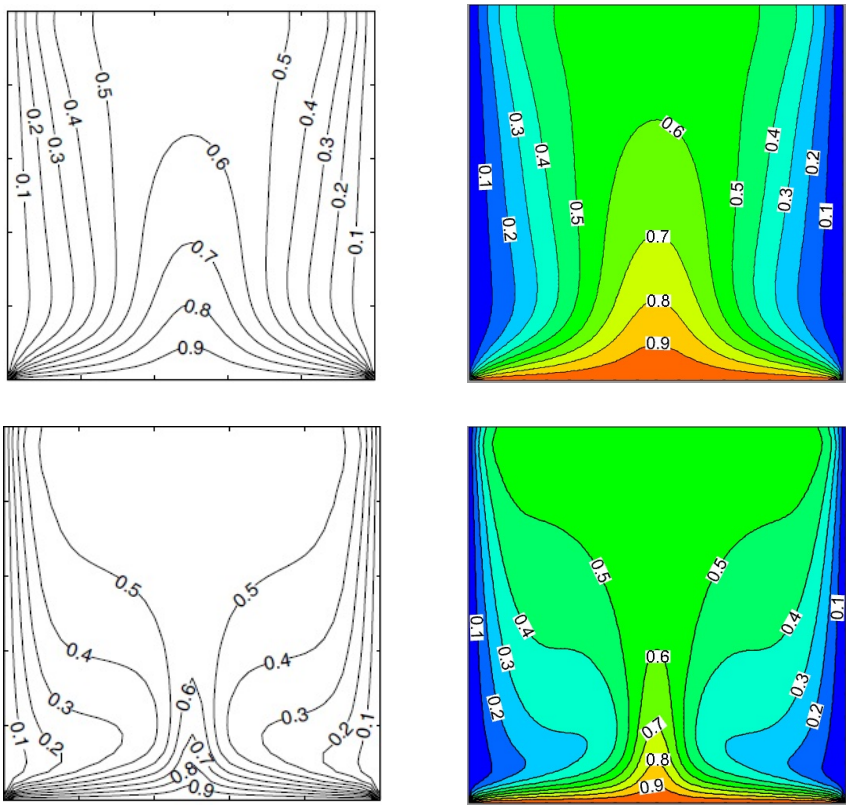

Figure 6.2: Validation of results via isotherm lines obtained in the present investigation (right side) and those in Basak et al.'s [15] work (left side) for $Pr = 0.71, Ra = 10^6, \varepsilon = 1$ in case of newtonian fluids

about the vertical midline, i.e., $X = \frac{1}{2}$ of the porous cavity due to symmetry of the thermal boundary conditions. This symmetric nature of boundary conditions also results in the formation of counter-rotating vortices in both the halves (left & right) of the cavity. In each vortex cell, the local fluid gets heat from the partially heated bottom wall of the cavity. Hence, the density of the fluid in the vicinity of the heated wall reduces, which results in the development of buoyancy forces. The fluid moves upward due to density difference, and then faces the adiabatic upper wall of the cavity. After, then the fluid moves horizontally toward the cooled side walls. The vertical side walls absorb heat from the moving fluid, and then fluid moves downward due to the increase in its density. The fluid moved as a result of the simultaneous heating and cooling effect.

Numerical results in terms of streamlines for varying Da, Ra, φ, and $\varepsilon = 0.8$ are shown in figures (6.3-6.6). Streamlines pattern for three different volume fractions of hybrid nanoparticles $\varphi = 1\% - 3\%$ are illustrated in figures (6.3-6.5). Streamlines profile for varying Ra, Da at fixed length of heated zone ($\varepsilon = 0.8$) and volume fraction $\varphi = 1\%$ is depicted in figure 4. It is observed from the figure that flow circulation strongly depends on the Darcy number. At a low Darcy number, flow circulation is weak at any value of the Rayleigh number. The strength of the flow enhances at a higher value of Da due to which fluid rises in the upward direction from the middle portion of the bottom towards the cold vertical walls forming symmetric rolls in both the halves of the cavity in the anticlockwise and clockwise direction. This happens because the porous medium offers less resistance at a higher value of Da. This phenomenon is clearly visible at $Ra = 10^6$ and $Da = 10^{-3}$. This is because as we go on increasing the value of Ra, buoyancy forces increase. Therefore, flow circulation inside the cavity enhances, as seen from the greater magnitude of streamlines. The flow circulation near the center is more compared to side walls due to the no-slip boundary condition. In figure 6.4, streamlines are plotted for nanoparticles volume fraction $\varphi = 2\%$. It can be seen from the figure that flow circulation further enhances with the increment in the volume fraction of solid nanoparticles, and also a similar pattern of streamlines is observed for varying Ra and Da. Also, in figure 6.5, a similar streamlines profile for $\varphi = 3\%$ is depicted. Overall, it is depicted from the figures that streamline become sharper at extreme values of Ra, Da at any volume fraction of hybrid nanoparticles (φ)

In figure 6.6, the streamlines are illustrated for low and high values of governing parameters, i.e., Ra, Da, φ with the different length of heating zone $\varepsilon = 0.2, 0.5, 0.8$ to see its impact on hydrodynamic characteristics (streamline profile). As the value of governing parameters increases, the intensity of flow circulation augments, and streamlines become sharper, whereas the length of the heated zone increases from 0.2 to 0.8, the structure of flow

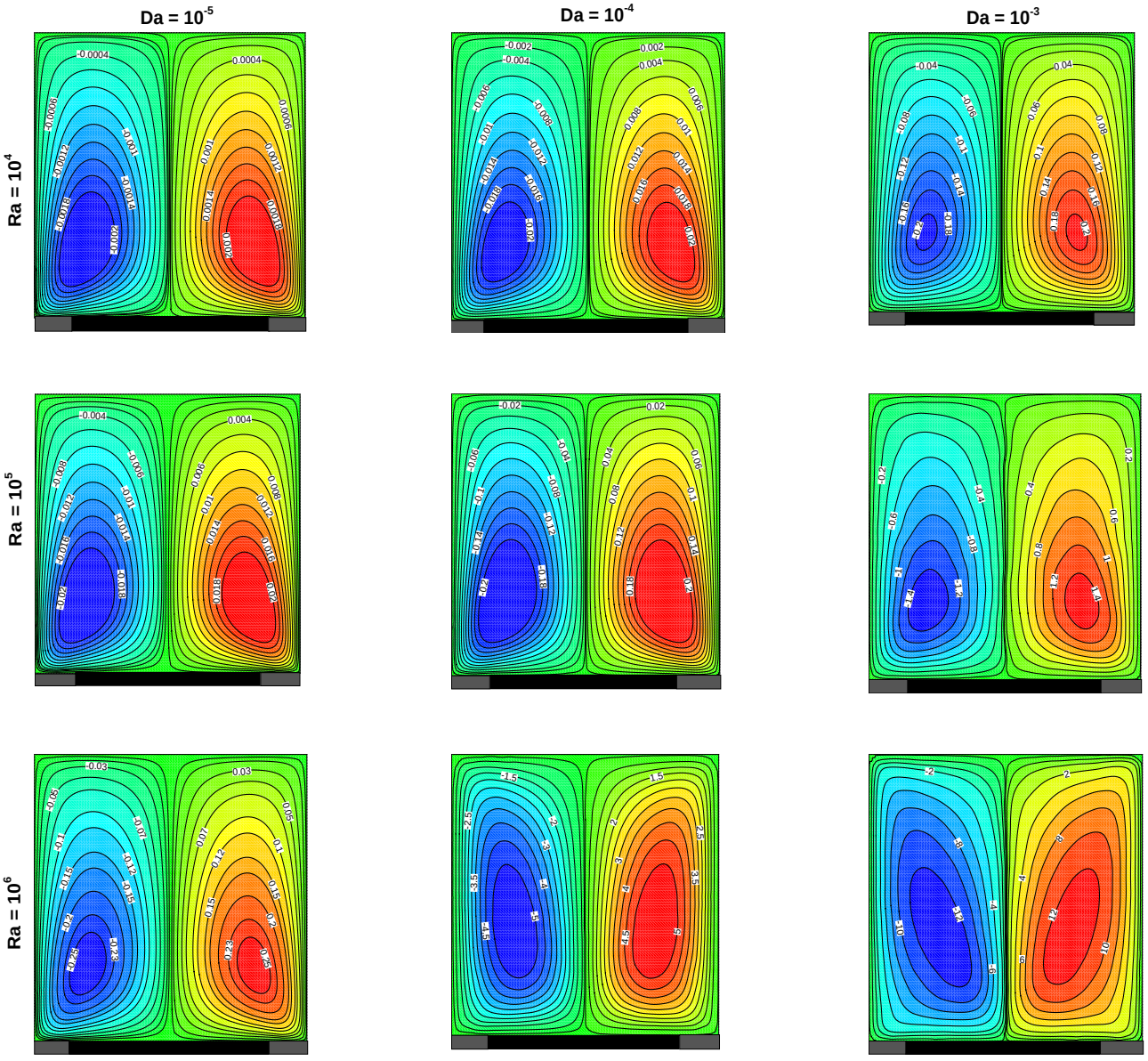

Figure 6.3: Streamlines plots for varying Ra, Da at fixed value of $\varphi = 1\%, \varepsilon = 0.8, Pr = 6.2$

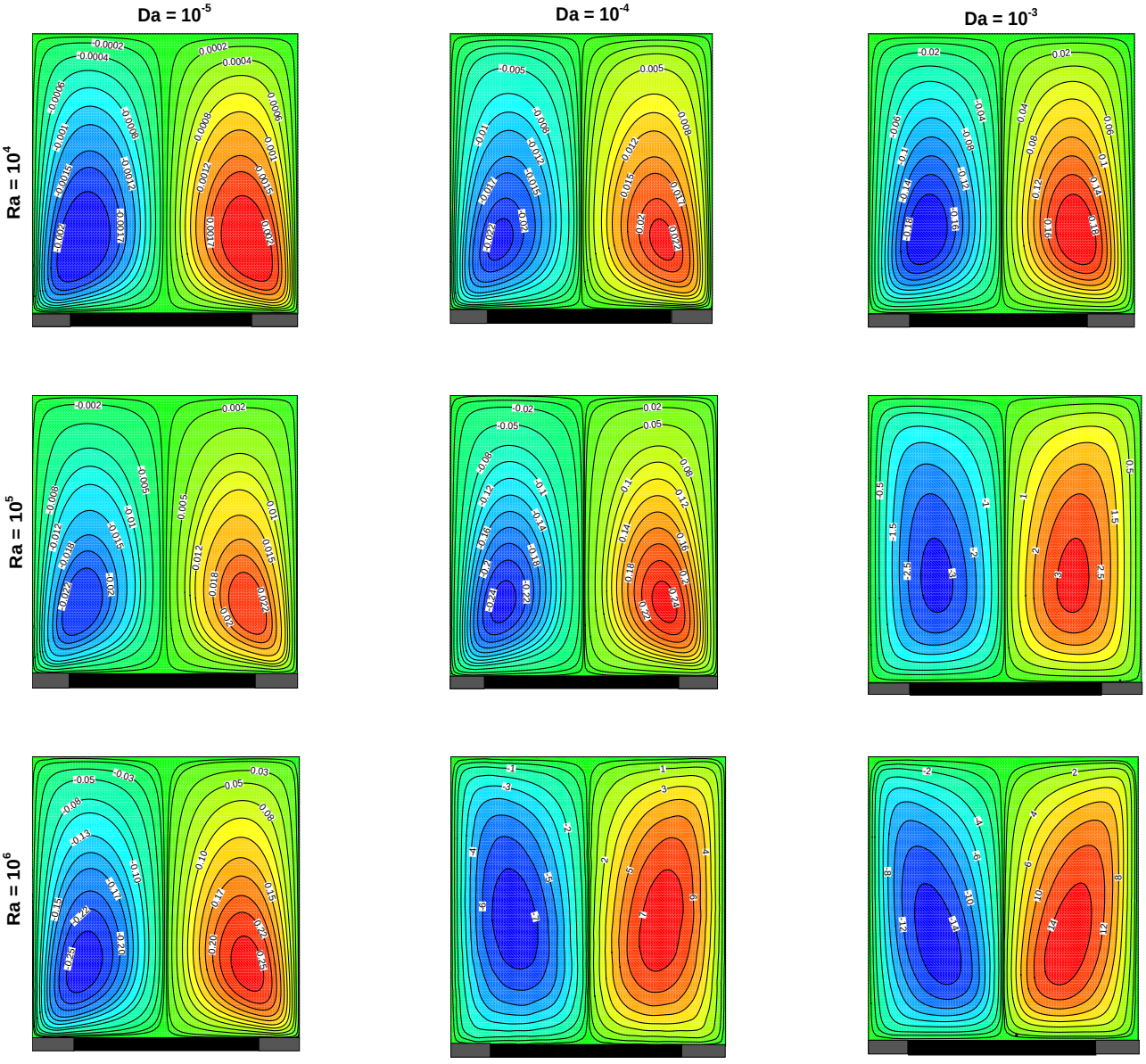

Figure 6.4: Streamlines plots for varying Ra, Da at fixed value of $\varphi = 2\%, \varepsilon = 0.8, Pr = 6.2$

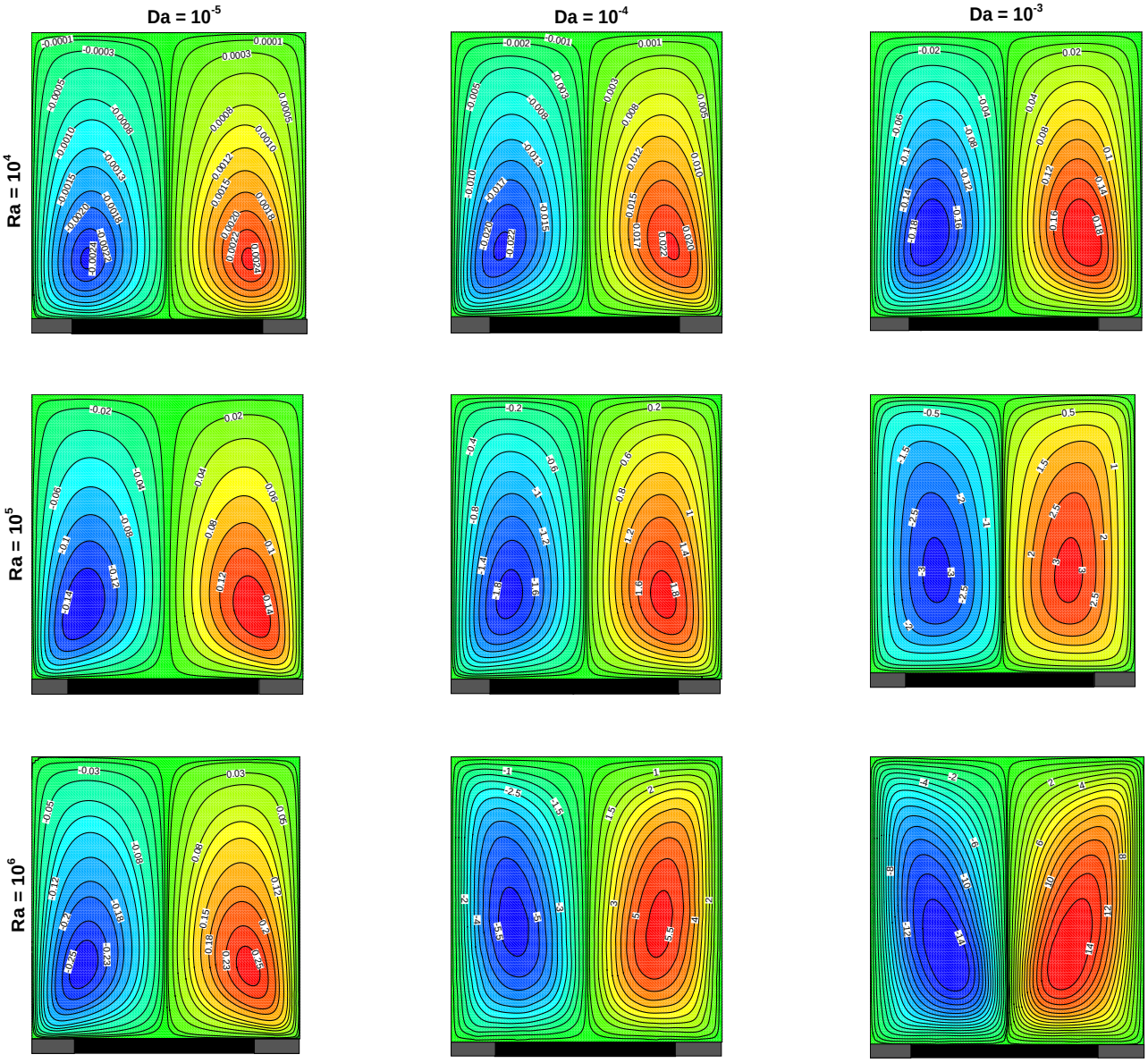

Figure 6.5: Streamlines plots for varying Ra, Da at fixed value of $\varphi = 3\%, \varepsilon = 0.8, Pr = 6.2$

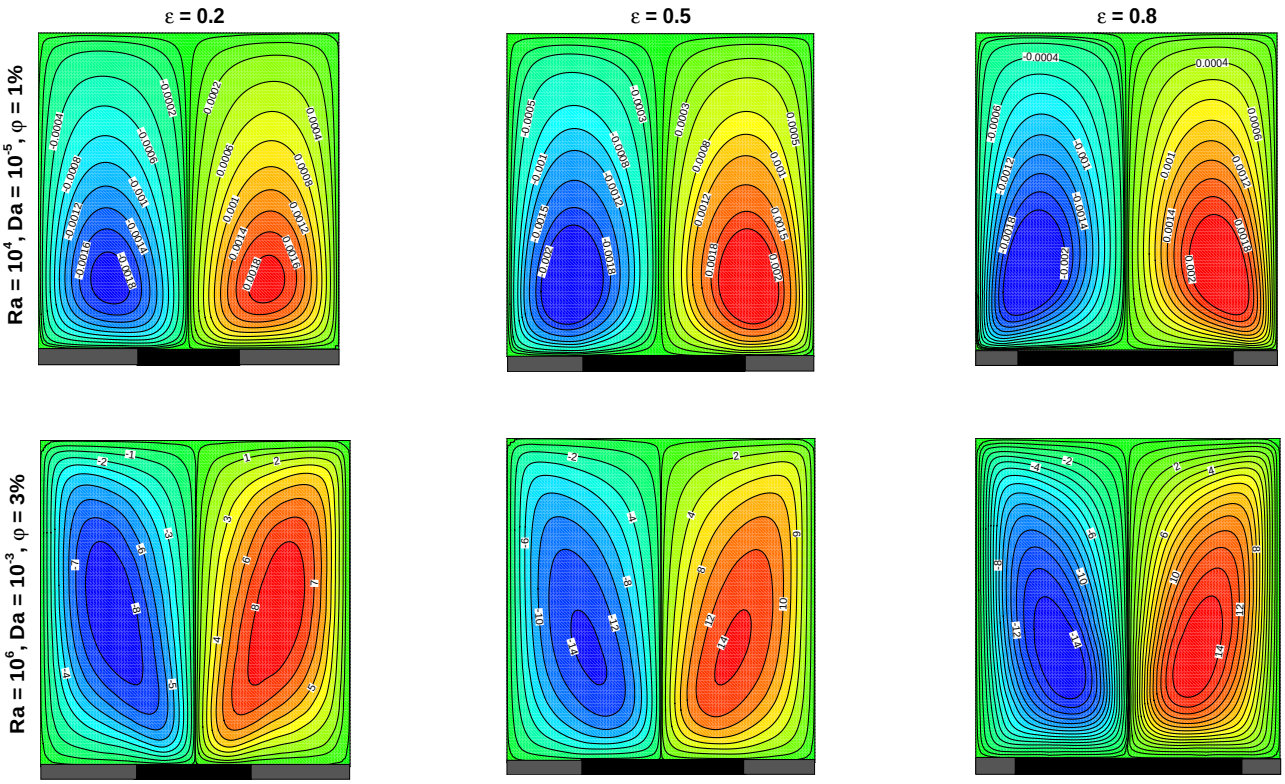

Figure 6.6: Streamline plots for varying ε, Ra, Da at fixed value of $Pr = 6.2$

changes, and the center of circulation shifts horizontally towards cold walls. It is observed from the figure that as the length of the heated portion of the bottom wall augments at fixed values of Ra, Da and φ, flow circulation becomes more intense. The figure also shows that the center of circulation exhibits complex behavior as the values of all governing parameters increase. Furthermore, as the length of the heating zone changes, the center of circulation shifts vertically downwards and moves horizontally towards cold vertical walls, as shown in the figure.

The figures show the temperature distribution inside the porous cavity with varying values of Da, Ra, and φ, as well as a fixed value of $\varepsilon = 0.8$. Figure 6.7 depicts isotherms for $\varphi = 1\%$ with varying values of Da, Ra. The figure shows that at low Da and Ra values, almost all the isotherms are smooth curves near the heated bottom wall. At this stage, conduction is the only mode of heat transfer due to low momentum and temperature gradients. Furthermore, as the magnitude of streamlines increases with an increase in the value of Ra from 10^4 to 10^6, the recirculation near the central regimes increases. As a result, isotherms begin to deform and shift towards cold vertical walls. The fluid circulates more at extreme Ra values, taking heat from the bottom wall and transferring it to the cold vertical walls, resulting in more noticeable heat exchange between the sides and bottom

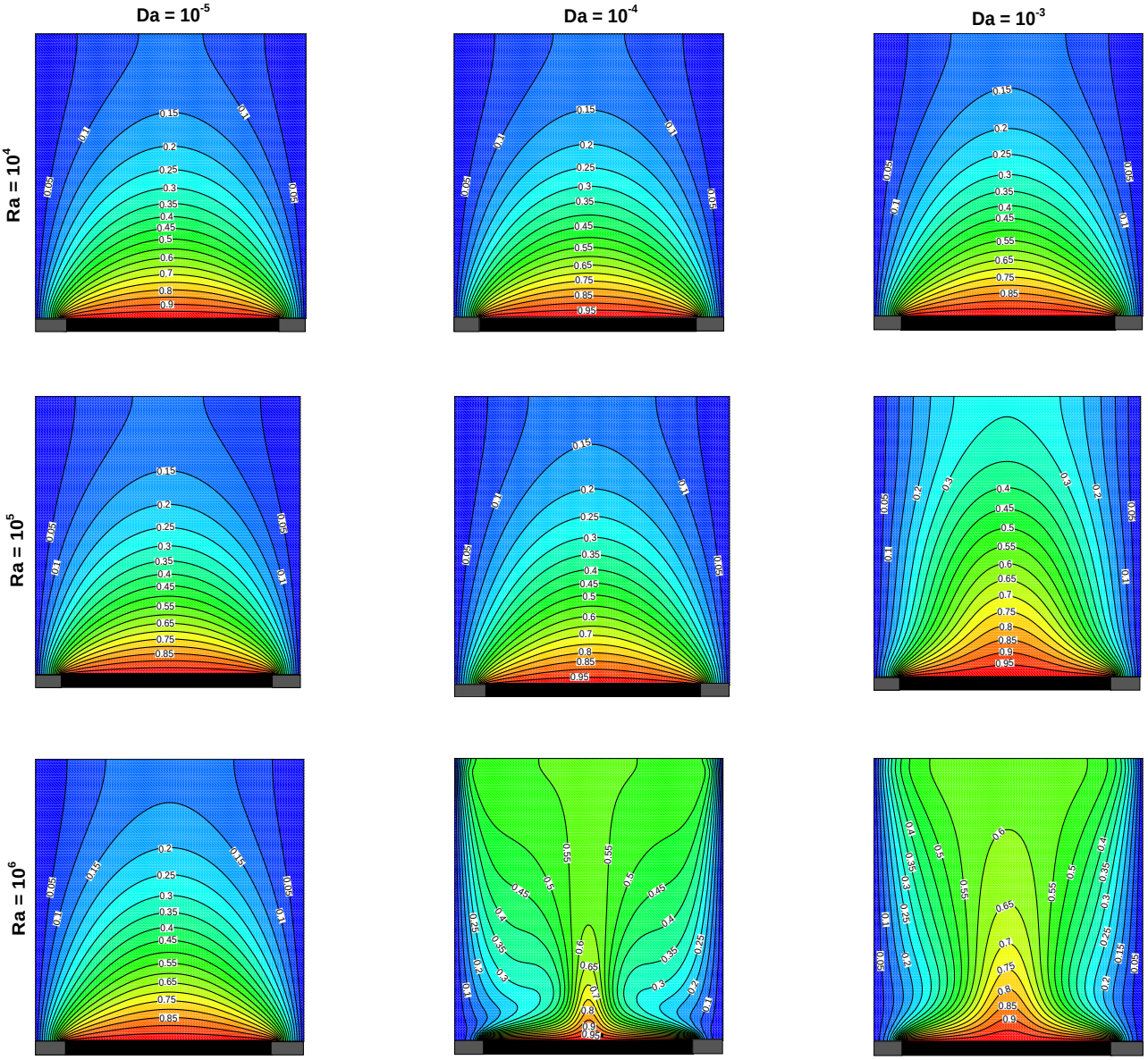

Figure 6.7: Isotherm plots for varying Ra, Da at fixed value of $\varphi = 1\%, \varepsilon = 0.8, Pr = 6.2$

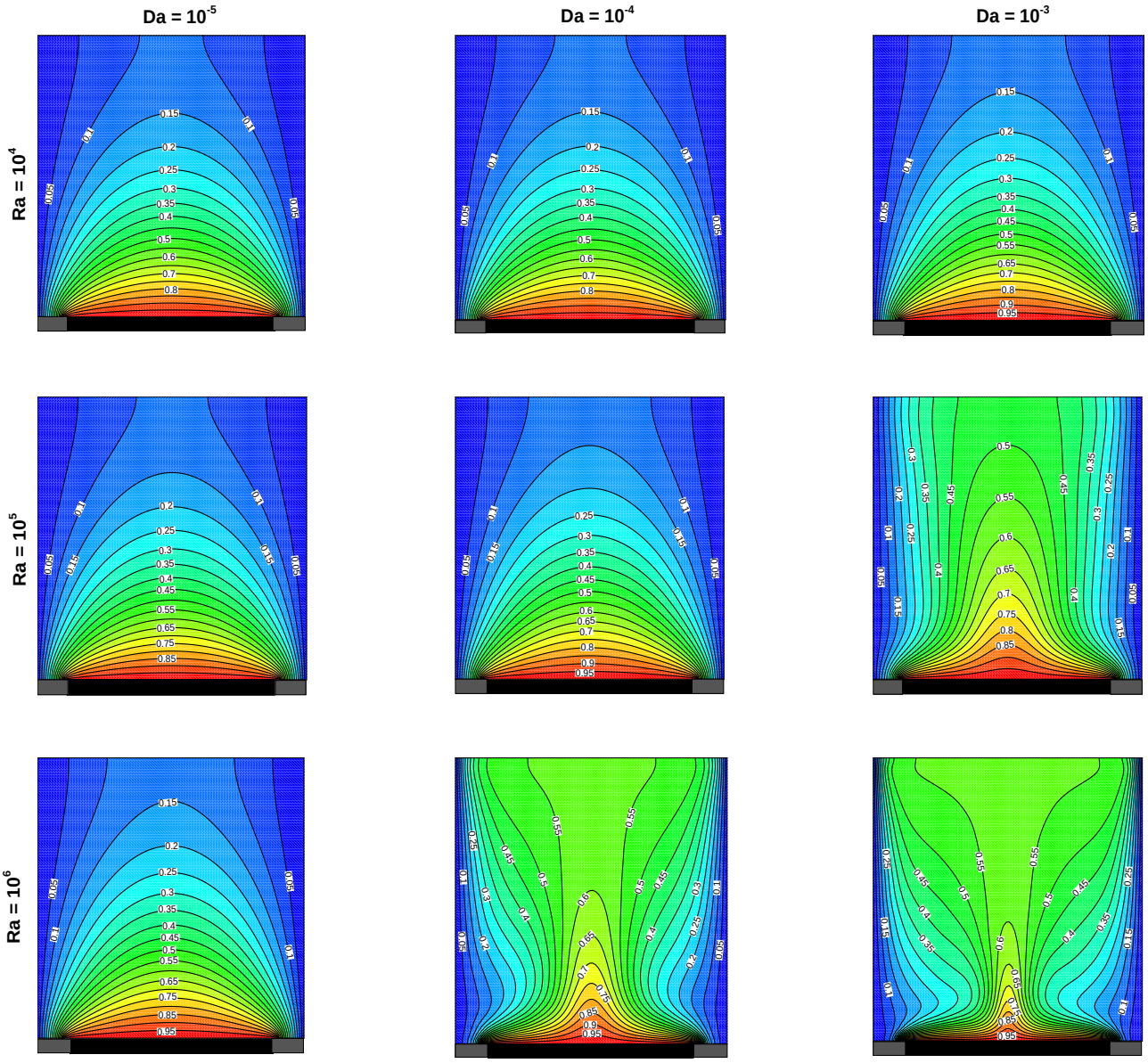

Figure 6.8: Isotherm plots for varying Ra, Da at fixed value of $\varphi = 2\%, \varepsilon = 0.8, Pr = 6.2$

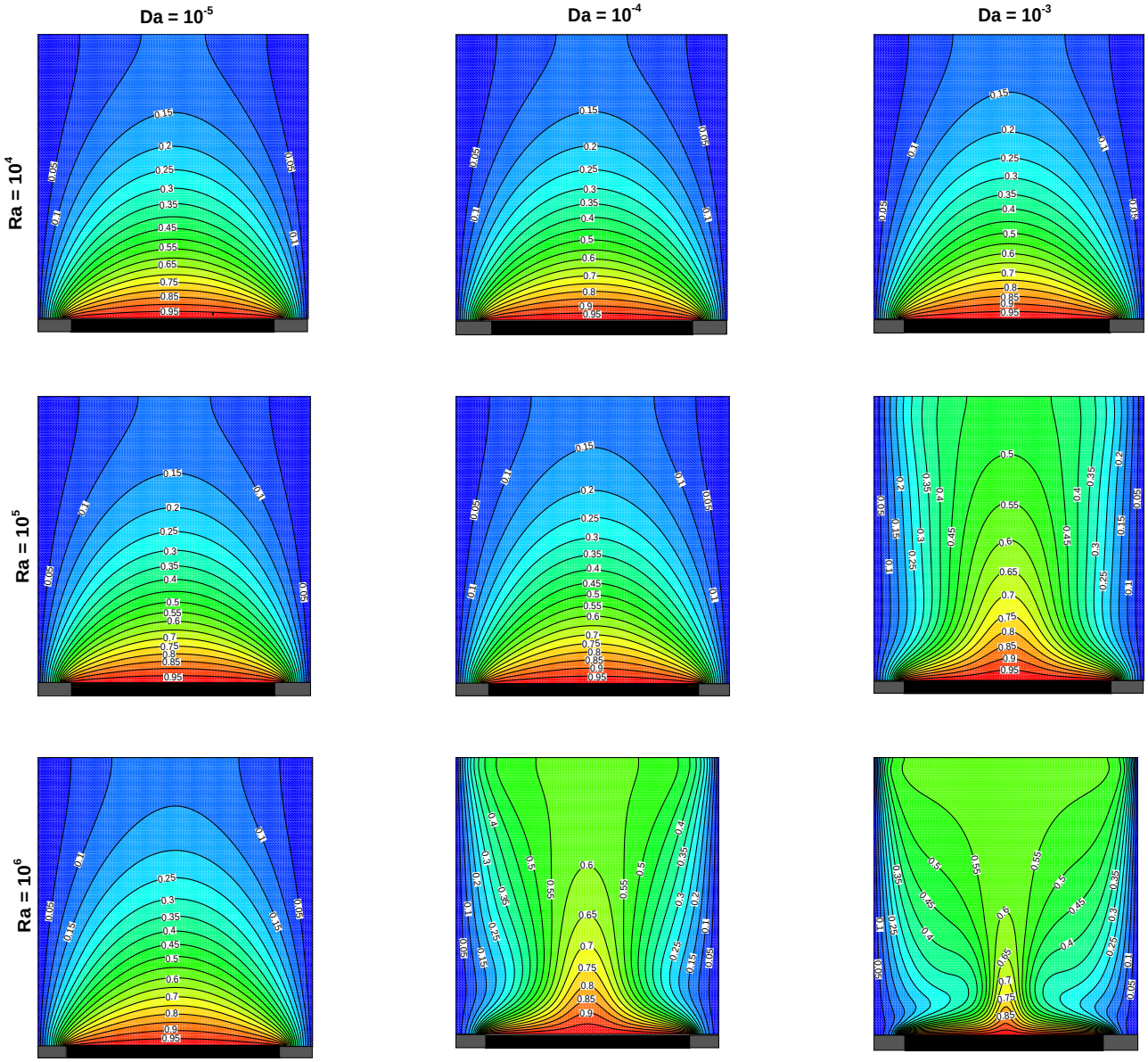

Figure 6.9: Isotherm plots for varying Ra, Da at fixed value of $\varphi = 3\%, \varepsilon = 0.8, Pr = 6.2$

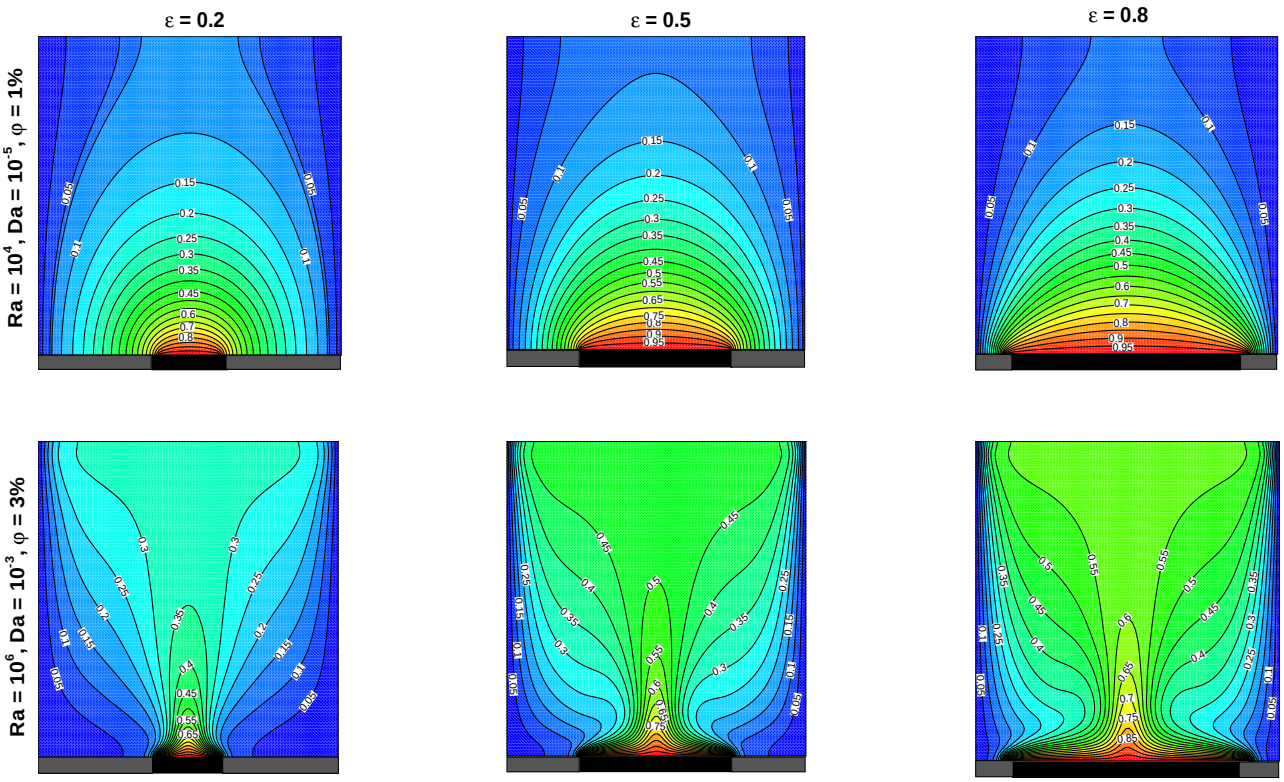

Figure 6.10: Isotherm plots for varying ε, Ra, Da at fixed value of $Pr = 6.2$

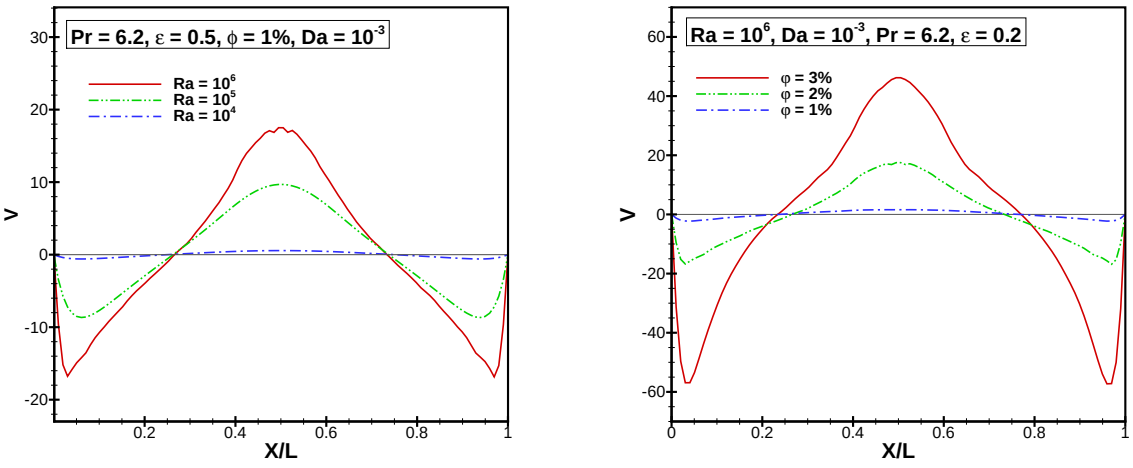

(a) (b)

Figure 6.11: vertical velocity component profile along horizontal midplane

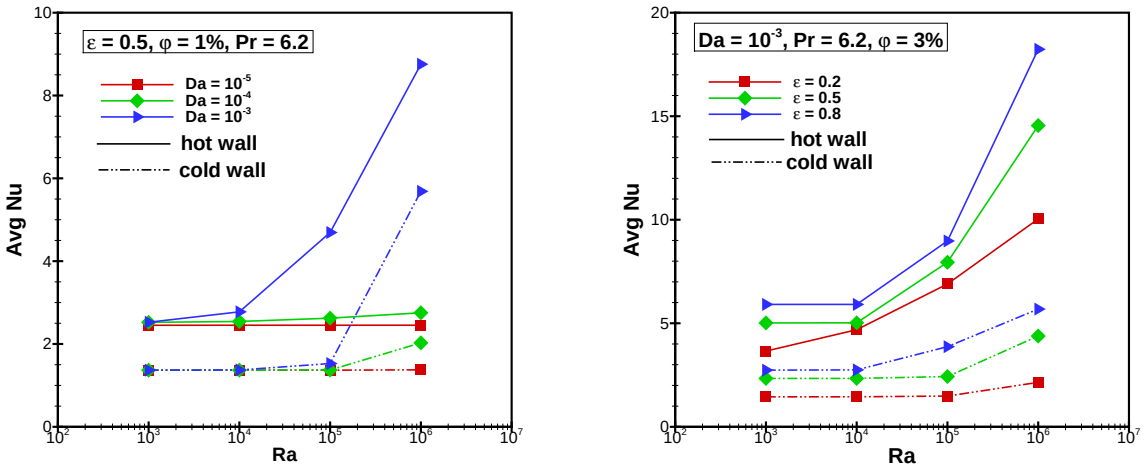

(a)

(b)

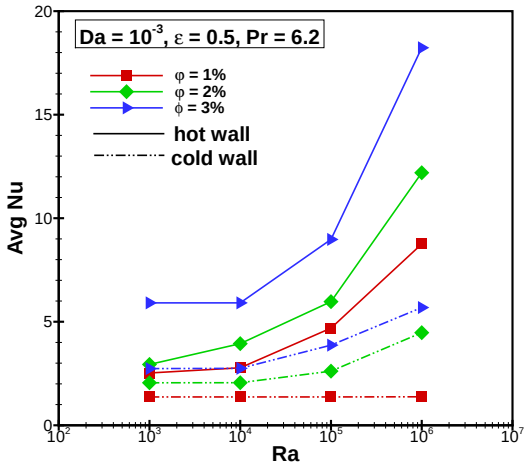

(c)

Figure 6.12: Average Nusselt number (Avg Nu) at hot and cold wall by varying Ra with Da, φ, ε (a) $\varepsilon = 0.5, \varphi = 1\%, Pr = 6.2$ (b) $Da = 10^{-3}, \varphi = 3\%, Pr = 6.2$ (c) $\varepsilon = 0.5, Da = 10^{-3}, Pr = 6.2$

walls. Temperature contours for $\varphi = 2\%$ are shown in figure 6.8. It is well known that the flow circulation improves with an increase in the volume fraction of nanoparticles, resulting in an increase in heat transfer, and that this process continues for $\varphi = 3\%$. (figure 6.9).

The influence of the varying heating length zone and extreme values of the remaining parameters on isothermal contours is shown in figure 6.10. It can be seen from the figure that temperature contours occupy most of the cavity with the increasing length of the heated zone. Furthermore, it is observed that heat exchange occurs for low values of all the governing parameters due to conduction only for any heated zone length. As the values of Ra, Da and φ are increasing, isotherms change their structure. The smooth curves that were previously symmetrical about the vertical midplane begin to deform and push towards the cold walls. As a result, heat transfer to the cold vertical walls increases due to enhanced buoyancy-driven flow circulation. There is more heat exchange between the cold vertical walls and the bottom wall when all of the parameters are set to their maximum values.

In figure 6.11, vertical velocity components are plotted along the horizontal midplane at $Y = \frac{1}{2}$ for varying values of φ and Ra. The vertical velocity component for different values of Ra is shown in figure 6.11a. It can be seen from the figure that velocity increases with an increase of Ra. This happens because the buoyancy force increases for the higher value of Ra. It is also noted from the figure that for any value of Ra, velocity is maximum at the center of the cavity, and then it changes its direction along the vertical side walls. This change in the direction of the velocity (upward to downward) takes place at two points inside the cavity regardless of the different values of the Rayleigh number. Similarly, in figure 6.11b vertical velocity component is demonstrated for varying values of φ. As the volume fraction of nanoparticles increases, the flow velocity increases in the vertical direction and is maximum at the center of the cavity.

6.3.2 Average Nusselt number (Avg Nu)

Figure 6.12 depicts the variations in heat transfer, i.e., the average Nusselt number, for the selected range of parameters. The figure shows that as φ, Ra, Da, and ε increase, so does the value of the average Nusselt number. When compared to cold walls, the rate of heat transfer is faster at the hot wall. Figure 6.12a shows the average Nusselt number for different values of Ra and Da while holding the other parameters constant. Figure shows that the variations in heat transfer rate remain nearly constant for $Da = 10^{-5}, 10^{-4}$ for all values of Ra. Because the fluid moves slowly inside the cavity at low permeability values of

the porous medium (Darcy number), heat transfer occurs solely through conduction. For $Ra > 10^5$, the heat transfer coefficient increases significantly at $Da = 10^{-3}$. At $Da = 10^{-3}$ and $Ra = 10^6$, there is a significant increase in heat transfer at the cold walls. Figure 6.12b depicts the variation of the average Nusselt number (ε) and Rayleigh number (Ra) for different heated zone lengths. The figure shows that for $Ra > 10^4$, the rate of heat transfer increases with all values of heated length zone at the hot wall, whereas there is no significant variation in the average Nusselt number at the cold wall. Figure 6.12c depicts the variation in heat transfer rate with different volume fractions. As the volume fraction of nanoparticles increases, so does the thermal conductivity of the fluid, and thus the rate of heat transfer.

Concluding Remarks

The current study examined the flow and heat transfer characteristics of a Al_2O_3/SiO_2 hybrid nanofluid in a partially heated square porous cavity. The penalty finite element method is used to solve the flow problem's governing equations numerically. The effect of various key parameters on the hydrodynamic flow and thermal field is obtained. The following findings from the aforementioned investigation are noteworthy:

- The impact of increasing the volume fraction of nanoparticles on streamlines and isotherm contours is significant. With increasing φ values, the average Nusselt number varies significantly.
- At higher values of Darcy number and Rayleigh number, buoyancy force increases. Thus, increased flow circulation occurs due to convection at extreme values of Da and Ra resulting in more heat transfer towards the cold vertical walls. The coefficient of heat transfer augments at extreme values of these parameters
- The flow circulation increases with the length of the heated zone, and its influence is more pronounced at extreme values of all governing parameters. The average Nusselt number rises as the heated length zone expands.

Chapter 7

Summary and Future Scope

7.1 Summary

Fluid Mechanics is one of the oldest and richest branches of Mechanics,applied Physics as well as Mathematical sciences. Fluid Mechanics has been studied and researched from early days of science and developed with the evolution of science. The subject has great depth for the application as it has tremendous applications in many branches of science and engineering including biological and environmental sciences. In addition it has great importance in Oceanography, Meteorology, glaciology, study of blood flow, gliding motility of bacteria, heat and mass transfer, aerodynamics, etc. We are literally immersed in fluids our bodies are primarily water and simply cannot live without water and air. Not only a fluids and there complex physics is of general interest but it is widely recognized that fluid mechanics is an essential part of human lives. Especially there is occurrence of the nanofluids, non-Newtonian fluids, whose study has been attracted much more attention because of their practical applications in engineering and industry particularly in extraction of crude oil from petroleum products, food processing and construction engineering.

Non Newtonian fluids are those which do not obey the Newtons law of viscosity, though they are highly viscous fluids. The Navier-stokes equations are the foundation of fluid mechanics and these are non-linear partial differential equations. In few cases, the exact solution of these equations are possible and these solutions further narrow downs when we study the mechanics of non-Newtonian fluids. These fluids are very important from industrial point of view and many physical problems involve such fluids, for example, blood, shampoo, ketchup, tooth paste, Grease, etc.

In the present thesis, flow, heat, and mass transfer characteristics of different kinds of fluids such as nanofluids, hybrid nanofluids, non-Newtonian fluid (Casson fluid, Erying-Powell fluid) through one and two-dimensional geometries have been investigated. The well-known Navier-Stokes equations govern fluid flow problems include basic equations such as conservation of mass, momentum, and energy, which are non-linear partial differential equations. The analytical solution of such equation is possible in rare cases only. So,

we utilized the numerical scheme (finite element method) to solve these equations. The following is a summary of all proposed models, as well as the future scope of the current research work:

Chapter 1 provides the background of the proposed study, its development, applications, and other physical aspects involved in studying heat and mass transfer problems. We investigated the flow of nanofluids and gyrotactic micro-organisms through a non-linear inclined stretching sheet in Chapter 2. The addition of micro-organisms to the base fluid, and the nanoparticles, is intended to provide stability to the suspension. Moreover, we used a variable magnetic field in the direction parallel to the y-axis. The main findings of this study show that as the angle of inclination increases fluid velocity decreases while temperature, concentration, and density of micro-organisms enhance. Furthermore, we discovered that the skin friction coefficient, Sherwood number, and Nusselt number decrease as the thermophoresis parameter and buoyancy ratio parameter increases. On the other hand, the motile micro-organisms density number rises by increasing the micro-organisms concentration difference parameter and the Peclet number.

In Chapter 3, we analyzed the bio-convective flow of nanofluids over a heated surface. In this problem, we have utilized a generalized model for heat, and mass flux (Catteneo-Christov double diffusion model). These theories are actively under investigation to resolve some drawbacks of the well-known Fourier's Law and Fick's Law. According to these models, heat is transported as thermal waves with finite speed, and on a similar basis mass is as well. We discovered that increasing the thermal relaxation parameter and solutal relaxation lowers the temperature and concentration of nanoparticles. With increasing values of the thermal relaxation parameter, the skin friction coefficient, and Nusselt number increase. Also, the Sherwood number rises as the solutal relaxation parameter is increased.

In Chapter 4, we examined the flow of non-Newtonian fluid through an exponential stretching sheet. For investigating the flow, heat and mass transfer traits of non-Newtonian fluids, we used the Erying-Powell fluid model. We used the Erying-Powell fluid model to investigate the flow, heat, and mass transfer traits of non-Newtonian fluids. This flow model is unique because it mathematically describes the flow behavior of Newtonian fluids at low and high shear rates but deviates at intermediate shear stresses. Furthermore, in this study, we considered the impact of chemical reactions. This study shows that increasing ϵ (high shear rate) causes an increase in the velocity profile in x and y directions while increasing ς causes a reverse pattern. The chemical reaction parameter affects the concentration of fluid particles, and it is observed that the concentration profile declines with an increase in the chemical reaction parameter.

For investigating flow and heat transfer in a two-dimensional system, we have chosen a

square porous cavity with a partially heated bottom. The phenomenon of free convective heat transfer in cavities is an attractive topic of research because, in cavities, no external source such as electric power is required to induce convectional heat transfer. Due to the absence of power sources, convectional heat transfer in cavities is free from magnetic noise, fee, and sound. In most of the industrial and engineering applications such as air conditioning devices, food processing industries, float glass production, disposal of nuclear waste, ceramic processing, geothermal systems cavities filled with porous media are used because dissipation area of porous is greater than conventional fins thereby enhancing heat convection. Also, The irregular motion of the fluid flow around the individual pores mixes the fluid more effectively. For analysis of results, we have plotted streamlines and isotherms. Also, we have calculated the avg Nusselt number. In chapter 5, we examined the flow of Casson fluid in a square porous cavity. Casson fluid is a particular type of non-Newtonian fluid that flows only when the applied stress is more than the critical value known as yield stress and behaves as solid below the critical value of yield stress. In this study, we concluded that with an increase in permeability of the porous medium (Darcy number) and Casson fluid parameter (γ), the intensity of flow circulation and temperature distribution inside the cavity enhances. Also, the coefficient of heat transfer (avg Nusselt number) enhances with an increase in the values of these parameters.

In recent years, due to the development of technology scientists, can combine the nanofluids of different characters in a single host fluid which has further improved thermophysical properties. This advanced class of nanofluids is called hybrid nanofluids which contain nanoparticles of different nature in a single host fluid. It is found that due to synergistic effects, hybrid nanofluids have more heat transfer rate compared to regular nanofluids. In chapter 6, we considered the flow of a hybrid nanofluid in a localized heated porous cavity. The results obtained in this study reveals that with an increase in volume fraction of nanoparticles intensity of circulation, temperature distribution and avg Nusselt number rises.

7.2 Future Scope

The present research problems has enormous scope for further research work. The work presented in this thesis provides the theoretical and numerical framework for studying the steady incompressible flow of fluids through one and two-dimensional systems. In the present work, we have analyzed the flow behavior of nanofluids, Casson fluid, Erying-

Powell fluid. Since, there are many other challenging engineering problems which involve flow characteristics of more complex fluids. Thus, this work can be extended to examine the flow behavior of some another kind of non-Newtonian fluids. In the present we have examined the flow traits through stretching sheets and square cavity. This work can be further extended to examine the heat and mass transfer through lid driven cavities, rectangular cavities, cylinders or more complex geometries. Also, the proposed work can be further extended to generalized the flow characteristics in the 3D-fluid flow where on the one hand, the problem becomes realistic. On the other hand, it becomes difficult to handle not only theoretically but also computationally. One can also extend the proposed problems to more complex geometries, which are relevant for industrial applications. Needless to mention that the numerical technique adopted in the thesis may not work well for these problems. Hence, a more robust and computationally cheap numerical scheme for different problems may be required.

Bibliography

[1] Abolbashari MH, Freidoonimehr N, Nazari F, Rashidi MM, Analytical modeling of entropy generation for casson nano-fluid flow induced by a stretching surface, *Advanced Powder Technology* 26(2) (2015) 542–552.

[2] Akbar NS, Ebaid A, Khan ZH, Numerical analysis of magnetic field effects on Eyring-Powell fluid flow towards a stretching sheet, *Journal of Magnetism and Magnetic Materials* 382 (2015) 355–358.

[3] Akbarinia A, Abdolzadeh M, Laur R, Critical investigation of heat transfer enhancement using nanofluids in microchannels with slip and non-slip flow regimes, *Applied Thermal Engineering* 31 (4) (2011) 556–565.

[4] Aksoy Y, Pakdemirli M, Khalique CM, Boundary layer equations and stretching sheet solutions for the modified second grade fluid, *International Journal of Engineering Science* 45(10) (2007) 829–841.

[5] Al-Farhany K, Turan A, Numerical study of double diffusive natural convective heat and mass transfer in an inclined rectangular cavity filled with porous medium, *International Communications in Heat and Mass Transfer*, 39(2) (2012) 174–181.

[6] Al-Odat MQ, Damseh RA, Al-Azab TA, Thermal boundary layer on an exponentially stretching continuous surface in the presence of magnetic field effect, *International Journal of Applied Mechanics and Engineering* 11(2) (2006) 289–299.

[7] Alawi OA, Sidik NAC, Xian HW, Kean TH, Kazi SN, Thermal conductivity and viscosity models of metallic oxides nanofluids, *International Journal of Heat and Mass Transfer* 116 (2018) 1314–1325.

[8] Aman S, Al-Mdallal Q, Khan I, Heat transfer and second order slip effect on MHD flow of fractional Maxwell fluid in a porous medium, *Journal of King Saud University-Science* 32(1) (2020) 450–458.

[9] Ashraf MB, Hayat T, Alsaedi A, Three-dimensional flow of eyring-powell nanofluid by convectively heated exponentially stretching sheet, *The European Physical Journal Plus* 130(1) (2015) 1–16.

[10] Ashraf MB, Hayat T, Shehzad SA, Malaikah H, Three-dimensional flow of a viscoelastic fluid on an exponentially stretching surface, *Journal of Applied Mechanics and Technical Physics* 57(3) (2016) 446–456.

[11] Batchelor G, Heat transfer by free convection across a closed cavity between vertical boundaries at different temperatures, *Quarterly of Applied Mathematics* 12(3) (1954) 209–233.

[12] Bachok N, Ishak A, Nazar R, Flow and heat transfer over an unsteady stretching sheet in a micropolar fluid, *Meccanica* 46(5) (2011) 935–942.

[13] Bachok N, Ishak A, Pop I, Flow and heat transfer characteristics on a moving plate in a nanofluid, *International Journal of Heat and Mass Transfer* 55 (4) (2012) 642–648.

[14] Badruddin IA, Zainal ZA, Narayana PA, Seetharamu KN, Heat transfer in porous cavity under the influence of radiation and viscous dissipation, *International Communications in Heat and Mass transfer* 33(4) (2006) 491–499.

[15] Basak T, Paul RS, Pop I, Natural convection in a square cavity filled with a porous medium: effects of various thermal boundary conditions, *International Journal of Heat and Mass Transfer*, 49 (2006) 1430–1441

[16] Baytas AC, Pop I, Free convection in a square porous cavity using a thermal nonequilibrium model, *International Journal of Thermal Sciences* 41(9) (2002) 861–870.

[17] Beavers GS, Joseph DD, Boundary conditions at a naturally permeable wall, *Journal of Fluid Mechanics* 30(1) (1967) 197–207.

[18] Beckermann C, Ramadhyani S, Viskanta R, Natural convection flow and heat transfer between a fluid layer and a porous layer inside a rectangular enclosure, *Journal of Heat Transfer* 109 (2) (1987) 363–370.

[19] Beckermann C, Viskanta R, Ramadhyani S, Natural convection in vertical enclosures containing simultaneously fluid and porous layers, *Journal of Fluid Mechanics* 186 (1988) 257–284.

[20] Beg OA, Uddin MJ, Khan W, Bioconvective non-newtonian nanofluid transport in porous media containing micro-organisms in a moving free stream, *Journal of Mechanics in Medicine and Biology* 15 (05) (2015) 1550071.

[21] Beg OA, Multi-physical computational modelling of nanofluid bioconvection flows, *A. Sohail, Z. Li (Eds.): Computational Approaches in Biomedical Nano-Engineering* (2019) 100–130.

[22] Begum N, Siddiqa S, Sulaiman M, Islam S, Hossain MA, Gorla RS, Numerical solutions for gyrotactic bioconvection of dusty nanofluid along a vertical isothermal surface, *International Journal of Heat and Mass Transfer* 113 (2017) 229–236.

[23] Begum N, Siddiqa S, Hossain MA, Nanofluid bioconvection with variable thermophysical properties, *Journal of Molecular Liquids* 231 (2017) 325–332.

[24] Bhargava R, Sharma S, Bhargava P, Takhar HS, MHD heat and mass transfer of micropolar fluid flow over a stretching sheet, *International Journal of Fluid Mechanics Research* 34(1) (2007).

[25] Bhargava R, Sharma S, Takhar HS, Beg OA, Bhargava P, Numerical solutions for micropolar transport phenomena over a nonlinear stretching sheet, *Nonlinear Analysis: Modelling and Control* 12 (2007) 45–63.

[26] Bhargava R, Beg OA, Sharma S, Zueco J, Finite element study of nonlinear two-dimensional deoxygenated biomagnetic micropolar flow, *Communications in Nonlinear Science and Numerical Simulation* 15(5) (2010) 1210–1223.

[27] Bhattacharyya K, Boundary layer flow and heat transfer over an exponentially shrinking sheet, *Chinese Physics Letters* 28(7) (2011) 074701.

[28] Bhattacharyya K, Hayat T, Alsaedi A, Exact solution for boundary layer flow of casson fluid over a permeable stretching/shrinking sheet, *Journal of Applied Mathematics and Mechanics* 94(6) (2014) 522–528.

[29] Bianco V, Nardini S, Manca O, Enhancement of heat transfer and entropy generation analysis of nanofluids turbulent convection flow in square section tubes, *Nanoscale research letters* 6 (1) (2011) 252.

[30] Bingham E, The behavior of plastic materials, *Bulletin of US bureau of standards* 13 (1916) 309–353.

[31] Bird RB, Stewart WE, Lightfoot EN, **Transport phenomena**, John Wiley & Sons, 2006.

[32] Boyd J, Buick JM, Green S, Analysis of the casson and carreau-yasuda non-newtonian blood models in steady and oscillatory flows using the lattice boltzmann method, *Physics of Fluids* 19(9) (2007) 093103.

[33] Buongiorno J, Convective transport in nanofluids, *Journal of Heat Transfer* 128 (3) (2005) 240–250.

[34] Brinkman HC, On the permeability of media consisting of closely packed porous particles, *Flow, Turbulence and Combustion* 1(1) (1949) 81–86.

[35] Cao BY, Guo ZY, Equation of motion of a phonon gas and non-Fourier heat conduction, *Journal of Applied Physics*, 102(5) (2007) 053503.

[36] Casson N, A flow equation for pigment-oil suspensions of the printing ink type, *Rheology of disperse systems* (1959).

[37] Cattaneo C, On heat conduction, *Acts Sem. Mat. Phys. Univ. Modena* 3 (1948) 83–101.

[38] Chakraborty T, Das K, Kundu PK, Framing the impact of external magnetic field on bioconvection of a nanofluid flow containing gyrotactic microorganisms with convective boundary conditions, *Alexandria Engineering Journal* 57(1) (2018) 61–71.

[39] Chakravarty S, Mandal PK, Unsteady flow of a two-layer blood stream past a tapered flexible artery under stenotic conditions, *Computational Methods in Applied Mathematics* 4(4) (2004) 391–409.

[40] Chamkha AJ, Miroshnichenko IV, Sheremet MA, Numerical analysis of unsteady conjugate natural convection of hybrid water-based nanofluid in a semicircular cavity, *Journal of Thermal Science and Engineering Applications* 9 (4) (2017).

[41] Chandra A, Chhabra RP, Influence of power-law index on transitional Reynolds numbers for flow over a semi-circular cylinder, *Applied Mathematical Modelling* 35 (12) (2011) 5766–5785.

[42] Chandra A, Chhabra RP, Laminar free convection from a horizontal semi-circular cylinder to power-law fluids, *International Journal of Heat and Mass Transfer* (11–12) (2012) 2934–2944.

[43] Chhabra RP, Richardson JF, **Non-Newtonian flow and applied rheology: engineering applications**, Butterworth-Heinemann, 2011.

[44] Char MI, et al., Heat transfer of a continuous, stretching surface with suction or blowing *Journal of Mathematical Analysis and Applications* 135 (2) (1988) 568–580.

[45] Chen C, Hsiao S, Transport phenomena in enclosed porous cavities, *Transport phenomena in porous media* (1998) 31–56.

[46] Cheng P, Minkowycz WJ, Free convection about a vertical flat plate embedded in a porous medium with application to heat transfer from a dike, *Journal of Geophysical Research* 82(14) (1977) 2040–2044.

[47] Cheng P, Heat transfer in geothermal systems, *Advances in heat transfer* 14 (1979) 1–105.

[48] Chevalley J, An adaptation of the Casson equation for the rheology of chocolate, *Journal of texture studies* 22(2) (1991) 219–229.

[49] Chiam T, Micropolar fluid flow over a stretching sheet, *Journal of Applied Mathematics and Mechanics* 62(10) (1982) 565–568.

[50] Chiam T, Hydromagnetic flow over a surface stretching with a power-law velocity, *International Journal of Engineering Science* 33(3) (1995) 429–435.

[51] Choi S, J. Eastman J, **Enhancing thermal conductivity of fluids with nanoparticles**, 1995.

[52] Christov C, On frame indifferent formulation of the maxwell–cattaneo model of finite-speed heat conduction, *Mechanics Research Communications* 36(4) (2009) 481–486.

[53] Churchill S, **Viscous flows** Butterworths, 1988.

[54] Cokelet GR, Merrill EW, Gilliland ER, Shin H, Britten A, Wells Jr RE, The rheology of human bloodmeasurement near and at zero shear rate, *Transactions of the Society of Rheology* 7(1) (1963) 303–317.

[55] Crane LJ, Flow past a stretching plate, *Journal for Applied Mathematics and Physics* 21 (4) (1970) 645–647.

[56] Dai W, Wang H, Jordan PM, Mickens RE, Bejan A, A mathematical model for skin burn injury induced by radiation heating, *International Journal of Heat and Mass Transfer* 51(23-24) (2008) 5497–5510.

[57] Darcy H, Les Fontanies Publiques de la ville de Dijon, Dalmont, Paris (1856).

[58] Das SK, Choi SU, Yu W, Pradeep T, **Nanofluids: science and technology** John Wiley & Sons, 2007.

[59] Dash RK, Mehta KN, Jayaraman G, Casson fluid flow in a pipe filled with a homogeneous porous medium, *International Journal of Engineering Science* 34(10) (1996) 1145–1156.

[60] Das SK, Putra N, Thiesen P, Roetzel W, Temperature dependence of thermal conductivity enhancement for nanofluids, *Journal of Heat Transfer* 125(4) (2003) 567–574.

[61] Das K, Duari PR, Kundu PK, Nanofluid bioconvection in presence of gyrotactic microorganisms and chemical reaction in a porous medium, *Journal of Mechanical Science and Technology* 29 (11) (2015) 4841–4849.

[62] Demirel CS, Birben NC, Bekbolet M, A comprehensive review on the use of second generation TiO2 photocatalysts: Microorganism inactivation, *Chemosphere* 211 (2018) 420–448.

[63] Ding Y, Alias H, Wen D, Williams RA, Heat transfer of aqueous suspensions of carbon nanotubes (cnt nanofluids), *International Journal of Heat and Mass Transfer* 49 (1-2) (2006) 240–250.

[64] Dong Y, Cao BY, Guo ZY, Generalized heat conduction laws based on thermomass theory and phonon hydrodynamics, *Journal of Applied Physics*, 110(6) (2011) 063–504.

[65] Dwivedi S, Dubey S. On the stability of steady-states of a two-dimensional system of ferromagnetic nanowires, *Journal of Applied Analysis* 23(2) (2017) 89–100.

[66] Elbashbeshy EM, Heat transfer over a stretching surface with variable surface heat flux, *Journal of Physics D: Applied Physics* 31(16) (1998) 1951.

[67] Eldabe NT, Hassan AA, Mohamed MA, Effect of couple stresses on the MHD of a non-Newtonian unsteady flow between two parallel porous plates, *Zeitschrift fr Naturforschung A* 58(4) (2003) 204–210.

[68] Esfe MH, Yan WM, Akbari M, Karimipour A, Hassani M, Experimental study on thermal conductivity of dwcnt-zno/water-eg nanofluids, *International Communications in Heat and Mass Transfer* 68 (2015) 248–251.

[69] Ferdows M, Uddin MJ, Afify A, Scaling group transformation for MHD boundary layer free convective heat and mass transfer flow past a convectively heated nonlinear radiating stretching sheet, *International Journal of Heat and Mass Transfer* 56 (1–2) (2013) 181 – 187.

[70] Fernandes VA, Muller AJ, Sandoval AJ, Thermal, structural and rheological characteristics of dark chocolate with different compositions, *Journal of Food Engineering* 116(1) (2013) 97–108.

[71] Fick A, About diffusion, *Annals of Physics* 170 (1) (1855) 59–86.

[72] Fish J, Belytschko T, **A first course in finite elements**, John Wiley & Sons, New York, 2007.

[73] Forchheimer P, Water movement through the ground, magazine of the Association of German Engineers 45 (1901) 1782-1788.

[74] Fourier B, Joseph JB, **The analytic theory of heat**, The University Press, 1878.

[75] Garcia-Ochoa F, Casas JA, Apparent yield stress in xanthan gum solutions at low concentrations, *The Chemical Engineering Journal and the Biochemical Engineering Journal* 53(3) (1994) B41–B46.

[76] Gebhart B, Effects of viscous dissipation in natural convection, *Journal of fluid Mechanics* 14(2) (1962) 25–32.

[77] Ghigo A, Lagree PY, Fullana JM, A time-dependent non-newtonian extension of a 1d blood flow model, *Journal of Non-Newtonian Fluid Mechanics* 253 (2018) 36–49.

[78] Gholinia M, Hosseinzadeh K, Mehrzadi H, Ganji DD, Ranjbar AA, Investigation of MHD EyringPowell fluid flow over a rotating disk under effect of homogeneousheterogeneous reactions, *Case Studies in Thermal Engineering* 13 (2019) 100356.

[79] Ghorai S, Hill N, Wavelengths of gyrotactic plumes in bioconvection, *Bulletin of mathematical biology* 62(3) (2000) 429–450.

[80] Gireesha B, Archana M, Gorla RR, Makinde OD, MHD three dimensional double diffusive flow of casson nanofluid with buoyancy forces and nonlinear thermal radiation over a stretching surface, *International Journal of Numerical Methods for Heat & Fluid Flow* 27(12) (2017) 2858–2878.

[81] Gobin D, Goyeau B, Neculae A, Convective heat and solute transfer in partially porous cavities, *International Journal of Heat and Mass Transfer* 48(10) (2005) 1898-1908.

[82] Ghorai S, Hill NA, Development and stability of gyrotactic plumes in bioconvection, *Journal of Fluid Mechanics* 400 (1999) 1–31.

[83] Gorla RS, Sidawi I, Free convection on a vertical stretching surface with suction and blowing, *Applied Scientific Research* 52(3) (1994):247–257.

[84] Gupta P, Gupta A, Heat and mass transfer on a stretching sheet with suction or blowing, *The Canadian Journal of Chemical Engineering* 55 (6) (1977), 744–746.

[85] Haddad S, Thermal instability in brinkman porous media with cattaneo–christov heat flux, *International Journal of Heat and Mass Transfer* 68 (2014) 659–668.

[86] Han S, Zheng L, Li C, Zhang X, Coupled flow and heat transfer in viscoelastic fluid with CattaneoChristov heat flux model, *Applied Mathematics Letter* 38 (2014) 87–93.

[87] Hamid M, Usman M, Khan ZH, Haq RU, Wang W, Heat transfer and flow analysis of Casson fluid enclosed in a partially heated trapezoidal cavity *International Communications in Heat and Mass Transfer* 108 (2019) 104284.

[88] Hartnett JP, Kostic M, Heat transfer to newtonian and non-newtonian fluids in rectangular ducts, *Advances in Heat Transfer* 19 (1989) 247–356.

[89] Hassanien I, Gorla RS, Mixed convection boundary layer flow of a micropolar fluid near a stagnation point on a horizontal cylinder, *International Journal of Engineering Science* 28 (2) (1990) 153–161.

[90] Hayat T, Iqbal Z, Qasim M, Obaidat S, Steady flow of an Eyring Powell fluid over a moving surface with convective boundary conditions *International Journal of Heat and Mass Transfer* 55(7-8) (2012) 1817-1822.

[91] Hayat T, Shehzad SA, Alsaedi A, Alhothuali MS, Mixed convection stagnation point flow of Casson fluid with convective boundary conditions *Chinese Physics Letters* 29(11) (2012) 114704.

[92] Hayat T, Awais M, Asghar S, Radiative effects in a three-dimensional flow of MHD Eyring-Powell fluid, *Journal of the Egyptian Mathematical Society* 21(3) (2013) 379–384.

[93] Hayat T, Ashraf MB, Alsaedi A, Shehzad SA, Convective heat and mass transfer effects in three-dimensional flow of Maxwell fluid over a stretching surface with heat source, *Journal of Central South University* 22(1) (2015) 717–726.

[94] Hayat T, Gull N, Farooq M, Ahmad B, Thermal radiation effect in MHD flow of PowellEyring nanofluid induced by a stretching cylinder, *Journal of Aerospace Engineering* 29(1) (2016) 04015011.

[95] Hayat T, Khan MI, Waqas M, Alsaedi A, On CattaneoChristov heat flux in the flow of variable thermal conductivity EyringPowell fluid, *Results in Physics* 7 (2017) 446–450.

[96] Hayat T, Nadeem S, Heat transfer enhancement with AgCuO/water hybrid nanofluid, *Results in physics* 7 (2017) 2317–2324.

[97] F. Hecht, **Freefem++ v. 3.19-1**, Universite Pierre et Marie Curie, 2012.

[98] Heinrich J, Vionnet CA, The penalty method for the navier-stokes equations, *Archives of Computational Methods in Engineering* 2 (2) (1995) 51–65.

[99] Heris SZ, Esfahany MN, Etemad SG, Experimental investigation of convective heat transfer of al2o3/water nanofluid in circular tube, *International Journal of Heat and Fluid flow* 28 (2) (2007) 203–210.

[100] Herschel W, Bulkley R, Measurement of consistency as applied to rubber-benzene solutions, *Proceedings – American Society for Testing and Materials* 26 (1926), 621–633.

[101] Hill NA, Pedley TJ, Kessler JO, Growth of bioconvection patterns in a suspension of gyrotactic micro-organisms in a layer of finite depth, *Journal of Fluid Mechanics* 208 (1989) 509–543.

[102] Hill NA, Pedley TJ, Bioconvection, *Fluid Dynamics Research* 37 (1-2) (2005) 1–20.

[103] Hughes TJ, Liu WK, Brooks A, Finite element analysis of incompressible viscous flows by the penalty function formulation, *Journal of Computational Physics* 30(1) (1979) 1–60.

[104] Huh D, Matthews BD, Mammoto A, Zavala MM, Hsin HY, Ingber DE, Reconstituting organ-level lung functions on a chip, *Science* 328 (5986) (2010) 1662–1668.

[105] Ibrahim W, Shankar B, MHD boundary layer flow and heat transfer of a nanofluid past a permeable stretching sheet with velocity, thermal and solutal slip boundary conditions, *Computers & Fluids* 75 (2013) 1 – 10.

[106] Ibrahim W, The effect of induced magnetic field and convective boundary condition on mhd stagnation point flow and heat transfer of nanofluid past a stretching sheet, *IEEE Transactions on Nanotechnology* 14(1) (2015) 178–186.

[107] Ibrahim W, Three dimensional rotating flow of Powell-Eyring nanofluid with non-Fouriers heat flux and non-Ficks mass flux theory, *Results in Physics* 8 (2018) 569–577.

[108] Imran A, Rana MA, Siddiqui A, Study of a EyringPowell Fluid in a Scraped Surface Heat Exchanger, *International Journal of Applied and Computational Mathematics* 4(1) (2018) 1–20.

[109] Ingham DB, Pop I, **Transport phenomena in porous media**, Elsevier, 1998.

[110] Ingham DB, Pop I, **Transport phenomena in porous media III**, Elsevier, 2005.

[111] Jana S, Salehi KA, Zhong WH, Enhancement of fluid thermal conductivity by the addition of single and hybrid nano-additives, *Thermochimica acta* 462 (1-2) (2007) 45–55.

[112] Jena PK, Brocchi EA, Motta MS, In-situ formation of CuAl2O3 nano-scale composites by chemical routes and studies on their microstructures, *Materials Science and Engineering: A* 313(1-2) (2001) 180–186.

[113] Johnson C, **Numerical solution of partial differential equations by the finite element method**, Courier Corporation, 2012.

[114] Kapoor S, Rawat S, Study of buoyancy driven free convective flow of a micropolar fluid through a darcy-forchheimer porous medium with mutable thermal conductivity, *Indian Journal of Pure & Applied Physics* 55 (10) (2017) 754–763.

[115] Kataria HR, Patel HR, Radiation and chemical reaction effects on mhd casson fluid flow past an oscillating vertical plate embedded in porous medium, *Alexandria Engineering Journal* 55(1) (2016) 583–595.

[116] Kelson NA, Desseaux A, Effect of surface conditions on flow of a micropolar fluid driven by a porous stretching sheet, *International journal of engineering science* 39(16) (2001) 1881–1897.

[117] Khan MS, Alam MM, Ferdows M, Effects of magnetic field on radiative flow of a nanofluid past a stretching sheet, *Procedia Engineering* 56 (2013) 316 – 322.

[118] Khan NS, Bioconvection in second grade nanofluid flow containing nanoparticles and gyrotactic microorganisms, *Brazilian Journal of Physics* 48(3) (2018) 227-241.

[119] Khan W, Pop I, Boundary-layer flow of a nanofluid past a stretching sheet, *International Journal of Heat and Mass transfer* 53(11-12) (2010) 2477–2483.

[120] Khan W, Makinde O, Khan Z, Mhd boundary layer flow of a nanofluid containing gyrotactic microorganisms past a vertical plate with navier slip, *International Journal of Heat and Mass Transfer* 74 (2014) 285–291.

[121] Kreith F, Black WZ, **Basic heat transfer**, Harper & Row, New york 1980.

[122] Kumar R, Kumar J, A population balance model with simultaneous aggregation and breakage for the synthesis of Titanium dioxide nanoparticles, *Indian Society of Industrial and Applied Mathematics*, (2013).

[123] Kuznetsov AV, Avramenko AA, Effect of small particles on this stability of bioconvection in a suspension of gyrotactic microorganisms in a layer of finite depth. *International Communications in Heat and Mass Transfer* 31(1) (2004) 1–10.

[124] Kuznetsov AV, The onset of bioconvection in a suspension of gyrotactic microorganisms in a fluid layer of finite depth heated from below, *International Communications in Heat and Mass Transfer* 32(5) (2005) 574–582.

[125] Kuznetsov AV, The onset of nanofluid bioconvection in a suspension containing both nanoparticles and gyrotactic microorganisms, *International Communications in Heat and Mass Transfer* 37 (10) (2010) 1421–1425.

[126] Kuznetsov AV, Nield D, Natural convective boundary-layer flow of a nanofluid past a vertical plate, *International Journal of Thermal Sciences* 49 (2) (2010) 243 – 247.

[127] Kuznetsov AV, Nield D, Double-diffusive natural convective boundary-layer flow of a nanofluid past a vertical plate, *International Journal of Thermal Sciences*, 50(5) (2011) 712–717.

[128] Latiff NAA, Uddin MJ, Beg OA, Ismail AI, Unsteady forced bioconvection slip flow of a micropolar nanofluid from a stretching/shrinking sheet, Proceedings of the Institution of Mechanical Engineers, Part N: *Journal of Nanomaterials, Nanoengineering and Nanosystems* 230 (4) (2016) 177–187.

[129] Li H, Liu S, Dai Z, Bao J, Yang X, Applications of nanomaterials in electrochemical enzyme biosensors, *Sensors* 9 (11) (2009) 8547–8561.

[130] Li H, Ha CS, Kim I, Fabrication of carbon nanotube/sio2 and carbon nanotube/sio2/ag nanoparticles hybrids by using plasma treatment, *Nanoscale research letters* 4 (11) (2009) 1384–1388.

[131] Li JJ, Xu H, Raees A, Zhao QK, Unsteady mixed bioconvection flow of a nanofluid between two contracting or expanding rotating discs, *Zeitschrift fur Naturforschung A* 71(3) (2016) 261–272.

[132] Liu IC, Wang HH, Peng YF, Flow and heat transfer for three-dimensional flow over an exponentially stretching surface, *Chemical Engineering Communications* 200(2) (2013) 253–268.

[133] Lu D, Kahshan M, Siddiqui A, Hydrodynamical study of micropolar fluid in a porous-walled channel: Application to flat plate dialyzer, *Symmetry* 11(4) (2019) 541.

[134] Mabood F, Khan W, Ismail AM, Mhd boundary layer flow and heat transfer of nanofluids over a nonlinear stretching sheet: a numerical study, *Journal of Magnetism and Magnetic Materials* 374 (2015) 569–576.

[135] Madhesh D, Kalaiselvam S, Experimental analysis of hybrid nanofluid as a coolant, *Procedia Engineering* 97 (2014) 1667–1675.

[136] Mahanthesh B, Gireesha B, Shashikumar N, Hayat T, Alsaedi A, Marangoni convection in casson liquid flow due to an infinite disk with exponential space dependent heat source and cross-diffusion effects, *Results in Physics* 9 (2018) 78–85.

[137] Mahapatra TR, Nandy SK, Gupta AS, Magnetohydrodynamic stagnation-point flow of a power-law fluid towards a stretching surface, *International Journal of Non-Linear Mechanics* 44(2) (2009) 124–129.

[138] Mahian O, Kianifar A, Kalogirou SA, Pop I, Wongwises S, A review of the applications of nanofluids in solar energy, *International Journal of Heat and Mass Transfer* 57(2) (2013) 582–594.

[139] Makinde O, Aziz A, Boundary layer flow of a nanofluid past a stretching sheet with a convective boundary condition, *International Journal of Thermal Sciences* 50 (7) (2011) 1326–1332.

[140] Makulati N, Kasaeipoor A, Rashidi M, Numerical study of natural convection of a water–alumina nanofluid in inclined c-shaped enclosures under the effect of magnetic field, *Advanced Powder Technology* 27 (2) (2016) 661–672.

[141] Malik MY, Khan I, Hussain A, Salahuddin T, Mixed convection flow of MHD Eyring-Powell nanofluid over a stretching sheet: A numerical study, *AIP advances* 5(11) (2015) 117118.

[142] Mansour MA, Siddiqa S, Gorla RS, Rashad AM, Effects of heat source and sink on entropy generation and MHD natural convection of Al2O3-Cu/water hybrid nanofluid filled with square porous cavity, *Thermal Science and Engineering Progress* 6 (2018) 57–71.

[143] Maxwell JC, **A treatise on electricity and magnetism**, Oxford: Clarendon Press, 1 (1873).

[144] Mehryan S, Kashkooli FM, Soltani M, Raahemifar K, Fluid flow and heat transfer analysis of a nanofluid containing motile gyrotactic micro-organisms passing a nonlinear stretching vertical sheet in the presence of a non-uniform magnetic field; numerical approach, *PloS one* 11(6) (2016) e0157598.

[145] Mernone A, Mazumdar J, Lucas S, A mathematical study of peristaltic transport of a casson fluid, *Mathematical and Computer Modelling* 35(7-8) (2002) 895–912.

[146] Misra J, Pandey S, Peristaltic transport of blood in small vessels: study of a mathematical model, *Computers & Mathematics with Applications* 43(8-9) (2002) 1183–1193.

[147] Mliki B, Abbassi MA, Omri A, Zeghmati B, Effects of nanoparticles brownian motion in a linearly/sinusoidally heated cavity with mhd natural convection in the presence of uniform heat generation/absorption, *Powder Technology* 295 (2016) 69–83.

[148] Motsa SS, Hayat T, Aldossary OM, MHD flow of upper-convected Maxwell fluid over porous stretching sheet using successive Taylor series linearization method, *Applied Mathematics and Mechanics* 33(8) (2012) 975–990.

[149] Muhammad N, Nadeem S, Mustafa T, Squeezed flow of a nanofluid with cattaneo–christov heat and mass fluxes, *Results in physics* 7 (2017) 862–869

[150] Mukhopadhyay S, Layek GC, Samad SA, Study of MHD boundary layer flow over a heated stretching sheet with variable viscosity, *International journal of heat and mass transfer* 48(21-22) (2005) 4460-4466.

[151] Mukhopadhyay S, Vajravelu K, Diffusion of chemically reactive species in casson fluid flow over an unsteady permeable stretching surface, *Journal of Hydrodynamics* 25(4) (2013) 591–598.

[152] Mukhopadhyay S, Vajravelu K, Van Gorder RA, Casson fluid flow and heat transfer at an exponentially stretching permeable surface, *Journal of Applied Mechanics* 80(5) (2013).

[153] A. Munir, J. Wang, H. Zhou, Dynamics of capturing process of multiple magnetic nanoparticles in a flow through microfluidic bioseparation system, IET nanobiotechnology 3 (3) (2009) 55–64.

[154] Mustafaa M, Hayat T, Obaidat S, Boundary layer flow of a nanofluid over an exponentially stretching sheet with convective boundary conditions, *International Journal of Numerical Methods for Heat & Fluid Flow* 23(6) (2013) 945–959.

[155] Mustafa M, Cattaneo-Christov heat flux model for rotating flow and heat transfer of upper-convected Maxwell fluid, *AIP Advances* 5 (2015) 047–109.

[156] Mutuku WN, Makinde OD, Hydromagnetic bioconvection of nanofluid over a permeable vertical plate due to gyrotactic microorganisms, *Computers & Fluids* 95 (2014) 88–97.

[157] Mythili D, Sivaraj R, Influence of higher order chemical reaction and non-uniform heat source/sink on casson fluid flow over a vertical cone and flat plate, *Journal of Molecular Liquids* 216 (2016) 466–475.

[158] Nadeem S, Lee C, Boundary layer flow of nanofluid over an exponentially stretching surface, *Nanoscale Research Letters* 7(1) (2012) 1–6.

[159] Nakamura M, Sawada T, Numerical study on the flow of a non-newtonian fluid through an axisymmetric stenosis, *Journal of Biomechanical Engineering* 110 (2) (1988) 137–143.

[160] Nandalur AA, Kamangar S, Badruddin IA, Heat transfer in a porous cavity in presence of square solid block, *International Journal of Numerical Methods for Heat & Fluid Flow* 29(2) (2019) 640–656.

[161] Nazeer M, Ahmad F, Saeed M, Saleem A, Naveed S, Akram Z, Numerical solution for flow of a EyringPowell fluid in a pipe with prescribed surface temperature, *Journal of the Brazilian Society of Mechanical Sciences and Engineering* 41(11) (2019) 1–10.

[162] D.A. Nield, A. Bejan, **Convection in porous media**, Springer, 2006.

[163] Nield D, Kuznetsov AV, The cheng–minkowycz problem for natural convective boundary-layer flow in a porous medium saturated by a nanofluid, *International Journal of Heat and Mass Transfer* 52(25–26) (2009) 5792 – 5795.

[164] Nirmalkar N, Chhabra RP, Poole RJ, Laminar forced convection heat transfer from a heated square cylinder in a Bingham plastic fluid, *International Journal of Heat and Mass Transfer* 56 (1–2) (2013) 625–639.

[165] Nithiarasu P, Seetharamu KN, Sundararajan T, Natural convective heat transfer in a fluid saturated variable porosity medium, *International Journal of Heat and Mass Transfer* 40(16) (1997) 3955-3967.

[166] Nguyen CT, Roy G, Gauthier C, Galanis N, Heat transfer enhancement using al2o3–water nanofluid for an electronic liquid cooling system, *Applied Thermal Engineering* 27 (8-9) (2007) 1501–1506.

[167] Ochoa-Tapia JA, Whitaker S, Momentum transfer at the boundary between a porous medium and a homogeneous fluid-I. Theoretical development, International Journal of Heat and Mass Transfer, 38(14) (1995) 2635–2646.

[168] Oh ST, Lee JS, Sekino T, Niihara K, Fabrication of Cu dispersed Al2O3 nanocomposites using Al2O3/CuO and Al2O3/Cu-nitrate mixtures, *Scripta materialia* 44(8-9) (2001) 2117–2120.

[169] Oudina FM, Bessaih R, Numerical simulation of natural convection heat transfer of copper-water nanofluid in a vertical cylindrical annulus with heat sources, *Thermophysics and Aeromechanics* 26(3) (2019) 325–334.

[170] Oudina FM, Reddy NK, Sankar M, Heat source location effects on buoyant convection of nanofluids in an annulus, *Advances in Fluid Dynamics* (2021) 923–937.

[171] Patel M, Timol MG, Numerical treatment of PowellEyring fluid flow using method of satisfaction of asymptotic boundary conditions (MSABC), *Applied Numerical Mathematics* 59(10) (2009) 2584–2592.

[172] Panda S, Martha SC. Interaction of water waves with small undulations on a porous bed in a two-layer ice-covered fluid, *Journal of Marine Science and Application* 12(4) (2013) 381–392.

[173] Pedley TJ, Hill N, Kessler JO, The growth of bioconvection patterns in a uniform suspension of gyrotactic micro-organisms, *Journal of Fluid Mechanics* 195 (1988) 223–237.

[174] Pedley TJ, Kessler JO, Hydrodynamic phenomena in suspensions of swimming microorganisms, *Annual Review of Fluid Mechanics* 24(1) (1992) 313–358.

[175] Platt JR, "Bioconvection Patterns" in Cultures of Free-Swimming Organisms, *Science* 133(3466) (1961) 1766-1767.

[176] Poonia M, Bhargava R, Finite element study of EyringPowell fluid flow with convective boundary conditions, *Journal of Thermophysics and Heat Transfer* 28(3) (2014) 499–506.

[177] Pop I, Sheremet M, Free convection in a square cavity filled with a casson fluid under the effects of thermal radiation and viscous dissipation, *International Journal of Numerical Methods for Heat & Fluid Flow* 27(10) (2017) 2318–2332.

[178] Pop I, Ingham DB, **Convective heat transfer: mathematical and computational modelling of viscous fluids and porous media**, Elsevier, 2001.

[179] Poulikakos D, Bejan A, Selimos B, Blake K, High rayleigh number convection in a fluid overlaying a porous bed, *International Journal of Heat and Fluid Flow* 7(2) (1986) 109–116.

[180] Powell RE, Eyring H, Mechanisms for the relaxation theory of viscosity, *Nature* 154(3909) (1944) 427–428.

[181] Prasad V, Kulacki FA, Convective heat transfer in a rectangular porous cavity effect of aspect ratio on flow structure and heat transfer, *Journal of Heat Transfer* 106(1) (1984) 158–165.

[182] Qi H, Guo X, Transient fractional heat conduction with generalized cattaneo model, *International Journal of Heat and Mass Transfer* 76 (2014) 535–539.

[183] Rahman MM, Pop I, Effects of second-order slip and viscous dissipation on the analysis of the boundary layer flow and heat transfer characteristics of a casson fluid, *Sultan Qaboos University Journal for Science* 21(1) (2016) 48–63.

[184] Rana P, R. Bhargava R, Flow and heat transfer of a nanofluid over a nonlinearly stretching sheet: A numerical study, *Communications in Nonlinear Science and Numerical Simulation* 17 (1) (2012) 212–226.

[185] Rana S, Mehmood R, Akbar NS, Mixed convective oblique flow of a casson fluid with partial slip, internal heating and homogeneous–heterogeneous reactions, *Journal of Molecular liquids* 222 (2016) 1010–1019.

[186] Rashad AM, Nabwey HA, Gyrotactic mixed bioconvection flow of a nanofluid past a circular cylinder with convective boundary condition, *Journal of the Taiwan Institute of Chemical Engineers* 99 (2019) 9–17.

[187] Rashidi MM, Erfani E, A new analytical study of MHD stagnation-point flow in porous media with heat transfer, *Computer & Fluids* 40 (2011) 172–178.

[188] Rashidi MM, Ganesh NV, Hakeem AA, Ganga B, Buoyancy effect on MHD flow of nanofluid over a stretching sheet in the presence of thermal radiation, *Journal of Molecular Liquids* 198 (2014) 234–238.

[189] Rao AS, Sainath S, Rajendra P, Ramu G, Mathematical modelling of hydromagnetic casson non-newtonian nanofluid convection slip flow from an isothermal sphere, *Nonlinear Engineering* 8(1) (2019) 645–660.

[190] Reddy JN, On penalty function methods in the finite-element analysis of flow problems, *International Journal for Numerical Methods in Fluids* 2(2) (1982) 151–171.

[191] Reddy JN, **An Introduction to the Finite Element Method**, McGraw-Hill, New York, 1993.

[192] Reddy JN, Gartling DK, **The finite element method in heat transfer and fluid dynamics**, CRC press, 2010.

[193] Reddy JN, **An Introduction to Nonlinear Finite Element Analysis: with applications to heat transfer, fluid mechanics, and solid mechanics**, OUP Oxford, 2014.

[194] Reher EO, Haroske D, Kohler K, Chem Technol, *Chem Technol* 21(3) (1969):137-143.

[195] Rehman FU, Nadeem S, Rehman HU, Haq RU, Thermophysical analysis for three-dimensional MHD stagnation-point flow of nano-material influenced by an exponential stretching surface, *Results in Physics* 8 (2018) 316–323.

[196] Rohni AM, Ahmad S, Pop I, Flow and heat transfer over an unsteady shrinking sheet with suction in nanofluids, *International Journal of Heat and Mass Transfer* 55 (7-8) (2012) 1888–1895.

[197] Rohsenow WM, Hartnett JP, Ganic EN, **Handbook of heat transfer fundamentals**, New York. 1985.

[198] Sadaka G, **Freefem++, a tool to solve pdes numerically**, arXiv preprint arXiv:1205.1293.

[199] Saini S, Sharma YD, Numerical study of nanofluid thermo-bioconvection containing gravitactic microorganisms in porous media: Effect of vertical through flow, *Advanced Powder Technology* 29(11) (2018) 2725–2732.

[200] Saghir M, Heat and mass transfer in a multi-porous cavity, *International communications in heat and mass transfer* 25(7) (1998) 1019–1030.

[201] Sakiadis BC, Boundary-layer behavior on continuous solid surfaces: I boundary-layer equations for two-dimensional and axisymmetric flow, *AIChE Journal* 7(1) (1961) 26–28.

[202] Sankar D, Lee U, Two–fluid casson model for pulsatile blood flow through stenosed arteries: A theoretical model, *Communications in Nonlinear Science and Numerical Simulation* 15(8) (2010) 2086–2097.

[203] Santhosh N, Radhakrishnamacharya G, Chamkha AJ, Flow of a Jeffrey fluid through a porous medium in narrow tubes, *Journal of Porous Media* 18 (1) (2015) 71–78.

[204] Sarkar J, Ghosh P, Adil A, A review on hybrid nanofluids: recent research, development and applications, *Renewable and Sustainable Energy Reviews* 43 (2015) 164–177.

[205] Siegel R, **Thermal radiation heat transfer**, CRC press, 2001.

[206] Singh A, Thorpe G, Natural convection in a confined fluid overlying a porous layer-a comparison, *Indian Journal of Pure and Applied Mathematics* 26(1) (1995) 81–95.

[207] Shaw S, Sibanda P, Sutradhar A, Murthy P, Magnetohydrodynamics and soret effects on bioconvection in a porous medium saturated with a nanofluid containing gyrotactic microorganisms, *Journal of Heat Transfer* 136 (5) (2014) 052601.

[208] Sheikholeslami M, Gorji-Bandpy M, Ganji DD, Soleimani S, Effect of a magnetic field on natural convection in an inclined half-annulus enclosure filled with Cuwater nanofluid using CVFEM, *Advanced Powder Technology* 24(6) (2013) 980-991.

[209] Sheikholeslami M, Gorji-Bandpy M, Ganji D, MHD free convection in an eccentric semi-annulus filled with nanofluid, *Journal of the Taiwan Institute of Chemical Engineers* 45(4) (2014) 1204 – 1216.

[210] Sheikholeslami M, Hayat T, Alsaedi A, On simulation of nanofluid radiation and natural convection in an enclosure with elliptical cylinders, *International Journal of Heat and Mass Transfer* 115 (2017) 981–991.

[211] Sheikholeslami M, Seyednezhad M, Nanofluid heat transfer in a permeable enclosure in presence of variable magnetic field by means of CVFEM, *International Journal of Heat and Mass Transfer* 114 (2017) 1169–1180.

[212] Sheikholeslami M, Shehzad SA, Magnetohydrodynamic nanofluid convection in a porous enclosure considering heat flux boundary condition, *International Journal of Heat and Mass Transfer* 106 (2017) 1261–1269.

[213] Sheikholeslami M, Shehzad SA, CVFEM for influence of external magnetic source on Fe3O4-H2O nanofluid behavior in a permeable cavity considering shape effect, *International Journal of Heat and Mass Transfer* 115 (2017) 180–191.

[214] Sheikholeslami M, Rokni HB, Magnetic nanofluid flow and convective heat transfer in a porous cavity considering Brownian motion effects, *Physics of Fluids* 30(1) (2018) 012003.

[215] Sheikholeslami M, Rokni HB, Numerical simulation for impact of Coulomb force on nanofluid heat transfer in a porous enclosure in presence of thermal radiation, *International Journal of Heat and Mass Transfer* 118 (2018) 823–831.

[216] Sheikholeslami M, Mehryan SA, Shafee A, Sheremet MA, Variable magnetic forces impact on magnetizable hybrid nanofluid heat transfer through a circular cavity, *Journal of Molecular Liquids* 277 (2019) 388–396.

[217] Sheremet MA, Pop I, Conjugate natural convection in a square porous cavity filled by a nanofluid using Buongiornos mathematical model, *International Journal of Heat and Mass Transfer* 79 (2014) 137–145.

[218] Sheremet MA, Pop I, Nazar RJ, Natural convection in a square cavity filled with a porous medium saturated with a nanofluid using the thermal nonequilibrium model with a Tiwari and Das nanofluid model, *International Journal of Mechanical Sciences* 100 (2015) 312-321.

[219] Sidik NA, Adamu IM, Jamil MM, Kefayati GH, Mamat R, Najafi G, Recent progress on hybrid nanofluids in heat transfer applications: a comprehensive review, *International Communications in Heat and Mass Transfer* 78 (2016) 68–79.

[220] Sirohi V, Timol MG, Kalathia NL, Numerical treatment of Powell-Eyring fluid flow past a 90 degree wedge, *Reg. J. Energy Heat Mass Transfer* 6(3) (1984) 219–228.

[221] Sirohi V, Timol MG, Kalthia NL, Powell-Eyring model flow near an accelerated plate, *Fluid Dynamics Research* 2(3) (1987) 193.

[222] Sivasankaran S, Bhuvaneswari M, Natural convection in a porous cavity with sinusoidal heating on both sidewalls, *Numerical Heat Transfer, Part A: Applications* 63(1) (2013) 14–30.

[223] Straughan B, Thermal convection with the cattaneo–christov model, *International Journal of Heat and Mass Transfer* 53 (1-3) (2010) 95–98.

[224] Suresh S, Venkitaraj K, Selvakumar P, Chandrasekar M, Synthesis of al2o3–cu/water hybrid nanofluids using two step method and its thermo physical properties, *Colloids and Surfaces A: Physicochemical and Engineering Aspects* 388(1-3) (2011) 41–48.

[225] Suresh S, Venkitaraj KP, Selvakumar P, Chandrasekar M, Effect of Al2O3Cu/water hybrid nanofluid in heat transfer, *Experimental Thermal and Fluid Science* 38 (2012) 54–60.

[226] Sui J, Zheng L, Zhang X, Boundary layer heat and mass transfer with Cattaneo–Christov double-diffusion in upper-convected Maxwell nanofluid past a stretching sheet with slip velocity, *International Journal of Thermal Sciences* 104 (2016) 461–468.

[227] Tayebi T, Chamkha AJ, Free convection enhancement in an annulus between horizontal confocal elliptical cylinders using hybrid nanofluids, *Numerical Heat Transfer, Part A: Applications* 70 (10) (2016) 1141–1156.

[228] Tayebi T, Chamkha AJ, Buoyancy-driven heat transfer enhancement in a sinusoidally heated enclosure utilizing hybrid nanofluid, *Computational Thermal Sciences: An International Journal* 9 (5) (2017).

[229] Thumma T, Beg OA, Sheri SR, Finite element computation of transient dissipative double diffusive magneto-convective nanofluid flow from a rotating vertical porous surface in porous media, *Proceedings of the Institution of Mechanical Engineers, Part N: Journal of Nanomaterials, Nanoengineering and Nanosystems* 231(2) (2017) 89–108.

[230] Tibullo V, Zampoli V, A uniqueness result for the cattaneo–christov heat conduction model applied to incompressible fluids, *Mechanics Research Communications* 38(1), 77–79 (2011).

[231] Toghraie D, Chaharsoghi VA, Afrand M, Measurement of thermal conductivity of ZnOTiO 2/EG hybrid nanofluid, *Journal of Thermal Analysis and Calorimetry* 125(1) (2016) 527–535.

[232] Trevisan OV, Bejan A, Natural convection with combined heat and mass transfer buoyancy effects in a porous medium, *International Journal of Heat and Mass Transfer* 28(8) (1985) 1597–1611.

[233] Turan O, Chakraborty N, Poole RJ, Laminar natural convection of Bingham fluids in a square enclosure with differentially heated side walls, *Journal of Non-Newtonian Fluid Mechanics* 165 (15–16) (2010) 901–913.

[234] Tzirakis K, Botti L, Vavourakis V, Papaharilaou Y, Numerical modeling of non-newtonian biomagnetic fluid flow, *Computers & Fluids* 126 (2016) 170–180.

[235] Uddin MJ, Beg OA, Ghose PK, Ismael AIM, Numerical study of non-Newtonian nanofluid transport in a porous medium with multiple convective boundary conditions and nonlinear thermal radiation effects, *International Journal of Numerical Methods for Heat and Fluid Flow* 26(5) (2016) 1–25.

[236] Uddin MJ, Khan W, Qureshi S, Beg OA, Bioconvection nanofluid slip flow past a wavy surface with applications in nano-biofuel cells, *Chinese Journal of Physics* 55 (5) (2017) 2048–2063.

[237] Ullah I, Alkanhal TA, Shafie S, Nisar KS, Khan I, Makinde OD, MHD slip flow of casson fluid along a nonlinear permeable stretching cylinder saturated in a porous medium with chemical reaction, viscous dissipation, and heat generation/absorption, *Symmetry* 11(4) (2019) 531.

[238] Walawender WP, Chen TY, Cala DF, An approximate Casson fluid model for tube flow of blood, *Biorheology* 12(2) (1975) 111–119.

[239] Walker KL, Homsy GM, Convection in a porous cavity, *Journal of Fluid Mechanics* 87(3) (1978) 449–474.

[240] Waqas H, Khan SU, Hassan M, Bhatti MM, Imran M, Analysis on the bioconvection flow of modified second-grade nanofluid containing gyrotactic microorganisms and nanoparticles, *Journal of Molecular Liquids* 291 (2019) 111231.

[241] Wen D, Ding Y, Experimental investigation into convective heat transfer of nanofluids at the entrance region under laminar flow conditions, *International journal of heat and mass transfer* 47 (24) (2004) 5181–5188.

[242] Xuan Y, Li Q, Heat transfer enhancement of nanofluids, *International Journal of heat and fluid flow* 21(1) (2000) 58–64.

[243] Yildiz C, Arici M, Karabay H, Comparison of a theoretical and experimental thermal conductivity model on the heat transfer performance of al2o3-sio2/water hybrid-nanofluid, *International Journal of Heat and Mass Transfer* 140 (2019) 598–605.

[244] Zalba B, Marin JM, Cabeza LF, Mehling H, Review on thermal energy storage with phase change: materials, heat transfer analysis and applications, *Applied Thermal Engineering* 23(3) (2003) 251–283.

[245] Zhang L, Ding Y, Povey M, York D, Zno nanofluids–a potential antibacterial agent, *Progress in Natural Science* 18(8) (2008) 939–944.

[246] Zhang S, Zhao D, **Advances in magnetic materials: processing, properties, and performance**, CRC press, 2017.

[247] Zhao Q, Xu H, Tao L, Unsteady bioconvection squeezing flow in a horizontal channel with chemical reaction and magnetic field effects, Mathematical Problems in Engineering (2017).

.

.

.

Appendix

Numerical Methods The basic idea behind all numerical techniques is to perform calculations at a small number of points and then with the help of solutions obtained at specified, results are interpolated for the whole domain (either surface or volume). All numerical methods begin with a speculative assumption. Following the receipt of the results, there are various methods of varifying accuracy of results and minimization of error.

Finite Element Method Finite element method (FEM) is a higher order numerical method that was originally developed to solve structural problems but is now used as a mathematical tool to solve linear and nonlinear ordinary or partial differential equations as well as integral equations. The finite element method not only overcomes the limitations of traditional variational methods but it also possesses the characteristics of a powerful computational technique. This method is so general that it can be used to solve a wide range of engineering problems, such as heat and mass transfer, fluid mechanics, chemical processing, solid mechanics, electrical systems, and many others. The basics steps involved in this method are summarized below :

- **Discretization of the domain into elements:**

    1. The whole domain is divided into a finite number of subdomains, which is called the discretization of the domain. Each subdomain is called an element. Subdomain may be one dimensional (line elements) or two dimensional (triangle, rectangle or quadrilateral). The collection of elements is called the finite-element mesh. The intersection of any two elements is termed as inter-element boundary. The intersection points or intermediate points are called the nodes.

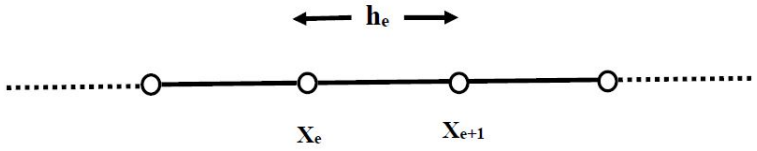

Discretization of one-dimensional domain

    2. The geometric properties needed for the problem are generated, which indicates the position of the elements.

- **Interpolation function:** The finite element approximation ($U^e(x, y)$) over an element Ω^e must satisfy the following conditions in order for the approximate solution

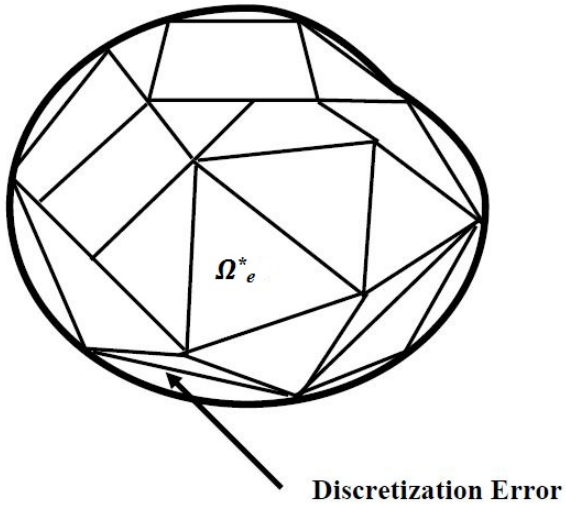

Discretization of two-dimensional domain

to be convergent to the true one:

1. U^e must be continuous over the element and differentiable, as required in the weak form of the problem.
2. The polynomial used to represent U^e must be complete.
3. All terms in the polynomial should be linearly independent.

- **Element Equations:** The derivation of finite element equations, i.e., algebraic equations among the unknown parameters of the finite element approximation, involves the following steps:
  1. A typical element is isolated from the mesh and variational formulation of the given problem over the typical element is constructed.
  2. Assume the form of the approximate solution over a typical finite element.
  3. The element matrix is called as stiffness matrix is constructed by using the element interpolation functions. The interpolation functions depend upon the type of element (geometry, number of nodes and number of primary unknowns per node).
- **Assembly of Element Equations:** In the continuous finite element method local elements and vectors are assembled in the assembly routine.
- **Imposition of Boundary Conditions:** The essential and natural boundary conditions are imposed on the equations.
- **Solve algebraic system:** The resulting algebraic system is solved (iteratively) using

linear algebra routines.

Penalty Finite Element Method The basic idea behind the Penalty finite element method [191] is similar to Lagrange's multiplier method which allows us to reformulate the problem with constraints as one without constraints. The method can be explained by considering an example of steady state flow of viscous incompressible fluid in a closed domain Ω^*. Here, we assumed that speed of flow is low (inertial effects are neglected), such a flow is called stokes flow and the governing Stokes equations for the flow problem are given as:

Conservation of Mass

$$\frac{\partial u}{\partial x} + \frac{\partial v}{\partial y} = 0 \tag{A1}$$

Conservation of Momentum

$$\frac{\partial P}{\partial x} - \frac{\partial}{\partial x}\left(2\mu\frac{\partial u}{\partial x}\right) - \frac{\partial}{\partial y}\left[\mu\left(\frac{\partial u}{\partial y} + \frac{\partial v}{\partial x}\right)\right] - f_x = 0, \tag{A2}$$

$$\frac{\partial P}{\partial y} - \frac{\partial}{\partial y}\left(2\mu\frac{\partial v}{\partial y}\right) - \frac{\partial}{\partial x}\left[\mu\left(\frac{\partial u}{\partial y} + \frac{\partial v}{\partial x}\right)\right] - f_y = 0 \tag{A3}$$

The corresponding boundary conditions are given below:

$$h_x = 2\mu\frac{\partial u}{\partial x}n_x + \mu\left(\frac{\partial u}{\partial y} + \frac{\partial v}{\partial x}\right)n_y - Pn_x \quad \text{on} \quad \Gamma_1^* \tag{A4}$$

$$h_y = 2\mu\frac{\partial v}{\partial y}n_y + \mu\left(\frac{\partial u}{\partial y} + \frac{\partial v}{\partial x}\right)n_x - Pn_y \quad \text{on} \quad \Gamma_1^* \tag{A5}$$

$$u = u^*, \quad v = v^* \quad \text{on} \quad \Gamma_2^* \tag{A6}$$

The variational formulation of equations $A2$-$A3$ over an element Ω^{*e} can be obtained by using weight functions w_1, w_2 and integrate over an element:

$$\int_{\Omega^{*e}} w_1\left\{ - \frac{\partial}{\partial x}\left(2\mu\frac{\partial u}{\partial x}\right) - \frac{\partial}{\partial y}\left[\mu\left(\frac{\partial u}{\partial y} + \frac{\partial v}{\partial x}\right)\right] - f_x\right\}dxdy = 0, \tag{A7}$$

$$\int_{\Omega^{*e}} w_2\left\{ - \frac{\partial}{\partial y}\left(2\mu\frac{\partial v}{\partial y}\right) - \frac{\partial}{\partial x}\left[\mu\left(\frac{\partial u}{\partial y} + \frac{\partial v}{\partial x}\right)\right] - f_y\right\}dxdy = 0, \tag{A8}$$

The pressure term and equation $A1$ does not appear in the weak form. This is because the continuity equation is automatically satisfied by the velocity field (u, v) when they are subject to the constraint $\frac{\partial u}{\partial x} + \frac{\partial v}{\partial y} = 0$.

Now, after doing integration by parts and applying boundary conditions, we get the following form of equations:

$$\int_{\Omega^{*e}} \left[2\mu \frac{\partial w_1}{\partial x}\frac{\partial u}{\partial x} + \mu \frac{\partial w_1}{\partial y}\left(\frac{\partial u}{\partial y} + \frac{\partial v}{\partial x}\right) - w_1 f_x \right] dxdy - \oint_{\Gamma^*} w_1 h_x ds = 0 \qquad (A9)$$

$$\int_{\Omega^{*e}} \left[2\mu \frac{\partial w_2}{\partial y}\frac{\partial v}{\partial y} + \mu \frac{\partial w_2}{\partial x}\left(\frac{\partial u}{\partial y} + \frac{\partial v}{\partial x}\right) - w_2 f_y \right] dxdy - \oint_{\Gamma^*} w_2 h_y ds = 0 \qquad (A10)$$

The linear and bilinear form of the equations $A9$-$A10$ is given by:

$$I(w_1, w_2) = \int_{\Omega^{*e}} (f_x w_1 + f_y w_2) dxdy + \oint_{\Gamma^*} (h_x w_1 + h_y w_2) ds, \qquad (A11)$$

$B((w_1, w_2), (u, v)) =$

$$\mu \int_{\Omega^{*e}} \left[2\left(\frac{\partial w_1}{\partial x}\frac{\partial u}{\partial x} + \frac{\partial w_2}{\partial y}\frac{\partial v}{\partial y} \right) + \left(\frac{\partial w_1}{\partial y} + \frac{\partial w_2}{\partial x} \right)\left(\frac{\partial u}{\partial y} + \frac{\partial v}{\partial x} \right) \right] dxdy. \qquad (A12)$$

The corresponding quadratic functional can be written as

$J(u, v) = \frac{1}{2} B((u, v), (u, v)) - l(u, v)$

$$J(u, v) = \mu \int_{\Omega^{*e}} \left[\left(\frac{\partial u}{\partial x} \right)^2 + \left(\frac{\partial v}{\partial y} \right)^2 + \frac{1}{2}\left(\frac{\partial u}{\partial y} + \frac{\partial v}{\partial x} \right)^2 \right] dxdy$$

$$- \int_{\Omega^{*e}} (f_x u + f_y v) dxdy - \oint_{\Gamma^*} (h_x u + h_y y) ds. \qquad (A13)$$

We here state that the equations ($A2$ - $A3$) which govern the steady state incompressible flow of viscous fluid has made equivalent to minimizing $J(u, v)$ $(A13)$ subjected to the constraint
$H(u, v) \equiv \frac{\partial u}{\partial x} + \frac{\partial v}{\partial y} = 0.$

Now, the constrained problem is reformulated with the help of penalty function method as an unconstrained problem by minimizing the modified functional, which is given as
$J_p(u, v) = J(u, v) + \frac{1}{2}\Gamma \int_{\Omega^*} [H(u, v)]^2 dxdy,$
The necessary conditions for the minimizing the J_p are: $\delta^* u J_p = 0, \delta^* v J_p = 0$

$\delta^* u J_p = \delta^* u J + \Gamma \int_{\Omega^{*e}} H(u,v)\delta^* u H(u,v) dxdy.$

$$\delta^* u J_p = \int_{\Omega^{*e}} \left[2\mu \frac{\partial \delta^* u}{\partial x}\frac{\partial u}{\partial x} + \mu \frac{\partial \delta^* u}{\partial y}\left(\frac{\partial u}{\partial y} + \frac{\partial v}{\partial x}\right)\right] dxdy$$

$$- \int_{\Omega^{*e}} \delta^* u f_x dxdy - \oint_{\Gamma^e} \delta^* u h_x ds + \Gamma \int_{\Omega^{*e}} \frac{\partial \delta^* u}{\partial x}\left(\frac{\partial u}{\partial x} + \frac{\partial v}{\partial y}\right) dxdy = 0. \qquad (A14)$$

$$\delta^* v J_p = \int_{\Omega^{*e}} \left[2\mu \frac{\partial \delta^* v}{\partial y}\frac{\partial v}{\partial y} + \mu \frac{\partial \delta^* v}{\partial x}\left(\frac{\partial u}{\partial y} + \frac{\partial v}{\partial x}\right)\right] dxdy$$

$$- \int_{\Omega^{*e}} \delta^* v f_y dxdy - \oint_{\Gamma^e} \delta^* v h_y ds + \Gamma \int_{\Omega^{*e}} \frac{\partial \delta^* v}{\partial y}\left(\frac{\partial u}{\partial x} + \frac{\partial v}{\partial y}\right) dxdy = 0. \qquad (A15)$$

The above said equations (equations $A14$ - $A15$) represents the weak form of the penalty finite method model. Here the point to be noticed that the pressure, which is the lagrange multiplier is not included explicitly in the weak form, although it appears in the boundary stresses h_x and h_y. Now we consider the interpolation function for the velcity field as: $u = \sum_{j=1}^{n} u_j \Psi_j^e, v = \sum_{j=1}^{n} v_j \Psi_j^e$ and $\delta^* u = \Psi_i, \delta^* v = \Psi_i$. By using these interpolation function for the velocity field, the penalty finite element model takes the form,

$$\begin{bmatrix} [\overline{L^{11}}] & [\overline{L^{12}}] \\ [\overline{L^{21}}] & [\overline{L^{22}}] \end{bmatrix} \begin{bmatrix} \{u\} \\ \{v\} \end{bmatrix} = \begin{bmatrix} \{K^1\} \\ \{K^2\} \end{bmatrix} \qquad (A15)$$

where $[\overline{L^{11}}] = [L^{11}] + \Gamma[R^{11}]$, $[\overline{L^{12}}] = [L^{12}] + \Gamma[R^{12}]$, and $[\overline{L^{22}}] = [L^{22}] + \Gamma[R^{22}]$. Also each L^{ij}, R^{ij} and K^i are submatrices of order (2×2) and (2×1), respectively. These submatrices are defined as:

$$R_{ij}^{11} = \int_{\Omega^{*e}} \frac{\partial \Psi_i}{\partial x}\frac{\partial \Psi_j}{\partial x} dxdy, \quad R_{ij}^{12} = \int_{\Omega^{*e}} \frac{\partial \Psi_i}{\partial x}\frac{\partial \Psi_j}{\partial x} dxdy, \quad R_{ij}^{22} = \int_{\Omega^{*e}} \frac{\partial \Psi_i}{\partial x}\frac{\partial \Psi_j}{\partial x} dxdy$$

$$K_i^1 = \int_{\Omega^{*e}} f_x \Psi_i dxdy + \oint_{\Gamma^{*e}} h_x \Psi_i ds, \quad K_i^2 = \int_{\Omega^{*e}} f_y \Psi_i dxdy + \oint_{\Gamma^{*e}} h_y \Psi_i ds \qquad (A16)$$

The penalty parameter is calculated from the equation given below:

$$\Upsilon_\Gamma = -P_\Gamma^e = \Gamma H(u_\Gamma, v_\Gamma) = \Gamma\left(\frac{\partial u_\Gamma}{\partial x} + \frac{\partial v_\Gamma}{\partial y}\right)$$